Chitosan mediated DNA condensation as a basis for gene delivery: Influence of polyelectrolyte molecular parameters on the condensation behavior

Signe Danielsen

A thesis in partial fulfillment of the requirements for the degree
Doctor Scientiarum

Department of Physics
Norwegian University of Science and Technology
Trondheim, Norway 2004

Acknowledgments

This work has been carried out at the Department of Physics at The Norwegian University of Science and Technology (NTNU) in the period 2000-2004. The financial support from the Norwegian Research Council through a strategic program in Medical Technology and the Department of Physics, NTNU, to carry out the study is highly acknowledged.

I will take the opportunity to thank several people that have been important for me during the work with the PhD:

First of all I would like to thank my supervisor professor Bjørn T. Stokke for introducing me to the field of polyelectrolyte complexes and for guiding me through the work. The amount of knowledge he has shared with me through the numerous of discussions is highly appreciated. I also want to thank my co-supervisor professor Catharina de Lange Davies for her interest and discussions during these years.

Further, I would like to thank the members of the Biophysics group at NTNU for making the years here memorable. My colleagues Gjertrud and Pawel are especially thanked for their contributions in several ways, both scientific and non-scientific. The many helpful discussions with professor Thor-Bernt Melø are also highly appreciated.

The high-quality chitosan samples provided by professor Kjell Morten Vårum is highly appreciated. I also thank Sabina P. Strand for collaboration and discussions.

I am grateful to Professor Helen G. Hansma who gave me the opportunity to visit her lab at the Department of Physics at University of California Santa Barbara and allowed me to use her lab to perform experiments. The people in the Hansma-lab are all thanked for contributing to making my stay in Santa Barbara such a memorable time. Emin Oroudjev and Thomas Gutsmann are especially thanked for their contributions in both scientific and non-scientific discussions.

Finally, I would like thank my friends and family for being encouraging, giving me confidence and reminding me of the world outside 'polyelectrolytes'. I am especially grateful to Robert for being patient and supportive even in my most frustrated and psychotic periods.

Trondheim, October 2004

Signe Danielsen

Table of Contents

Abbreviations v

List of papers vi

Summary viii

1 Introduction 1

1.1 Introduction to gene therapy 1

1.1.1 Historical background 1

1.1.2 Barriers to gene delivery 3

1.2 Gene delivery system, an approach towards non-viral vectors 5

1.2.1 Naked DNA and physical methods 6

1.2.2 Cationic lipids 7

1.2.3 Cationic polymers 8

1.2.4 The use of chitosan as a potential system for gene delivery 9

1.3 Polycation-induced DNA condensation 11

1.3.1 DNA structure 12

1.3.2 Polyelectrolyte properties of DNA 14

1.3.2.1 The Poisson-Boltzmann equation 14

1.3.2.2 Counterion condensation 15

1.3.2.3 Charge correlations 16

1.3.3 DNA-polycation complex formation 17

2 Aim of the thesis 21

3 Summary of the papers 22

3.1 Paper I 22

3.2 Paper II 22

3.3 Paper III 23

3.4 Paper IV 24

3.5 Paper V 24

4 General discussion 25

4.1 Structure and stability of DNA-chitosan complexes 25

4.1.1 Effect of chitosan molecular parameters on its ability to compact DNA 26

4.1.2 Effect of solution parameters on the DNA-chitosan complexation 29

4.1.3 Polyelectrolyte complexation, DNA as a part of the general picture 30

4.1.4 Polyplex stability 34

Concluding remarks 36

References 38

Appendix A-1
A.1 Image analysis A-1
A.2 DNA labeling for CLSM imaging A-3
A.3 Immobilization of chitosan to mica and DNA to the AFM tip A-4

Abbreviations

AFM	Atomic force microscopy
bp	Base pairs
CLSM	Confocal laser scanning microscopy
DNA	Deoxyribonucleic acid
DP	Degree of polymerization
EtBr	Ethidium bromide
F_A	Degree of acetylation
HDP	High degree of polymerization
I	Ionic strength
GAG	Glycosaminoglycan
HA	Hyaluronic acid
L_c	Contour length
LDP	Low degree of polymerization
Lipoplex	Liposome-DNA complex
L_p	Persistence length
PA	Polyanion
PB	Poisson Boltzman
PC	Polycation
pDNA	Plasmid DNA
PEI	Poly(ethylenimine)
PLL	Poly-L-lysine
Polyplex	Polyelectrolyte complex (polyanion-polycation)
RNA	Ribonucleic acid
T	Temperature
TM-AFM	Tapping mode atomic force microscopy

List of papers

I. **Signe Danielsen**, Kjell M. Vårum, and Bjørn T. Stokke. 2004: Structural analysis of chitosan mediated DNA condensation by AFM: Influence of chitosan molecular parameters. *Biomacromolecules*. 5:928-936, 2004.

II. **Signe Danielsen**, Sabina Strand, Catharina de Lange Davies, and Bjørn T. Stokke: Glycosaminoglycan destabilization of DNA-chitosan polyplexes for gene delivery depends on chitosan chain length and GAG properties. Accepted for publication in *Biochim Biophys Acta*, 2004.

III. Gjertrud Maurstad, **Signe Danielsen**, and Bjørn T. Stokke: Analysis of compacted semiflexible polyanions visualized by atomic force microscopy: Influence of chain stiffness on the morphologies of polyelectrolytes. *J. Phys. Chem. B*. 107:8172-8180, 2003.

IV. **Signe Danielsen*** and Gjertrud Maurstad*, and Bjørn T. Stokke: DNA-polycation complexation and polyplex stability in the presence of competing polyanions. Accepted for publication in *Biopolymers*, 2004.

V. **Signe Danielsen**, Emin Oroudjev, Thomas Gutsmann, Bjørn T. Stokke, and Helen G. Hansma: Chitosan-mica interactions by force-spectroscopy: a model system for DNA-chitosan condensation.

* The authors contributed equally to the work

Contributions to the papers:

The papers are based on projects that have involved collaboration with other people. The contribution to the papers, in which parts of the experimental work is carried out by others, is therefore given below:

Paper III: Experimental work and data analysis involving the DNA data.

In all papers, data extraction and data analysis were carried out by employing novel programs implemented in either IDL (paper I-IV) or Igor Pro (paper V). The implementation of these programs was carried out by others.

Summary

Polycation mediated gene delivery has emerged as a promising alternative to the use of viral vectors for gene therapy. Although yielding significantly lower transfection efficiency than viral vectors, the use of polycations possess advantages over viruses such as reduced immune response and the possibility of carrying large DNAs at low cost. The polycations will condense DNA into a more compact form that may allow easier transport through the extracellular matrix and probably across the cell membrane, as well as protect the DNA from nuclease attacks. The non-toxic and biodegradable polycation chitosan has shown great potential as a gene delivery vehicle, as high transfection efficiencies are reported. In this study the effect of chitosan molecular parameters like charge density (determined by the fractional content of acetylated units, F_A) and the degree of polymerization (DP) was evaluated for its ability to compact DNA. AFM-imaging revealed that chitosan compacted DNA into toroidal, rod-like and globular structures, with the dominant morphology depending on both F_A and DP of the chitosan. Furthermore, when reducing the chitosan DP, larger chitosan concentrations were required to obtain DNA condensates of a well defined morphology. However, whereas high DP (HDP) chitosans could form well defined structures even at pH 7.4, chitosan oligomers were unable to compact DNA even at very high stoichiometric ratios. This indicates that a minimum chitosan charge is required to cause DNA collapse. Studying other polyanion-polycation systems revealed that general electrostatics is important for the complex formation. Furthermore, employing polyanions with different chain stiffness (xanthan, DNA and alginate) and using different polycations (chitosan and poly-L-lysine) as condensation agents showed that the morphologies formed are to a large extent determined by the chain stiffness of the polyanion, as well as properties of the polycation which is believed to affect the intersegment interaction energy. The stability of the delivery system is identified to be important for its ability to mediate high transfection levels. Whereas high stability is required for the transport of the delivery system towards the cell, and intracellularly towards the nucleus, DNA needs to be released inside the cell to be expressed. The ability of the DNA-chitosan complexes to release DNA upon exposure to competing polyanions was identified to depend on the chitosan DP and concentration, as well as the properties of the competing polyanion. The glycosaminoglycans (GAGs) heparin and hyaluronic acid (HA) represent such competing polyanions. Whereas HA was unable to dissociated the DNA-chitosan complexes, exposure to heparin yielded a dissociation that depended on both the chitosan chain length and concentration. Both increasing chitosan concentration and DP resulted in complexes that

were more resistant towards dissociation. Furthermore, increased stability of the complexes was obtained upon increasing the temperature of the DNA-chitosan system. Thus, by controlling the chitosan molecular parameters such as F_A and DP, as well as the temperature in the system, it appears that both the morphology and the stability of the resulting DNA-chitosan complexes can be tuned. Such knowledge is of importance when attempting to optimize this system for gene delivery purposes.

1 Introduction

The condensation of DNA has attracted considerable attention for a long time and from a wide area of interests. This is motivated by the search for an understanding of the chromosomal packing of genes, the polyelectrolyte complexation and phase transitions in general, and, more recently, the condensation of gene vectors required for gene therapy. Advancement of gene therapy requires efficient gene delivery systems that can overcome the many barriers related to the transport and expression of the gene vector. This section thus starts with an introduction to the field of gene therapy and describes the major barriers involved. The most important gene delivery systems being under investigation are then presented, focusing on the polycation mediated DNA condensation which has received increasing interest during the last years. Although both molecular and solution parameters are identified to be important for the collapse transition of the DNA molecule, a detailed molecular understanding of the complexation process is still not achieved. In this study the polycation chitosan was employed to compact DNA and the complexation was studied at various conditions in an attempt to obtain more knowledge about the polycation-induced DNA condensation.

1.1 Introduction to gene therapy

Gene therapy is defined as the application of genetic principles to the treatment of human diseases [1]. The basis of gene therapy is to eliminate the cause of the disease by inserting genetic material into the cells instead of treating the symptoms as most of today's drugs do. By addition or modification of genes, the cell becomes able to produce enzymes or other proteins that were initially defective or missing. Gene therapy is thus regarded as a powerful tool for curing many hereditary diseases and multigenetic disorders. The introduction of nucleic acids to cells also provides the possibility of downregulating the expression of particular genes (e.g. oncogenes), predominantly by interaction with mRNA, representing a potential strategy for cancer treatment [2].

1.1.1 Historical background

The possibility of gene therapy in medicine began with the discoveries that a gene could be transferred within nucleic acids (Avery, MacLeod and McCarthy, 1944) and that viral

genomes could become a permanent part of cell genomes (Zinder and Lederberg, 1953) [1]. The first specific approach to carry out human gene therapy was in 1966 when the concept of genetic engineering of human beings was described. During the years 1966-1969 a theoretical discussion went on concerning the use of viruses for the benefit of man by introducing new genes into defective cells. It was suggested that by extracting the DNA molecules that code for certain proteins and chemically grafting these to the DNA of existing viruses, genes could be transferred to a cell by infection of this virus. In 1968 French Anderson wrote an article postulating how gene therapy one day could be accomplished. However, the editors of the journal (New England Journal of Medicine) rejected the article as too speculative, although very fascinating [3].

In 1970, the first genetic engineering experiment was carried out on humans and involved the administration of a virus to two German girls suffering from a genetic disease. Not everyone was enthusiastic about the experiment. Concerns were expressed that not enough was known about the potential consequences of such experiments, leading to a rise in the ethical discussion about the use of gene therapy. The concerns were related to the safety of the treatment and the potential misuse of genetic engineering. In the early 1970s sufficient progress was made in inserting genes into a mammalian DNA virus, and successful molecular cloning was created. This lead to the recognition of the enormous power of and danger related to this new technology. The first official guidelines for carrying out recombinant DNA research were published in 1976. By 1979 these guidelines became highly respected and the public's fear had greatly subsided [3].

In the beginning of 1980 retroviral-mediated gene transfer was developed in animal models. Successful gene therapy was carried out on fruit flies (*Drosophila*) and procedures were developed for inserting functional genes into the bone marrow of mice. The first genetic cure in a mammal was reported in 1984. However, problems concerning regulation of the production of the gene products, low transfection efficiency and safety of the treatment still remained major issues [4].

The first approved trial of gene transfer into humans took place in 1989, but did not involve gene therapy [5]. This trial was performed to track gene-marked immune cells after infusion into patients with advanced cancer [5, 6]. The first US federally approved gene therapy trial began in 1990 giving encouraging results that stimulated to further clinical trials. Since then

more than 300 clinical protocols have been approved worldwide and more than 3000 patients have carried genetically engineered cells in their body [7].

In 2002 a tragic setback was reported [8]. A three-year-old boy who had received gene therapy treatment developed a leukemia-like condition that was believed to be due to the gene therapy treatment. Until then, the treatment of this boy, and 10 other kids, was believed to be the first proof that gene-therapy could cure a life-threatening disease. However, rather than backing away from the field of gene therapy, experts are working on new strategies for gene delivery and seeking a deeper understanding of the risks involved.

The ethics of gene therapy in humans has been widely debated throughout all these years. There is still much to learn about how the human body works, and alteration of the genetic information in a patient may result in long-term side effects that are unpredictable at the present.

The ultimate goal of gene delivery research is the development of vectors that can be injected into the patient and target specific cells with the result of safe and efficient gene transfer that will cure the disease. This requires regulation in production of the gene product, preferably by the body's own signals. Furthermore, since the number of target cells is huge, the injection of a large number of vectors may be necessary, requiring cost-effective production of the gene vectors. So far gene therapy trials have been carried out on cells extracted from the patients and returning the gene-corrected cells into the patient. This procedure requires specialized techniques, is very expensive and requires scientific and medical expertise, thus being useful only in major medical centers and providing help only to a limited number of patients.

1.1.2 Barriers to gene delivery

Both the gene transfer to culture cells that are to be reimplanted into the patient and the administration of the gene via the intravenous route need to overcome several barriers for the gene therapy to be successful. As more is learned about how to package the injected DNA and to make tissue- and cell type specific delivery systems, the intravenous route would be the simplest and most desirable one. Such methods would be much more efficient and ensure treatment of a broad range of diseases and a large number of patients. The barriers discussed here therefore focus on those related to the intravenous route.

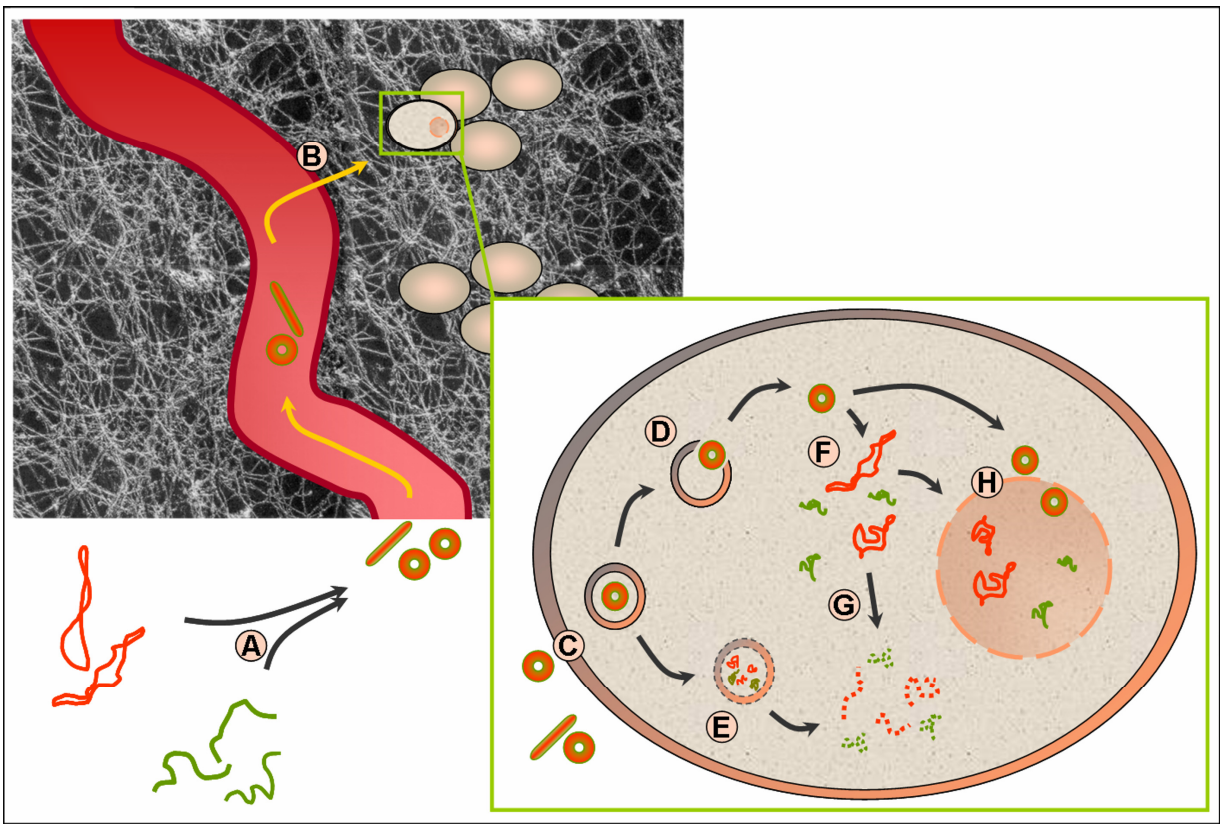

Figure 1: Schematic drawing of the DNA delivery pathways towards cells, illustrating the barriers related to transport from the blood vessels through the extracellular matrix, cellular uptake across the plasma membrane, intracellular release of DNA and nuclear targeting. The steps involved are: A. DNA complexation with a carrier; B. Transport across the capillary wall and through the extracellular matrix; C. Cellular uptake through endosomes; D. Endosomal escape; E. Degradation by lysosomes; F. Intracellular release of DNA; G. DNA degradation; H. Nuclear entry and expression.

Successful gene therapy consists of many steps, all requiring different expertise and approaches. Since improvement in the efficiency of each step is expected to yield an overall improvement of the delivery system, it is useful to consider the gene delivery as consecutive independent steps, which can be studied and improved separately. The main steps involved can be classified in the following way: administration of the gene to the body; delivery of the gene to the target cell and into the nucleus and expression of the therapeutic product (Figure 1).

An essential challenge of gene delivery is the fact that the DNA itself is highly negatively charged with a radius of gyration of several micrometers [9]. The distribution of a particle inside the body will depend on physical properties like the size, surface charge, interaction with serum proteins and interaction with the cell surface. It is therefore important to reduce the size of the DNA and mask the negative charges so that the molecule effectively can be transported towards the target cell.

The transport through extracellular matrix exposes the genetic material to nucleases, which have the potential of rapidly degrading DNA. To protect the DNA from being attacked by these enzymes, it needs to be packed into a compact form or be surrounded by a protective coat. A barrier related to cellular uptake is association of the delivery system to the cell surface for subsequent internalization. Similar to most macromolecules, cellular uptake of DNA occurs into membrane bound compartments by pinocytosis, adsorptive endocytosis, receptor-mediated endocytosis or phagocytosis [10]. The high negative charge of both DNA and the cell surface is believed to complicate the association of DNA to the surface [2, 10]. Development of a positively charged delivery system or conjugation of targeting ligands to the delivery system for the binding to cell surface receptors might therefore be favorable for cellular uptake. Following internalization, the delivery system needs to escape from the endosomes to prevent DNA from being transported to lysosomes where low pH and enzymes induce DNA degradation. After endosomal escape, DNA must be guided through the dense microfibril network within the cytosol to the nucleus. Similar to extracellular matrix, diffusion through cytosol is size-dependent with very large DNA molecules (~10^5 bp and ~10^3 bp, respectively) appearing to be immobile [11, 12]. For the DNA to be expressed, it needs to enter the nucleus. A majority of the delivery systems are identified to involve entry of DNA into the nucleus during cell division, requiring DNA to be stable until the next disassembly of the nuclear envelope [2]. Other strategies are therefore required for the nuclear entry of slowly dividing cells. Since structures with a diameter larger than ~10 nm are unable to passively diffuse through the nuclear pore complexes, methods involving targeting with nuclear localization sequences may be employed [2].

1.2 Gene delivery system, an approach towards non-viral vectors

Most research on gene therapy has focused on the use of recombinant viruses for the delivery of genes to the cells. The principle of viral gene delivery is that genes' viral functions may be replaced by genes encoding therapeutic functions which are transferred to defected cells by infection by these viruses. Approximately 75% of the recent clinical protocols involving gene therapy are based on virus-based vectors [13]. This is due to the high efficiencies, both with respect to delivery and expression, obtained with these vectors compared to other systems. However, safety concerns, limited DNA carrying capacity and difficult large-scale production have motivated the search for alternative delivery systems [2, 13]. The safety concerns are mainly related to the high immunogenicity developed after repeated administration, and

potential oncogenicity due to insertional mutagenesis upon incorporation of the viral genes into the genome [2, 13, 14].

Several methods have been proposed for the design of non-viral gene delivery systems. These involve artificial viruses that attempt to mimic the process of viral infection using synthetic materials, and DNA complexed with a carrier molecule like lipid, protein, peptide or another cationic polymer [15]. Non-viral systems show significantly lower safety risks than viral delivery systems and can be conjugated to cell targeting ligands to enable specific transport and uptake by the desired cells [2]. They are further capable of carrying large DNA molecules and can be produced in large quantities at low costs. However, transfection efficiencies are still low for these systems.

Non-viral delivery systems require the gene to be inserted into an appropriate expression vector such as a plasmid, which contains the gene of interest together with regulatory signals [4]. In addition to containing the therapeutic gene, the expression vector is typically composed of a promoter, specific sites necessary for correct processing of the transcribed RNA (splice site and polyadenylation site) and an enhancer. To overcome transport- and cellular barriers, and protect it from being attacked by nucleases, the plasmid DNA (pDNA) is mainly used in combination with a carrier. Although cationic polymers and cationic lipids are by far the most widely used carriers in non-viral gene delivery, other methods involving particle bombardment and the application of naked DNA also exist [2, 16].

1.2.1 Naked DNA and physical methods

Although possessing efficiencies that are far from those obtained when employing viral vectors, naked DNA is reported to yield surprisingly efficient gene transfer following injection to muscle and skin tissue *in vivo* [16]. No transfection is however observed *in vitro*, and the mechanism for cellular uptake of naked DNA is unknown. In most tissue the expression related to naked DNA administration is very brief, only in muscles is the expression observed to last for several months. Furthermore, naked DNA is unsuitable for targeting purposes and the poor transport properties make it a potential treatment only for local administration to tissues. Injection of naked DNA does not provoke specific immune response, but elicit immune stimulatory responses that make it useful for vaccine applications, but not for treating chronic diseases [16]. Naked DNA can also be injected directly into cells by microinjection, resulting in high transfection efficiency. However, only one cell at a time

can be injected, making it unsuitable when transfection of a large number of cells is required [4].

Two different devices have been developed to inject DNA into cells without the use of needles. One of them uses a high-pressure helium stream to deliver DNA-coated gold particles directly into the cytoplasm. This technique is referred to as the 'gene gun' and gives moderate transfection efficiency both *in vitro* and *in vivo* in skin [16]. The high frequency of immune responses observed makes gene-gun delivery an alternative to genetic vaccination. Compared to the injection into tissue, the gene-gun requires much smaller DNA doses [4]. The other device, called the Intraject or Jetgun, uses liquid under high pressure to deliver DNA into interstitial space and is reported to give stronger immune responses than needle injection [4].

DNA can also be transported directly across the cell membrane by means of an electric field. This method, electroporation, is believed to work by inducing areas of transient breakdown of the cell membrane, through which DNA can enter the cytoplasm. However, due to cell damage, the usefulness of this method has so far been limited [16].

1.2.2 Cationic lipids

In aqueous media cationic lipids are assembled into liposomes. Such cationic liposomes interact efficiently with the negatively charged DNA through electrostatic attractions, promoting the condensation of DNA into a more compact form [17-19]. Cationic liposomes-DNA complexes (lipoplexes) have been widely studied for both *in vitro* and *in vivo* gene delivery because of their safety, reduced immunogenicity, ease of preparation and potential packaging of significant amounts of DNA compared to viral vectors. It is suggested that DNA is sandwiched between many liposomal particles. Above a critical liposome concentration lipid fusion and DNA collapse are initiated, resulting in DNA being coated by a lipid bilayer [18]. Entrapment of DNA within this structure yields a lipoplex with a net positive charge that can interact with the negatively charged cell surface [17]. The cationic liposomes exhibit fusogenic properties that can induce fusion and/or destabilization of the plasma membrane, thus facilitating intracellular release [17]. Release of the encapsulated DNA into the cytoplasm is further facilitated by addition of neutral lipids into the liposome [19].

Several different cationic lipids have been synthesized to yield liposomes of low toxicity and high transfection efficiency. Different cationic lipids are known to exhibit different abilities to

mediate transfection, revealing that the structure of the cationic lipid is critical for its function as a gene carrier. However, no definite structure-activity relationship has clearly emerged so far [10, 17-19]. The main disadvantages of cationic liposomes have been their poor stability, heterogeneity, inactivation in blood by serum proteins, relatively low transfection efficiency and poor targeting properties [10, 16, 17, 19]. Improvements of the systems have, however, been done by using cationic polymers or peptides to compact DNA before mixing it with the lipid components, resulting in the formation of more compact lipoplexes of increased stability. It is believed that the reduced size will facilitate endocytosis and increase the circulation time *in vivo* [19]. The possibility of associating lipoplexes with targeting ligands has resulted in increased transfection in a large variety of cells, both dividing and non-dividing [17]. In addition to improvements of the cationic lipids used, cationic emulsions and micelles have recently been reported to represent significant improvements in both physical and biological activities, making them a promising alternative as a gene delivery system [10, 19].

1.2.3 Cationic polymers

Cationic polymers (polycations) interact with DNA through electrostatic interactions, causing DNA to condense into smaller structures. The compacted form of DNA protects it from degradation by nucleases [20-22] and is believed to make the transport through extracellular matrix easier due to the reduced physical size. Complexation of DNA with polycations yield positively charged complexes that interact efficiently with the negatively charged cell membrane, leading to internalization mainly through endocytosis [2, 19].

A wide range of polycations have been studied for their potential as gene carriers. The most widely studied polycations have been poly-L-lysine (PLL) [20, 21, 23-25] and poly(ethylenimine) (PEI) [24, 26-28], but also other cationic agents such as spermidine [29-32] and cobolthexamine [31, 33, 34], and polycations prepared by combinatorial chemistry [35-37] have been studied. PLL was one of the first polymers used for gene delivery [2, 10]. Although PLL is biodegradable, it exhibits modest to high toxicity [2]. Cellular uptake of DNA-PLL complexes is found to be efficient, but the transfection efficiency remains low when using PLL as a carrier. It has been suggested that this is due to the complexes not being able to escape the endocytotic pathway [2]. Studies have shown that DNA-PLL complexes aggregate at physiological conditions. Introducing polyethylene glycol (PEG) into the PLL chains has reduced both the cytotoxicity and aggregation of DNA-PLL complexes [38].

PEI has been reported to mediate both efficient cellular uptake of DNA-PEI complexes and high transfection efficiency. It is, in fact, considered to be the most efficient polymeric delivery system, providing efficiencies equal to or better than those based on cationic lipids [27, 28]. The ability of the DNA-PEI complexes to be released from the endosomes by the 'proton sponge' effect is believed to be a crucial factor for their high transfection efficiency. The 'proton sponge' is explained by the ability of PEI to buffer over a wide pH range causing an increased proton influx into the endosomes, compared to the non-buffering situation, leading to osmotic swelling of the endosomes and subsequently collapse of the membrane and release of the DNA-PEI complexes [27]. However, although PEI exhibit high transfection efficiencies, toxicity is rather high. The toxicity is reported to be reduced when using linear PEI of reduced molecular weight, or when using branched PEIs [2]. The ability of linear PEI to mediate cell cycle independent nuclear entry of DNA is important in the therapy of slowly dividing cells [2]. Similar to DNA-PLL complexes, aggregation of DNA-PEI complexes can be reduced by linking the PEI chains to PEG [38].

Although the properties of the polycation are reported to be important for its ability to mediate successful transfection, the exact relation between polycation properties and its transfection activity is still not known. Factors affecting the size, charge and stability of the DNA-polycation complexes are important for their ability to transfect cells. Since polycations display the possibility of being specifically tailored to optimize their gene carrying properties by altering the structural and chemical properties, they are good candidates for the design of efficient gene delivery systems. Furthermore, by conjugating the polycations to targeting ligands site-specific gene delivery through receptor mediated endocytosis can be obtained.

1.2.4 The use of chitosan as a potential system for gene delivery

The linear copolymer chitosan has emerged as an interesting polymeric gene carrier due to its non-toxic and biodegradable nature [22, 39, 40]. Chitosan is a partly or completely de-N-acetylated derivative of the naturally occurring polysaccharide chitin, which is one of the most abundant natural polysaccharides, primarily obtained from crustacean [41]. The molecular structure of chitosan consists of different compositions of (1→4)-β-linked N-acetyl-D-glucosamine and D-glucosamine residues (Figure 2), distributed randomly within the polymer [42]. The fraction of these residues in a chitosan sample is commonly described by the fraction of acetylated units, F_A.

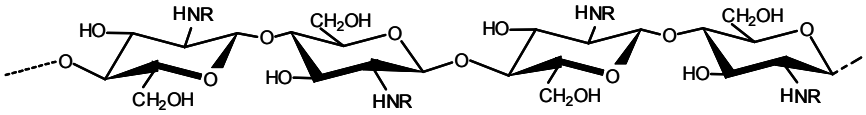

Figure 2: The chemical structure of chitosan, consisting of various compositions of acetylated (R = $COCH_3$) and de-acetylated (R = H) units.

Independent of F_A, the intrinsic pK_a value of the amino groups in the deacetylated units have been determined to be ~6.5 [43, 44], giving rise to the polycationic behavior of chitosan in neutral or acidic solutions. The effective charge density of chitosan can thus be controlled through the preparation of samples with different F_A, as well as by controlling the pH of the solutions. The pH will also affect the solubility of chitosans with $F_A < 0.6$ with increasing pH yielding decreased solubility [45].

The use of chitosan for gene delivery was first described by Mumper *et al* in 1995 [46]. Since then, several studies have explored the ability of chitosan to mediate gene transfer. Chitosan is reported to efficiently compact DNA and provide protection of DNA against degradation by nucleases [22, 40, 47]. The use of chitosan as a carrier has recently been reported to mediate high transfection efficiencies, comparable to that of PEI [47, 48], with lower toxicity towards cells than both PEI and PLL [40, 47, 49]. Several studies have reported that both F_A and chitosan chain length affect its ability to mediate high transfection efficiency [47, 50-52]. A F_A less than 0.35 has been suggested to be required to obtain complexes capable of transfecting cells *in vitro* [47]. Although chitosan is considered to be a non-toxic polymer, a dose dependent toxic response has been reported for high molecular weight chitosans [47, 49]. Reducing the chitosan chain length has been found to reduce the cytotoxicity [22, 49]. Chitosan chain length is also believed to affect the stability of the DNA-chitosan complexes, which is important as the complexes must withstand the transport towards the target while being able to release DNA intracellularly. Dissociation of the DNA-chitosan complexes is believed to be one of the critical rate-limiting steps for the transfection [47, 53]. Increased *in vitro* transfection has been reported upon reducing the chitosan chain length [51, 54]. This was suggested to be due to reduced stability of the complexes upon reducing the chain length, resulting in DNA being released from the complex more easily. Furthermore, the supercoiled form of pDNA was reported to be retained upon release from these complexes [54].

Cellular uptake of DNA-chitosan complexes is reported to take place through endocytosis [48, 52, 55]. Although endosomal escape is proposed to be a limiting step for the transfection [47], nuclear accumulation of the delivery vector has been detected following uptake of the

complexes [55], indicating that DNA (either free or complexed with chitosan) is able to escape the endosomes. Different mechanisms for the endosomal escape are proposed. Some suggest that the endosomal escape is due to endosomal buffering of the DNA-chitosan complexes, consistent with the 'proton sponge' hypothesis proposed by Boussif *et al* for the PEI-DNA delivery system [27], whereas other suggest that polymer degradation, causing increased osmolarity and lysosomal rupture, is crucial [47]. Studies comparing the transfection mediated by chitosan and PEI, respectively, have revealed differences in the kinetics of the gene expression. Chitosan mediated expression was found to reach its maximum levels significantly later than the PEI mediated expression [47, 54]. This was suggested to be due to different ability of these two polycations to mediate endosomal escape. Previous studies have also revealed that the chitosan system is less sensitive to the presence of serum than both the PEI system [48] and cationic liposomes [56].

The primary amine of chitosan has been used to chemically modify the chitosan structure in order to further improve the transfection efficiency. Conjugation of targeting ligands to these primary amines, giving a branched chitosan structure, has been reported to yield increased transfection efficiency [57-61]. Similar results were reported when using trimethylated chitosans, containing quaternary amines, the charge of which does not depend on pH [62]. The increased transfection compared to that obtained when using unmodified chitosan oligomers was suggested to be due to the increased interaction strength following increased charge and the increased solubility in neutral solutions [62].

1.3 Polycation-induced DNA condensation

The condensation of DNA is an important feature making it possible for the extended genes to fit into the cell nucleus. In the cell nucleus this condensation is provided by interactions with positively charged histone particles, resulting in DNA being wrapped around the histones to form nucleosomes.

Using polycations as the basis for DNA delivery systems has lately become a popular route for gene delivery as they provide an efficient way to condense the extended genes into smaller structures and at the same time mask the negative charges of DNA. However, to exploit the potential of polycations as gene carriers, suitable polymer structures need to be identified. This requires more knowledge about the mechanisms involved in the DNA-polycation complex formation, and how both molecular and solution parameters affect the formation and

stability of the complexes. Several details about the DNA-polycation complexation process still need to be resolved before a clear relationship between polycation molecular parameters and biological activity can be established.

To understand the condensation behavior of DNA upon mixing with oppositely charged multivalent ions, the polyelectrolyte properties of DNA must be considered. The structure and properties of DNA are therefore briefly described below to yield a basis for the discussion of polyelectrolyte complex (polyplex) formation. The polyelectrolyte properties are not restricted to DNA, but is a general description applying to charged polymers. The discussion of DNA-polycation complex formation thus involves treating DNA as a general polyelectrolyte with a certain chain stiffness and ionic properties. By studying other polymers, both polyanions and polycations, with different characteristics, the effect of various parameters on the complex formation can be better understood.

1.3.1 DNA structure

The importance of DNA as the basis of all living organisms (being responsible for storage, duplication and realization of the genetic information) has made it a widely studied polymer within many areas for more than fifty years [63-65]. Despite the large diversities of living creatures, carrying different genetic information, the physical shape of DNA is the same. The basic building blocks of DNA are nucleotides, each consisting of a sugar, a phosphate and a base. The 2-D arrangement of DNA involves a backbone of alternating sugars and phosphates in which the third carbon of one sugar ring is linked via a phosphate to the fifth carbon on the next sugar (Figure 3). Each sugar ring is attached to one of the four different bases adenine (A), cytosine (C), guanine (G) and thymine (T) that are responsible for coding the genetic information. The 3-D structure of DNA was discovered in 1953 by Watson and Crick [66]. Using the X-ray fiber diffraction patterns obtained by Franklin and Wilkins the structure of DNA as a double helix was elucidated. The bases from the two nucleotide strands are paired by complementary hydrogen bonding in the helix interior with phosphate-sugar backbones extending along the outside, thus minimizing electrostatic repulsions. Base pairing (the complementary principle) is very important and involves that in the double helix A always opposes T whereas G always opposes C (Figure 3). This complementary principle enables the two chains to unzip and serve as a template for the formation of another complementary chain, thus passing the genetic information on to the next generation of cells. The two strands

are antiparallel with base stacking playing an important role in stabilizing the helical structure of DNA.

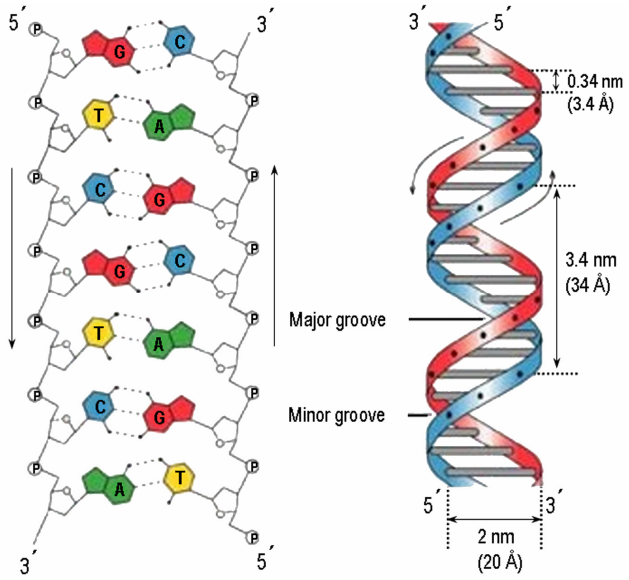

Figure 3: The DNA structure illustrated both by the 2-D structure (left), showing how two complementary strands are linked through hydrogen bonds between the bases, and the 3-D double helical structure (right) (http:/www.blc.arizona.edu/marty/411/modules/helix.html).

At physiological conditions DNA adopts the B-form in which the double helix is right-handed with ten base pairs (bp) per turn and with a diameter of 2 nm (Figure 3). The surface of the double helix has two distinct grooves, the major- and minor groove, which are important for the DNA function (e.g. specific binding of proteins). In this B-form configuration the bases are planar, perpendicular to the axis of the double helix, and spaced by 0.34 nm along the helix. The double helical structure makes the DNA molecule rather stiff with a persistence length (L_p) close to 50 nm, leading to very small excluded volume effects. This high stiffness is due to the fact that the molecule consists of two, rather than one, polymer chains and that rotation around single bonds is highly constrained for the double helical structure. The bending flexibility is only due to accumulation of small changes of angles between adjacent base pairs, making the DNA molecule best modeled as an elastic rod. For comparison the intrinsic L_p of single stranded DNA is ~1 nm [67].

DNA in living organisms appears as either linear or circular. In eucaryotes it has the linear form and is highly complexed with proteins (in particular histones), whereas in prokaryotes it is found to be covalently closed into a circular form, referred to as a plasmid [68]. Some virus particles contain linear DNA or DNA molecules that can interconvert between linear and circular forms, with the linear form being present inside the virus particle and the circular form in the host cell [69]. The double helix can be further coiled on itself to form a superhelix, or a supercoiled structure, yielding a more compact shape than its non-supercoiled counterpart [69].

1.3.2 Polyelectrolyte properties of DNA

DNA is a highly charged polyanion, with one negative charge per phosphate, giving rise to strong repulsion between the phosphate backbones. This high negative charge causes DNA to interact strongly with ions, particularly cations, in its environment. The polyelectrolyte behavior of DNA is important for the binding of charged ligands (proteins and drugs) and its condensation and packaging, being a result of interactions where Coulomb forces are important. The major tools for theoretical treatment of the DNA polyelectrolyte properties are the Poisson-Boltzmann (PB) equation and the counterion condensation theory.

1.3.2.1 The Poisson-Boltzmann equation

Analysis of the ionic properties of solutions often starts from the mean-field Poisson-Boltzmann (PB) theory, in which local fluctuations in the electrostatic potential are ignored [63, 70]. Instead, the potential is considered as time averaged, $\langle V(\mathbf{r})\rangle$, so that the local ion concentration (giving rise to the local charge density) can be expressed as a Boltzmann distribution. Inserting this distribution into the Poisson equation, which determines the local electrostatic field from the local charge density function, gives the mean-field PB equation:

$$\nabla^2 \langle V(\mathbf{r})\rangle = -\frac{e}{\varepsilon}\sum_i z_i n_i^{(0)} \exp\left[-\frac{z_i e \langle V(\mathbf{r})\rangle}{kT}\right] \tag{1.1}$$

where the sum goes over all ionic species, e is the elementary charge, ε the dielectric constant of the solution, k is the Boltzmann constant, T is the absolute temperature, and z_i and $n_i^{(0)}$ are the valence and bulk concentration, respectively of the ith species. At weak potentials, $\langle V(\mathbf{r})\rangle << kT / z_i e$, and requiring electroneutrality, the PB equation (1.1) can be linearized:

$$\nabla^2 \langle V(\mathbf{r})\rangle = \frac{e^2 \sum_i z_i^2 n_i^{(0)}}{\varepsilon kT} \langle V(\mathbf{r})\rangle = \kappa^2 \langle V(\mathbf{r})\rangle \tag{1.2}$$

This linearized PB equation is also referred to as the Debye-Hückel equation where $\kappa^{-1} = \left(\frac{\varepsilon kT}{e^2 \sum_i z_i^2 n_i^{(0)}}\right)^{-1/2}$ defines the Debye screening length. Such a linearization is valid

provided the potential is not too strong anywhere in the solution, which is often the case if the charges involved are small enough.

Considering a point-like charge surrounded by other point charges (counterions), the Debye screening length yields a measure of the range of the potential around the charge when screened by the counterions. Introducing the ionic strength I

$$I = \frac{1}{2}\sum z_i^2 n_i^{(0)} \tag{1.3}$$

κ^{-1} can be expressed as:

$$\kappa^{-1} = \left(\frac{\varepsilon kT}{2e^2 I} \right)^{-1/2} \tag{1.4}$$

At large distances these mobile counterions thus give rise to an exponentially decaying electrostatic potential.

1.3.2.2 Counterion condensation

Highly charged polyelectrolytes in solution will attract counterions from its surroundings and cause these to condense onto the polyelectrolyte, resulting in an apparent reduction in the polyelectrolyte charge [63, 70]. The counterion condensation can be understood as a competition between the energy gain associated with electrostatic interaction and the loss of entropy upon binding, attempting to minimize the free energy of the polyelectrolytes in solution.

The important parameter in determining whether counterions will condense onto the polyion is the charge density parameter, ξ:

$$\xi = \frac{e^2}{4\pi\varepsilon kTb} = \frac{b_j}{b} \tag{1.5}$$

Where b is the linear charge spacing and b_j ($= e^2 / 4\pi\varepsilon kT$) is the Bjerrum length, defined as the distance at which the Coulomb interaction between two fundamental charges equals the thermal energy. In aqueous solutions at room temperature b_j is equal to 0.71 nm. Counterion condensation is reported to be thermodynamically favorable if the charge density of the polyion exceeds a critical value where b becomes smaller than b_j, meaning that $\xi > 1/z$.

Assuming θ_z counterions of valence z being condensed per polyion charge, such counterion condensation cause the polyion charge to be reduced by a factor $r = z\theta_z = 1 - 1/z\xi$.

The condensed counterions are considered to be confined to a volume close to the rod, but are free to move along its backbone within this volume (territorially bound). The counterions that are not confined to this volume are considered to be free in the solution. For the counterion condensation theory to apply, the real polyelectrolyte chain must be replaced by a continuous line charge that can be treated as a straight line of infinite length. Interactions between polyions must further be neglected. The straight line approximation requires that $\kappa^{-1} < L_p$. Considering DNA with $L_p \sim 50$ nm, this is valid for ionic strengths larger than 37 mM. The requirement of infinite length is considered to be fulfilled when the polyion is much longer than κ^{-1}. Thus, the theory will break down at very low salt concentrations or for very short oligomers.

1.3.2.3 Charge correlations

Applying the mean-field PB-theory to calculate the forces between two surfaces of same charge, yields a repulsion of the surfaces. Further, the equilibrium spacing between condensed DNA helices has been reported to be too large for cross-linking by small multivalent ions to be responsible for driving the compaction [71]. The importance of counterion correlations has been investigated in order to explain the attraction between like-charged polyions [72, 73]. In a system with a highly charged macroion surrounded by counterions with a valence, z, larger than 1, the counterions will become strongly coupled, making the mean-field approximation inapplicable [73]. These correlations are due to strong interactions both between the counterions and between the macroion and the counterions, being important close to the macroion surface.

Correlations between multivalent counterions close to a highly charged macroion surface may form spontaneous overcharging of the surface. Thus, instead of charge reduction of the macroion charge due to shielding, multivalent counterions will adsorb on the macroion in amounts that might exceed the neutralization requirement, causing a charge inversion of the macroion [74]. Since correlation of monovalent ions is negligible, they will not induce charge inversion of a macroion. Their only role will be to screen the electrostatic potential around other polyions, thus acting to increase the charge inversion of a macroion by multivalent counterions [73]. This is explained by a decreased repulsion between the counterions due to

the screening by monovalent ions, making it possible for these to be packed closer together on the macroion surface.

1.3.3 DNA-polycation complex formation

Mixing DNA with oppositely charged multivalent ions leads to complex formation and, if DNA is sufficiently neutralized, a spontaneous collapse of the extended DNA molecules into compacted structures. The cation-induced condensation has been reported to be a two stage process in which cation binding and DNA condensation has been identified as two separate events [75]. Packing DNA into such compacted structures involves overcoming the coulombic barrier related to the negatively charged phosphates on the DNA. Other energetic barriers arise from the bending of the stiff double helix and the loss in configurational entropy when organizing the extended DNA molecule into well-defined structures. The binding of a multivalent cation to DNA is an exchange reaction where counterions are released both from the DNA and the multivalent cation, causing an increase in the overall entropy [75, 76]. Electrostatic interactions, accompanied by entropy gain upon counterion release, are thus driving the complex formation (Figure 4).

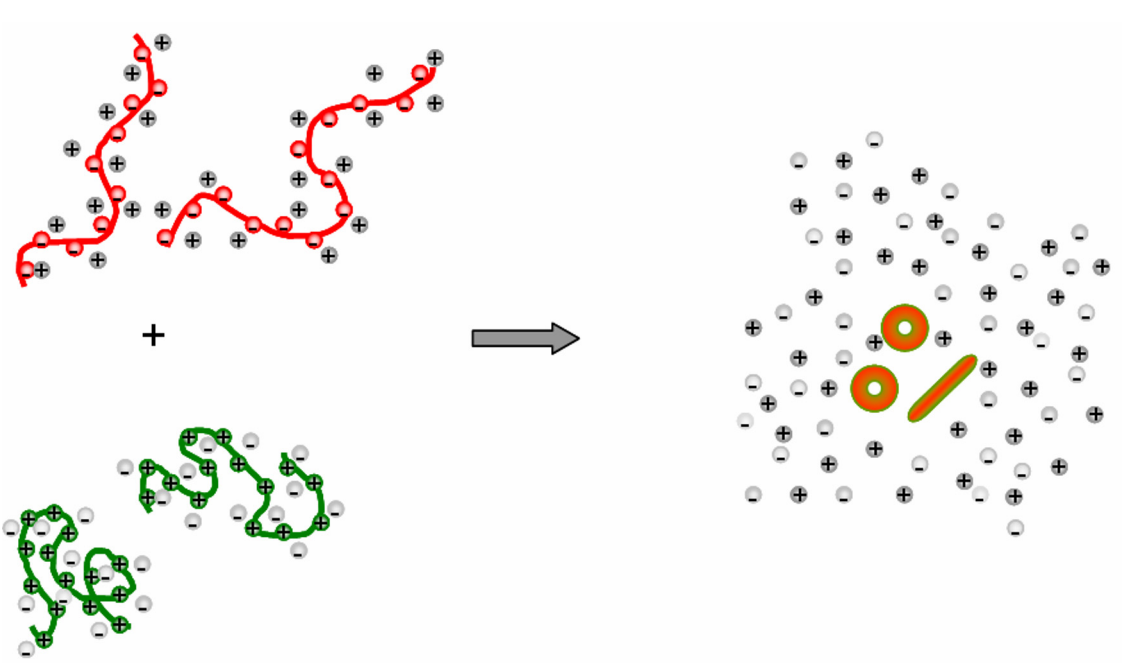

Figure 4: Polyelectrolyte complexation driven by the electrostatic interaction between DNA (red) and multivalent cations (green) with a concomitant release of counterions, yielding an increase in the overall entropy and the formation of compacted structures.

In general terms, DNA condensation is defined as a decrease in the volume occupied by DNA upon transition from the extended chain to a compacted state in which the volume fractions of

DNA and solvent are comparable. Since more than one DNA molecule is often involved in the condensed structure, condensation can be difficult to distinguish from aggregation or precipitation. The term condensation is thus generally confined to situations in which the aggregate is of finite size and ordered morphology [76] and commonly requires low polymer concentrations.

DNA condensation is provoked either by decreasing the repulsion between DNA segments, or by making the DNA-solvent interactions less favorable. Manning proposed a model for cation-induced DNA condensation in which the DNA helix will bend when its negative charges are sufficiently neutralized [77]. However, this is not a widely accepted driving force for the DNA condensation process, which is alternatively suggested to arise from lateral interaction between adjacent helices. Using Manning's counterion condensation theory, Wilson and Bloomfield showed that 90% of the DNA charge must be neutralized to overcome the electrostatic repulsion within the DNA molecule so that condensation can occur [30]. In aqueous solutions a valence of 3 or more is required to obtain 90% neutralization of the DNA phosphate charge, and thus to be able to induce a collapse transition of DNA [30]. In addition to electrostatic forces, correlated counterion fluctuations and hydration forces are important in explaining the overall attractive force stabilizing the condensed structure. Rouzina and Bloomfield developed an attraction theory in which the surface adsorbed counterions make up a two-dimensional lattice on the DNA surface [72, 76]. Since the binding to DNA is delocalized, the counterions are mobile [78]. When two DNA molecules with surface lattices approach each other closely, the lattices adjust in a complementary fashion so that the positive charges will position themselves opposite the negative charges, leading to a net attraction. The magnitude of this attraction is determined by the surface charge density and the solution dielectric constant. In aqueous solution this attraction is calculated to be stable with respect to disruptive thermal motions of the ions when the counterions have a valence of +3 or more [76]. The hydration forces have been suggested to be due to reconfiguration of the surface-bound water upon DNA condensation, being either repulsive or attractive [76, 79]. Whereas the repulsive component has been explained by polarization of water by polar groups on the DNA surface, attraction is believed to be driven by entropy increase upon rearrangement or release of water, or water bridging between two DNA helices. However, although identified as important for the behavior of biological systems, the exact origin of these hydration forces is still not known and it is believed that water structure effects are not sufficient for the understanding of these forces [80].

The condensation of DNA by multivalent cations is known to depend on both solution properties and details of the multivalent cation. Increasing the valence of the multivalent cation is reported to yield stronger binding to DNA [81, 82], with a concomitant increase in the extent of counterions released, thus being important for the compaction of DNA. The structure of the multivalent cation is reported to affect the morphology of the resulting condensates, with small modifications in the cationic structure altering the condensates [31, 83]. Also the ionic strength will affect the interaction strength between DNA and multivalent cations as the presence of salt will decrease the Debye screening length and make the entropy gain upon release of counterions smaller than in the absence of salt. The electrostatic interaction is thus reduced when increasing the ionic strength [75, 82].

Condensation of DNA by multivalent cations in dilute solutions typically yields the formation of toroidal and rod-like structures, with the condensation behavior depending on the properties of both the solution and the multivalent cation used. A lower limit of ~150 bp has been suggested for the DNA to be able to collapse into discrete particles of well-defined morphology, whereas a minimum length of approximately 400 bp has been proposed as a requirement for the formation of a toroidal morphology [33, 79]. It is further suggested that above a certain maximum length, DNA will be condensed into spherical globules rather than toroids. The dimensions of the toroidal and rod-like structures, determined in terms of thickness and contour length, have been reported to be similar, with neither one appearing to be a precursor of the other [76]. The formation of torus-shaped particles has received special attention as it is considered to reflect a balance between the energy penalty associated with the bending of a relatively stiff chain, and the attractive collapsing force [84]. Different models for the toroid formation have been suggested. Hud and colleagues proposed a kinetic model based on the probability of DNA forming loops [85]. Due to random thermal motions, a loop, in which two segments are juxtaposed and stabilized, is formed. Successive loops, precessing about the central axis of the toroid, are then formed and stabilized by the condensing agent, comprising the toroid. The dimension of the resulting toroid will be determined by the size of the first loop, which again will be determined by the DNA chain stiffness. In this model, all parts of the toroid will be bent with the same radius of curvature. It is therefore referred to as the constant radius of curvature model [85], in which the toroid develops through a nucleation and growth pathway. Another model, called the spool model, has suggested that DNA is wrapped circumferently in a continuous unidirectionaly fashion to form a toroid [86]. This was based on the observation of individual DNA strands from electron microscopy

photographs. In this spool-like model the radius of curvature would differ for the various DNA segments, requiring that DNA near the center of the toroid is subject to higher stress than DNA further out from the centre. Both real-time studies and theoretical simulations of the DNA condensation have indicated that the transition from the elongated coil state to the compacted form follows a nucleation-growth pathway [87-89]. The formation of a nucleation center is thus crucial for the development of a compacted structure. Since the first loop will determine the size of the toroid formed, this suggests a mechanism by which the size of the toroid can be controlled. Introduction of a static loop into the DNA has been shown to provide a site for toroid nucleation that will be favored over random polymer fluctuation and thus control the dimensions of the toroid [90]. The presence of A-tracts in the DNA molecule will induce bending of the DNA helix and has been found to induce the formation of toroids with a smaller diameter than what would be expected from the chain stiffness of DNA [90, 91]. Whereas the diameter of the toroids formed from a random DNA sequence has been reported to be ~65 nm [79], the presence of A-tracts in the DNA has been reported to induce the formation of toroids with a diameter of ~25 nm [91]. This further allowed DNA molecules shorter than the suggested critical length to form toroidal structures [91]. The packing of DNA within the toroidal condensates has been reported to result in a hexagonal ordering of the DNA strands with an interhelical spacing of 2.5-3.8 nm, depending on the polycation [92, 93]. Regions with non-hexagonal packing have also been identified and suggested to be due to crossover regions [94], consistent with the model proposed by Park *et al* [95].

2 Aim of the thesis

Attempts to develop efficient chitosan based systems for gene delivery require more knowledge about the DNA-chitosan complexation process, and how chitosan properties and solution parameters affect the structure and stability of the resulting complexes. Identification of the effect of these parameters is important when tuning the size, charge, morphology and stability of the complexes to optimize their gene delivery properties.

In this study the effect of chitosan molecular properties, such as F_A and DP, on its ability to compact DNA was investigated. Furthermore, since polyplex stability has been reported to be an important parameter to control, both for the transport and the subsequent release of the gene vector, the stability of the DNA-chitosan complexes was studied upon exposure to competing polyanions. The chitosan chain length has been of special interest for controlling this stability, and was further investigated here. To obtain a better understanding of the effect of polymer properties on the complexation process, the polyanion-polycation complexation was further evaluated by employing other polymers with varying chain stiffness and charge densities.

The structure and stability of the polyplexes were characterized by tapping mode atomic force microscopy (TM-AFM) and force spectroscopy. To obtain quantitative information about the morphology and dimensions of the structures, the AFM topographs were subject to image analysis as detailed in appendix A.1. Complexation and polyplex stability was also studied by employing an EtBr fluorescence assay, involving EtBr labeling of DNA followed by recording of the changes in fluorescence intensity upon DNA condensation and polyplex dissociation.

3 Summary of the papers

3.1 Paper I

The effect of chitosan molecular parameters like chain length and charge density (proportional to (1-F_A)) on its ability to compact DNA was studied by AFM imaging. Since DNA-chitosan complexes are being studied for their potential as a gene delivery system, the complexation in this study was performed at physiological-like conditions (pH 7.4 and ionic strength of 150 mM). High molecular weight chitosans were found to compact DNA into toroidal, rod-like and globular structures with the relative abundance depending on F_A. Increasing the F_A was found to yield a decrease in the toroid-to-rod ratio, indicating that the toroid is dominating the polyplex population for high intersegment interactions. In contrast to the relative abundance, the dimensions of the structures did not depend on the F_A, and was comparable for the toroidal and rod-like structures. The use of larger chitosan concentrations for complex formation resulted in flower-like and racquet-like structures, identified as intermediate states. The same toroidal and rod-like structures were observed when low molecular weight chitosans were used to compact DNA. However, to compensate for the reduced interaction strength following the reduction in chitosan chain length, larger concentrations of chitosan were required to obtain these structures.

3.2 Paper II

Polyplex stability is identified as an important property to control when designing efficient polycation based gene delivery systems. Reduction of the chitosan chain length (F_A = 0) for the optimalization of the chitosan based delivery system has led to the development of chitosan oligomers with well defined chain lengths which are reported to mediate high transfection efficiencies. In this study the ability of these chitosan oligomers to compact DNA, as compared to that of HDP chitosans, was studied by AFM imaging. Furthermore, the effect of chitosan chain length on the stability of the DNA-chitosan complexes was studied by exposing the polyplexes to the biological polyanions heparin and hyaluronic acid (HA). The degree of polyplex dissociation obtained upon exposure to these polyanions was measured by AFM imaging and an EtBr fluorescence assay, yielding recovery of the fluorescence signal upon release of DNA from the polyplexes. Both polycation and polyanion properties were

found to be important for the stability of the polyplexes, with increased chitosan chain length and concentration providing polyplexes that were more resistant towards dissociation. Of the two polyanions employed here, only heparin was able to cause dissociation of the polyplexes, with larger heparin concentrations being required for the dissociation of the more stable polyplexes. The chitosan chain length was also found to affect the morphology of the DNA-chitosan complexes to some extent. Hardly any toroidal structures were observed when compacting DNA with the shortest chitosans, while these structures made up a considerable fraction of the structures when long chitosans were used for the compaction.

3.3 Paper III

The effect of polyanion chain stiffness and intersegment attraction on the morphology of polyelectrolyte complexes was investigated by studying the polyanion-polycation complexation for various polyanions and polycations. Most experimental studies describing such complexation have so far focused on DNA. However, theoretical studies have implied that DNA is part of a more general picture. In this study the compaction of DNA by the polycation chitosan was compared to the compaction of the polyanions xanthan, acetan and alginate by the same polycation. These polyanions were chosen because they have persistence lengths higher and lower than that of DNA. From AFM imaging it was found that the polyplex morphologies depend on the chain stiffness of the polyanion, with toroidal structures appearing for persistence lengths of ~25 nm and larger. Whereas rod-like structures were formed for the intermediate chain stiffness, complexation of the stiffest polyanion xanthan with chitosan resulted in the formation of other types of structures, identified as intermediate states similar to those observed from Brownian dynamics. It was further found that a minimum xanthan chain length was required for the formation of toroidal structure, similar to what is reported for DNA. Comparing the dimensions of the toroidal structures resulting from compacting DNA and xanthan, respectively, showed that the toroids formed from DNA were shorter and thicker than those formed from xanthan. Xanthan and acetan were additionally compacted with PLL. PLL was found to yield looser complexes than chitosan, emphasizing that the molecular details of the polycation is important for the polyanion-polycation complex formation.

3.4 Paper IV

DNA compaction by the two polycations chitosan and PLL, respectively, were compared by employing the two techniques AFM imaging and EtBr fluorescence. Both techniques showed that the compaction behavior of DNA depended on the polycation properties. The presence of an additional polyanion (xanthan or alginate) in the solution was found to compete with DNA for polycation binding, resulting in a less efficient compaction of DNA. This was seen as a less efficient reduction in the DNA-EtBr fluorescence assay upon addition of polycation. Although the competing polyanions had different equivalent mass per unit charge, the degree to which DNA compaction was inhibited by the presence of these polyions was found to depend only on the DNA to polyanion charge ratio, indicating an electrostatically driven interaction. The stability of the DNA-polycation complexes when exposed to the competing polyanions was studied by recording the EtBr-DNA fluorescence recovery upon addition of the polyanions. Both polyanions were found to be able to dissociate the polyplexes. However, whereas xanthan did not discriminate between the polyplexes prepared from the two different polycations, alginate was more efficient in dissociating the DNA-PLL complexes compared to the DNA-chitosan complexes. The stability of the pDNA-chitosan complexes was found to increase when incubating the polyplexes at increased temperature. Such temperature treatment was also found to affect the morphology of the polyplexes, revealing that for this particular system the short rods are more energetically favorable than the toroid.

3.5 Paper V

The interaction between chitosan and a negatively charged solid surface (mica or AFM tip) was studied by employing AFM-based force spectroscopy. Varying both chitosan molecular parameters (F_A) and solution parameters (pH and ionic strength, I) showed that these parameters are important for the interaction strength, being strongest for low pH, low I, and low F_A as expected from electrostatic considerations. The solution parameters were also found to affect the shape of the force spectra, presumably reflecting the adsorption characteristics of chitosan onto mica at these conditions. Since chitosan conformation probably is of importance for its interaction with DNA, which is of electrostatic nature, the chitosan-surface interaction is believed to act as a model system for the DNA-chitosan interaction.

4 General discussion

Chitosan-mediated condensation of DNA vectors has emerged as a promising gene delivery system as it is reported to yield high transfection efficiency [40, 47, 48, 50, 51, 53-55]. Successful transfection requires overcoming the many barriers related to transport from blood vessels and through extracellular matrix, cellular uptake and transport through the cell cytosol towards the nucleus. Understanding the factors important for complexation, polyplex stability and transport properties is thus essential for the optimization of the delivery system. To understand why chitosan appear to be a promising candidate for gene delivery, the effect of both molecular parameters and solution parameters on the size, shape and stability of the resulting polyplexes needs to be evaluated. Transfection studies have shown that molecular parameters like the chitosan F_A and DP, as well as pH of the solution are important for the ability of DNA-chitosan complexes to transfect cells [47, 50, 51, 54, 56]. The influence of these parameters on the chitosan mediated DNA condensation was therefore investigated in this study.

The ability of a wide range of polycations to compact DNA and transfect cells has been investigated. Alongside the experimental studies, theories for a molecular understanding of the condensation behavior have been proposed. To understand the complexation behavior of DNA by chitosan, DNA was regarded as a part of a general picture where factors like chain stiffness and intersegment attraction were considered. By studying other polymers, both polyanions and polycations, with different characteristics, the effect of various parameters on the complex formation was investigated.

4.1 Structure and stability of DNA-chitosan complexes

The ability of chitosan to compact DNA into well-defined structures was found to depend on several factors, involving both molecular parameters (DP and F_A) and solution parameters (I and pH), as well as the temperature after complexation. In this section the compaction of DNA by various chitosans at different conditions is discussed. The DNA-chitosan compaction is further compared to other systems, placing it in a more generalized picture where electrostatic interactions are the main driving force.

4.1.1 Effect of chitosan molecular parameters on its ability to compact DNA

DNA condensation studies involving several different polycations have shown that the details of the compaction depend on the polycation [31, 35, 96, 97]. Varying the chitosan molecular parameters, like the degree of polymerization (DP) and degree of acetylation (F_A), was thus expected to affect the condensation behavior of DNA mediated by the interaction with chitosan. Although several studies have reported that chitosan efficiently compacts DNA [48, 53], only a limited set of chitosan molecular parameters have been explored for its ability to induce DNA condensation. By employing AFM imaging, it was here demonstrated that chitosan condense DNA (plasmid and linear DNA of ~4.4 kbp and ~2 kbp, respectively) into toroidal, rodlike and globular structures with the dominating topologies of the polyplexes depending on both the F_A and the DP of the chitosan (paper I and II). All chitosans were found to compact pDNA (~4.4 kbp) into structures with approximately a ten-fold reduction in the contour length and a ten-fold increase in the height compared to uncomplexed DNA (paper I). This implies that multiple DNA molecules not necessarily are involved in the DNA condensates, as previously suggested for DNA molecules shorter than 40 kbp [79]. The height analysis of the complexes further revealed considerable height variations within the complexes, indicating the coexistence of several packing modes within the complexes (paper I). Increasing the F_A of high DP (HDP, DP~1000) chitosans resulted in a decrease in the toroid to rod ratio, implying that the chitosan charge is important in determining the shape of the DNA-chitosan complexes (paper I). Since the main driving force of the DNA-chitosan interactions is of electrostatic origin, higher chitosan charge density is expected to mediate increased intersegment interactions. The type of structures formed thus appears to depend on the strength of the intersegment interaction with the toroid being the preferred structure for high intersegment attractions. The slightly higher pull-off forces observed for higher charged chitosans when pulling on chitosan physiosorbed onto mica supports the suggestion of increased intersegment attraction upon increasing the chitosan charge (paper V).

Transfection studies have shown that the most efficient DNA-chitosan delivery systems were obtained when reducing the chitosan F_A [47, 50]. An important aspect in polycation mediated gene delivery is, however, the high cytotoxicity related to the use of polycations with high valence. Further is the high stability of polyplexes resulting from highly charged polycations believed to be a limitation for the subsequent intracellular release of DNA [53, 98]. This is based on the increased interaction strength expected when increasing the valence of a multivalent ion that interacts with an oppositely charged polyion [81, 82, 99]. The polycation

valence is reported to be important for the efficiency of the polyplexes to transfect cells [51, 100]. Changing the chitosan DP provides a tool for changing the valence of the molecules without altering the F_A. Reduction in the chitosan chain length is reported to yield increased transfection efficiency [51] with chitosan oligomers having a DP of 15-21 (F_A = 0.0) being optimal for chitosan-mediated transfection *in vivo* in mouse lungs [54]. However, for these chitosan oligomers to mediate maximum transfection, larger concentrations are reported to be required compared to high molecular weight chitosans [50, 51, 54]. The effect of chitosan chain length on its ability to compact DNA was here studied by employing chitosans with DP ranging from 10 to 1000 (paper I and II). The low DP (LDP, DP < 100) chitosans were found to yield the same type of structures as HDP chitosans (paper I and II), but whereas HDP chitosans compacted DNA into well-defined structures at a charge ratio (+/-) less than 1 (when adjusted for pH in the solution) a larger charge ratio (+/-) was required to obtain these structures when DNA was compacted by LDP chitosans (paper I). The increased chitosan concentrations were believed to compensate for reduced interaction strength between chitosan and DNA associated with the reduced number of charged groups obtained when reducing the chitosan DP. Comparing polyplexes formed from HDP and LDP chitosans, respectively, showed that the resulting geometries depended on the chitosan chain length. Whereas hardly any toroids were observed when large excess amounts of chitosan were used for the complex formation, they made up a considerable fraction of the structures for the HDP chitosans (paper II). Although little is known about the relation between polyplex structure and transfection efficiency, the rodlike structures observed to a large extent when employing LDP chitosans might be able to passively diffuse through the nuclear pores and thus easily provide nuclear entry of the gene vector. This is based on reports stating that only the diameter of the complex, and not the length, represents a barrier for diffusion through the nuclear pores [2]. However, nuclear entry mediated by such passive diffusion requires the complexes to remain in their compacted state after endosomal escape and while present in the cytoplasm.

Studies have shown that the amount of chitosan used for DNA-chitosan complexation is important for the transfection efficiency of the system, with the optimal charge ratio (+/-) depending on the chitosan chain length [50, 51, 54]. Excessive amounts of polycations have been reported to increase the transfection efficiency of DNA-polycation complexes [35, 96, 101]. This might be due to effects of the charge ratio (+/-) on polyplex properties like the surface charge, size, shape and stability. The surface charge of the complexes is important for its interaction with other biological polyions in the cell surroundings, and with the negatively

charged cell membrane. Comparing the structures formed when complexing DNA with HDP or LDP chitosans in Milli-Q H_2O, showed that large concentrations of LDP chitosans yielded more fuzzy structures compared to HDP chitosans (paper II). Analyzing the structures further revealed that the type of structures and the height of the morphologies at different chitosan concentrations were affected by the chitosan chain length. Whereas the toroid-to-rod ratio was found to increase with increasing amount of chitosan when HDP chitosans were used, it was almost unaffected when complexation was performed with increasing amounts of LDP chitosans (paper II). The increase in chitosan concentration of HDP chitosans resulted in a reduction in the width of the height distribution and a shift in the peak towards smaller heights (paper I and II). Increasing the chitosan concentration of LDP chitosans did however not affect the height distribution of the resulting DNA-chitosan complexes (paper II).

The size, shape and stability of the structures might be important for e.g. the transport of the polyplexes towards the cell, cellular uptake and the release of DNA intracellularly. To study the diffusion and uptake of DNA-chitosan complexes in multicellular spheroids, fluorochrome-labeled DNA was complexed with chitosan (F_A = 0.01, DP~1000) and incubated with human osteosarcoma multicellular spheroids. Imaging the spheroids by confocal laser scanning microscopy (CLSM) revealed that the complexes were taken up by all cells throughout the spheroids (unpublished data). For this *in vitro* cellular system the extracellular matrix or the plasma membrane did not represent a major barrier for the delivery system. Similar results were obtained when incubating the spheroids with uncomplexed fluorochrome-labeled DNA, implying that a positively charged complex is not a prerequisite for cellular uptake in this model system. However, the extracellular space in the spheroids is small resulting in small diffusion distances compared to normal tissue or solid tumors. Further attempts to study the diffusion of DNA-chitosan complexes were carried out in agarose gels (0.2-2%) using the method of fluorescence recovery after photobleaching (unpublished data, for further details about the method see appendix A.2). However, the complexes formed large aggregates heterogeneously distributed in the gels, thus making it impossible to perform diffusion measurements. The largest aggregates and most heterogeneous distributions were obtained when low F_A chitosans, which are reported to yield highest levels of gene expression, were employed for the complex formation. A similar trend was observed when imaging the complexes with CLSM in a buffer solution (pH 7.4 and I = 150 mM). Furthermore, the tendency of aggregation was not affected by the chitosan molecular weight, in contrast to previous reports predicting that chitosan oligomers would yield less aggregated

shapes [54]. Although such aggregated structures could not be observed by AFM imaging, they might still be present in the solution in addition to the smaller and well-defined structures. This needs to be further evaluated.

4.1.2 Effect of solution parameters on the DNA-chitosan complexation

Since the driving force for the DNA-chitosan interactions is mainly electrostatic, changes in solution parameters that will affect the chitosan charge and/or the electrostatic potential surrounding the polyions are expected to affect the DNA-chitosan complexation behavior. Increasing the pH in the solution will reduce the effective chitosan charge by reducing the protonation of amine groups (pK_a ~6.5, [43, 44]) and is thus expected to yield weaker interaction with DNA and thus less stable complexes. Both increased pH and I have further been reported to induce dissociation of DNA-chitosan complexes [102].

The effect of pH and ionic strength on the interaction strength between DNA and chitosan was also supported by measuring the pull-off force when pulling on chitosan physiosorbed onto mica (paper V). Stronger interactions were measured for low pH and I as expected from general electrostatic considerations of increasing chitosan charge, as well as increased width of the electrostatic potential around the polymers. Similar effect of the solution parameters were observed on the interaction measured between chitosan covalently immobilized onto mica and DNA covalently anchored to the AFM tip (the immobilization procedure is described in A.3) (unpublished data). The strength of the interactions between DNA and chitosan was in the same range as those measured for the chitosan-mica interactions. Due to the similar response of these two systems, explained by non-specific electrostatic interactions, the chitosan-mica system appeared to be a model system for the DNA-chitosan interactions.

Although only about 10% of the chitosan amine groups are charged at physiological pH (7.4), all HDP chitosans were found to effectively compact DNA into well-defined structures at this high pH (paper I). It is reported that the apparent pK_a of a polycation will increase in the presence of a strong polyanion [103]. Chitosan is therefore believed to have a higher charge in the presence of DNA than would be expected from its pK_a value, which can explain its ability to form complexes at pH 7.4. However, whereas HDP chitosans were efficient in compacting DNA at physiological pH, LDP chitosans were found to be unable to compact DNA at this pH (unpublished data). Although it was observed that the reduced interaction strength related to the interaction between shorter chitosans and DNA could be compensated for by increasing

the chitosan concentration, there might be a lower limit for the chain length below which the chitosans are unable to induce DNA compaction, independent of the chitosan concentration. This is based on reports stating that for a multivalent ion to be able to compact DNA, a valence of three or more is required [30]. Thus, if the chitosans become too short, the valence might be reduced below this value, making it unable to cause DNA compaction.

Both pH and ionic strength were found to affect the type of structures formed when HDP chitosans at increasing concentrations were used to compact DNA (paper I and II). Whereas increased chitosan concentration in Milli-Q H_2O caused an increase in the fraction of rods (paper II), the opposite happened at pH 7.4 and I=150 mM with the concomitant development of other types of structures identified as intermediate (kinetically trapped) states (paper I). This identification was based on similarities with structures observed for the xanthan-chitosan system (paper III) [104]. Increasing I for the xanthan-chitosan system was found to increase the extent of aggregation, on the expense of the formation of well defined structures. The height distributions obtained for the DNA-chitosan complexes prepared in the two different solutions (Milli-Q H_2O and solution of pH 7.4 and I=150 mM) both became narrower with the peak shifted towards smaller heights upon increased chitosan concentration. Similarly, the contour length distributions were in both situations slightly shifted towards larger lengths (paper I and II). The conformation of chitosan at various conditions might be important for its interaction with DNA. Pulling experiments on chitosan physiosorbed onto mica revealed that both pH and I affect the adsorption characteristics of chitosan onto the surface, reflecting different conformations of chitosan at a charged surface at these conditions (paper V).

Increasing the ionic strength has been observed to cause polyplex dissociation [102, 105]. The apparently higher stability measured here in I=150 mM compared to in water when exposing the polyplex to a competing polyanion is therefore believed to be due to weaker interactions between the polyplex and this polyanion, indicating that the polyplex dissociation is driven by chitosan sequestration by the added polyanion (paper II).

4.1.3 Polyelectrolyte complexation, DNA as a part of the general picture

The collapse transition of semiflexible polymers has been described in a number of simulation studies and the morphology of the resulting structures is predicted to depend on factors like the polymer chain stiffness, chain length and the intersegment attraction [84, 106-108]. Due to its biological relevance, DNA is an extensively studied polymer which molecular details are

well known. DNA has therefore been the subject for most of the collapse transitions studies. Recent studies have shown that the main driving force in the compaction behavior is electrostatic interactions and that DNA fits into a general description (paper III and IV).

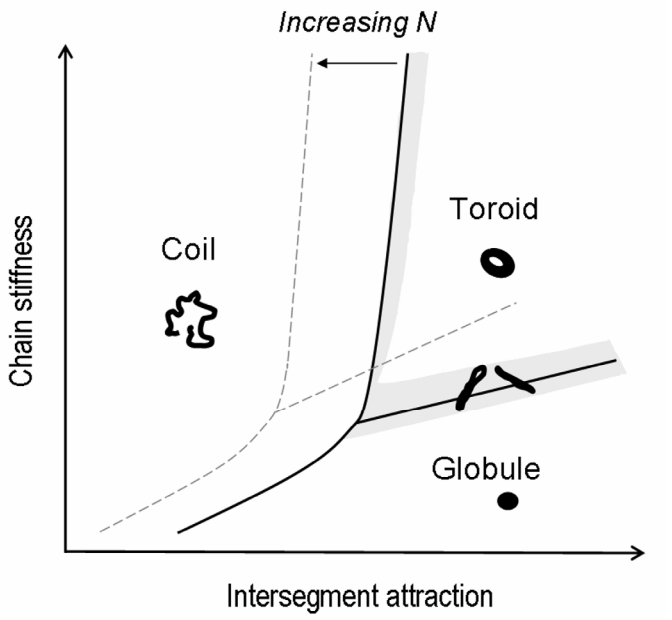

Figure 5: Schematic presentation of the theoretical state diagram illustrating the effect of chain stiffness and intersegment attraction on the collapse morphology of a semiflexible polymer. *N* represents the number of monomers in the polymer, and the grey areas represent transition regions in which a coexistence of different morphologies appear [84, 106].

The energy penalty associated with sharp bends of stiff polymers will oppose the formation of compact globular structures. A balance between the attractive collapsing force and the bending rigidity is reported to be important for the morphology of the collapsed structures. Simulation studies have led to the suggestion of the existence of a state diagram (Figure 5) predicting the relation between the polymer chain stiffness, intersegment attraction and the stability of various morphologies of the collapsed chains [84, 106, 109]. In many of the simulation studies the polymer collapse is induced by changes in the solvent quality. In a poor solvent the monomer-monomer interactions will be more favorable than the polymer-solvent interactions, leading to a collapse transition. Since the compaction is driven by short-range attraction, the precise nature of the forces is considered not to be important [106]. The framework set up by these studies is therefore employed also for the collapse transition mediated by the interaction between oppositely charged polyelectrolytes. For a rather stiff chain, the toroid is predicted to be the preferred structure, whereas the globule appears to be more favorable for more flexible chains. The transition between these regions is not sharp, but rather represents areas with a coexistence of different structures (grey areas in Figure 5).

Although the focus on toroid formation has been prominent in the literature about DNA condensation [10, 24, 76, 94, 110], this study showed that compaction of DNA with chitosan additionally yields a large fraction of rods (paper I, II and III). Furthermore, at some conditions rods were observed to be the dominating morphology with the presence of only a

few toroids (paper I and II). Whereas the toroidal structure has been predicted to be the most stable one for a rather stiff chain, the rod is predicted to be the most stable one when the chain stiffness is decreased [107, 111]. Since the intersegment interaction, which will be affected by the properties of the polycation, is also important for the structures formed, the relative stability of the different morphologies will also depend on the polycation. However, the presence of large amounts of rods in the DNA-chitosan system indicates that the chain stiffness of DNA is within a range where a coexistence of rod-like and toroidal structures occurs (Figure 5). By tuning the chitosan molecular parameters and the solution properties, the position of resulting polyplexes within the transition area varies. Comparing the structures formed in the DNA-chitosan system with those formed when compacting other polyanions, with chain stiffness different from that of DNA, by chitosan showed that the polyplex morphology depended on the chain stiffness of the polyanion (paper III). In the xanthan-chitosan system, xanthan having a persistence length of 120 nm, hardly any rods were seen, but rather toroids together with a number of morphologies identified as intermediate states (paper III). These were classified as intermediate states based on similarities with structures reported from Brownian dynamic studies, in which the polymer passes through several intermediate states (in which it might be kinetically trapped) on its way towards the most stable state [111]. When increasing the temperature of the system to overcome energetic barriers, these structures were observed to disappear with the concomitant formation of toroids, supporting the hypothesis that the toroids are the most stable structure for this system [104]. Similar heat treatment of the pDNA-chitosan system was found to cause an almost depletion of the toroidal structures in this system while provoking the formation of short rod-like structures, implying that rod-like structures are energetically favorable for this system (paper IV). Since destabilization of DNA-chitosan complexes indicated that toroidal structures were more difficult to dissociate than rod-like structures (paper II), rod-like structures with different free energies relative to the uncomplexed state might exist. The longer and thinner rods observed before heat treatment (paper I and II) probably represent intermediate states with slightly higher energy than the toroid, with both types of structures being transformed into short rods upon increasing the temperature of the system. Another possibility is that the most stable morphology depends on the properties of the polycation, with different chitosans yielding different final products in the folding process.

The observation that the average contour length, $<L_c>$, of the toroidal and rodlike DNA-chitosan polyplexes were similar, indicated that neither of the geometries were a precursor of

the other (paper I) [79]. Transitions between the different geometries, involving overcoming energy barriers in the transition from a local energy minimum to another more stable state, must thus involve unpacking, followed by a refolding**,** of the polyplexes.

Both the polycation charge density and the polycation concentration, relative to the polyanion, contribute to controlling the intersegment attraction, which are identified as an important parameter in determining the formation and stability of the morphologies [84, 109]. This was demonstrated by the observed effect on structures formed when increasing the chitosan charge density (paper I). The importance of the polycation properties for its interaction with DNA was also demonstrated by comparing the ability of chitosan and PLL, respectively, to compact DNA employing the EtBr fluorescence assay. Although a larger charge ratio (+/-) was required to cause efficient DNA compaction when more PLL was employed rather than chitosan, the overall compaction was more efficient when using PLL with the difference being more pronounced at low *I* (paper IV).

The polyanion chain length has been reported to affect its compaction behavior. Simulation studies have shown that the surface energy will become more important than the bending energy when the polymer chain length (*N*) increases, resulting in the coil-toroid transition taking place at weaker intersegment attractions [106]. This will result in the formation of globular structures as illustrated in Figure 5. The formation of globular structures upon increasing the DNA chain length was also demonstrated in this study. Whereas shorter DNAs (~2 kbp and ~4.4 kbp) yielded a blend of toroidal and rod-like structures when mixed with chitosan, independent of the linear or circular topology of DNA, the very long DNA (10 kpb) was observed to form only compact globular structures (paper IV). A lower limit for the DNA chain length has also been reported for its ability to form well-defined toroidal and rodlike structures. A minimum length of approximately 400 bp has been proposed as a requirement for the formation of toroidal DNA condensates. Furthermore, below ~150 bp it has been suggested that DNA is unable to collapse into discrete particles of a well defined morphology [33, 79]. The existence of a minimum chain length required for toroidal formation was also observed for the compaction of xanthan (paper III).

Comparing the toroidal structures formed when compacting xanthan and DNA, respectively, by chitosan, revealed different dimensions of the structures formed by these two systems. The optimum cyclization probability of wormlike chains undergoing thermal fluctuations is reported to depend on the ratio between the contour length and the persistence length [112].

Calculating this ratio for the experimentally observed xanthan and DNA toroids yielded almost the same value, which was almost the same as the reported optimum of the cyclization probability for semiflexible polymers (paper III). The larger diameter observed for the xanthan-chitosan toroids compared to that of DNA-chitosan toroids thus appeared to be a consequence of the higher chain stiffness of xanthan compared to DNA.

4.1.4 Polyplex stability

Polyplex stability is reported to be important for its function as an efficient gene delivery system where sufficient stability against environmental exposure must be combined with the ability to dissociate inside the cell [98]. The strength of the polyanion-polycation interaction is strongly affected by the valence of the polyions, with higher valence yielding stronger interactions [81, 82]. The polycation charge is thus expected to affect the polyplex stability. For the DNA-chitosan system, the high stability related to the interaction between DNA and high molecular weight chitosans is believed to be an important limitation for its function as a gene delivery system [47, 53]. Reducing the chitosan DP has been reported to yield increased transfection [51], with the highest transfection efficiency (*in vivo* in mouse lungs) observed for chitosan oligomers within a very narrow length interval [54]. Measuring the polyplex stability by exposing the polyplexes to the competing polyanion heparin, that might compete with DNA for chitosan binding, showed that the stability of the DNA-chitosan complexes increased with increasing chitosan chain length and concentration (paper II). Thus, the very long chitosans appear to be less efficient in releasing DNA.

Interaction with competing polyanions, extracellularly or intracellularly, may represent a barrier to gene delivery as they have the potential of binding to the positively charged complexes, thereby altering the size and charge, or causing polyplex dissociation. Exposing DNA-chitosan polyplexes to two important glycosaminoglycans, heparin and hyaluronic acid (HA), showed that both polycation and polyanion properties are important for the polyplex stability (paper II). Whereas exposure to heparin caused a polyplex dissociation that depended on the chain length and concentration of chitosan used for complex formation, HA was unable to cause any dissociation of the polyplexes (paper II). The different charge density of heparin and HA has been suggested as an explanation to this [113]. Exposing the DNA-chitosan complexes to alginate and xanthan supported this hypothesis (paper IV). Alginate and xanthan are two polyanions with very different chain stiffness and equivalent mass per unit charge, but with almost the same charge spacing intermediate to that of heparin and HA. However, since

the ability of heparin to cause polyplex dissociation appeared to be stronger than predicted by such charge interactions, while the opposite was the situation for HA, specific interactions between the polymers are also probably involved (paper II).

Changing the chitosan chain length is one of the ways to affect the charge density of chitosan, and thus tune the stability of the DNA-chitosan complexes. Other ways to tune this stability involve altering the chitosan F_A, changing the pH for complex formation and exposing the polyplexes to increased temperatures. The pH has been reported to be important for the transfection efficiency of DNA-chitosan complexes, with maximum transfection obtained at a pH of 7 [55, 56]. This might be related to the stability of the complexes, with too stable complexes being unable to release DNA inside the cell whereas low stability might cause the polyplexes to dissociate before they reach the cell. Such effects of pH on the transfection efficiency are suggested to be advantageous for selective gene delivery into tumor cells as the extracellular pH of tumors is lower than in normal tissue. Increasing the temperature during DNA-chitosan complex formation resulted in the formation of more stable polyplexes (paper IV). The higher temperature of the system thus facilitates the transition from kinetically trapped states to a lower free energy state. The transition into more stable structures was also found to involve changes in the polyplex morphology, emphasizing the relation between polyplex structure and stability as proposed by theoretical studies [84, 109].

Since different cells are reported to respond differently to various delivery systems [47, 48, 56], different cell types located in different types of tissues might thus possess different requirements when it comes to stability. The delivery systems must therefore probably be optimized for the specific cells, both with respect to chitosan DP, F_A and chitosan to DNA charge ratio (+/-).

Concluding remarks

The ability of chitosan to condense DNA into well defined structures was evaluated by employing TM-AFM, force spectroscopy and fluorescence spectroscopy. Both chitosan molecular parameters and solution properties were found to affect the condensation behavior of DNA as summarized schematically in Figure 6.

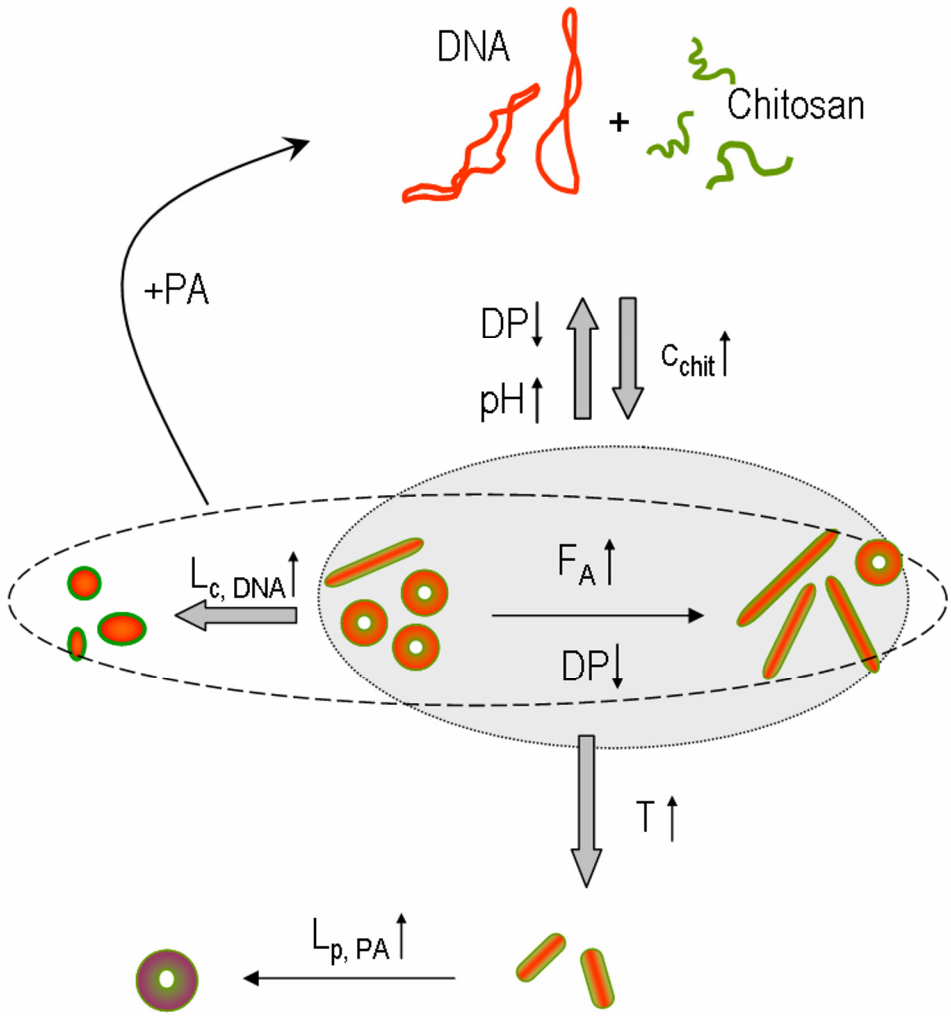

Figure 6: Summary of the chitosan-induced DNA condensation, illustrating how various factors affects the compaction behavior of DNA.

The main trends are:

- HDP chitosan efficiently compact DNA into well-defined structures with the toroid-to-rod ratio decreasing with increasing F_A.
- Increased chitosan concentrations (c_{chit}) are required for the formation of well-defined structures when employing LDP chitosans. This will compensate for the reduced interaction strength associated with reduced DP.

- Rods become the dominating morphology when the chitosan DP is reduced.
- In contrast to HDP chitosans, very short chitosans (oligomers) are unable to condense DNA at pH 7.4.
- The stability of the polyplexes upon exposure to competing polyanions (PA) depends on both the chitosan DP and the properties of the polyanion, with both electrostatic and more specific interactions being of importance. In general, increasing the chitosan DP result in increased stability of the complexes.
- Increasing the temperature of the DNA-chitosan system provide a transition into more stable structures. Whereas short rods appear to be the most stable structure for the DNA chitosan system, toroidal structures make up the most stable state when a stiffer polyanion (xanthan) is compacted by chitosan.

The results revealed that the structure and stability of the DNA-chitosan system can be tuned by varying chitosan F_A and DP, as well as solution properties like temperature, pH and ionic strength. This provides a basis for the selection of parameters when designing polycation-based gene delivery systems.

References

1. Wolff, J.A. & Lederberg, J. An early history of gene transfer and therapy. *Hum Gene Ther* **5**, 469-480 (1994).
2. Merdan, T., Kopecek, J. & Kissel, T. Prospects for cationic polymers in gene and oligonucleotide therapy against cancer. *Adv Drug Deliv Rev* **54**, 715-758 (2002).
3. Anderson, W.F. Human gene therapy: the inital concepts. In *Gene therapy for diseases of the lungs*. (ed Brigham, K.L.) 3-16 (Marcel Dekker Inc, New York, 1997).
4. Anderson, W.F. Prospects for human gene therapy. *Science* **226**, 401-409 (1984).
5. Miller, A.D. Human gene therapy comes of age. *Nature* **357**, 455-460 (1992).
6. Anderson, W.F. Human gene therapy. *Science* **256**, 808-813 (1992).
7. Anderson, W.F. Human gene therapy. *Nature* **392**, 25-30 (1998).
8. Check, E. A tragic setback. *Nature* **420**, 116-118 (2002).
9. Gelbart, W.M., Bruinsma, R.F., Pincus, P.A. & Parsegian, V.A. DNA-inspired electrostatics. *Phys Today* **53**, 38-44 (2000).
10. Kabanov, A.V., Felgner, P.L. & Seymour, L.W. (eds) *Self-assembling complexes for gene delivery:from laboratory to clinical trial*. (John Wiley & Sons, 1998).
11. Pluen, A., Netti, P.A., Jain, R.K. & Berk, D.A. Diffusion of macromolecules in agarose gels: Comparison of linear and globular configurations. *Biophys J* **77**, 542-552 (1999).
12. Lukacs, G.L., Haggie, P., Seksek, O., Lechardeur, D., Freedman, N. & Verkman, A.S. Size-dependent DNA mobility in cytoplasm and nucleus. *J Biol Chem* **275**, 1625-1629 (2000).
13. Luo, D. & Saltzman, W.M. Synthetic DNA delivery systems. *Nat Biotechnol* **18**, 33-37 (2000).
14. Crystal, R.G. Transfer of genes to humans: early lessons and obstacles to success. *Science* **270**, 404-410 (1995).
15. Ledley, F.D. Nonviral gene therapy: The promise of genes as pharmaceutical products. *Hum Gene Ther* **6**, 1129-1144 (1995).
16. Mountain, A. Gene therapy: the first decade. *Trends Biotechnol* **18**, 119-128 (2000).
17. Pedroso de Lima, M.C., Simões, S., Pires, P., Faneca, H. & Düzgünes, N. Cationic lipid-DNA complexes in gene delivery: from biophysics to biological applications. *Adv Drug Deliv Rev* **47**, 277-294 (2001).
18. Mahato, R.I., Rolland, A. & Tomlinson, E. Cationic lipid-based gene delivery systems: pharmaceutical perspectives. *Pharm Res* **14**, 853-859 (1997).
19. El-Aneed, A. An overview of current delivery systems in cancer gene therapy. *J Control Release* **94**, 1-14 (2004).
20. Kwoh, D.Y., Coffin, C.C., Lollo, C.P., Jovenal, J., Banaszczyk, M.G., Mullen, P., Phillips, A., Amini, A., Fabrycki, J., Bartholomew, R.M., Brostoff, S.W. & Carlo, D.J. Stabilization of poly-L-lysine/DNA polyplexes for in vivo gene delivery to the liver. *Biochim Biophys Acta* **1444**, 171-190 (1999).
21. Dash, P.R., Toncheva, V., Schacht, E. & Seymour, L.W. Synthetic polymers for vectorial delivery of DNA: characterisation of polymer-DNA complexes by photon correlation spectroscopy and stability to nuclease degradation and disruption by polyanion in vitro. *J Control Release* **48**, 269-276 (1997).

22. Richardson, S.C.W., Kolbe, H.V.J. & Duncan, R. Potential of low molecular mass chitosan as a DNA delivery system: biocompatibility, body distribution and ability to complex and protect DNA. *Int J Pharm* **178**, 231-243 (1999).

23. Hansma, H.G., Golan, R., Hsieh, W., Lollo, C.P., Mullen-Ley, P. & Kwoh, D. DNA condensation for gene therapy as monitored by atomic force microscopy. *Nucleic Acids Res* **26**, 2481-2487 (1998).

24. Tang, M.X. & Szoka, F.C. The influence of polymer structure on the interactions of cationic polymers with DNA and morphology of the resulting complexes. *Gene Ther* **4**, 823-832 (1997).

25. Liu, G., Molas, M., Grossmann, G.A., Pasumarthy, M., Perales, J.C., Cooper, M.J. & Hanson, R.W. Biological properties of poly-l-lysine-DNA complexes generated by cooperative binding of the polycation. *J Biol Chem* **276**, 34379-34387 (2001).

26. Godbey, W.T., Barry, M.A., Saggau, P., Wu, K.K. & Mikos, A.G. Poly(ethylenimine)-mediated transfection: A new paradigm for gene delivery. *J Biomed Mater Res* **51**, 321-328 (2000).

27. Boussif, O., Lezoualc'h, F., Zanta, M.A., Mergny, M.D., Scherman, D., Demeneix, B. & Behr, J.-P. A versatile vector for gene and oligonucleotide transfer into cells in culture and in vivo: Polyethylenimine. *Proc Natl Acad Sci U S A* **92**, 7297-7301 (1995).

28. Pollard, H., Remy, J.-S., Loussuouarn, G., Demolombe, S., Behr, J.-P. & Escande, D. Polyethylenimine but not cationic lipids promotes transgene delivery to the nucleus in mammalian cells. *J Biol Chem* **273**, 7507-7511 (1998).

29. Chattoraj, D.K., Gosule, L.C. & Schellman, J.A. DNA condensation with polyamines II. Electron microscopic studies. *J Mol Biol* **121**, 327-337 (1978).

30. Wilson, R.W. & Bloomfield, V.A. Counterion-induced condensation of deoxyribonucleic acid. A light-scattering study. *Biochemistry* **18**, 2192-2196 (1979).

31. Plum, G.E., Arscott, P.G. & Bloomfield, V.A. Condensation of DNA by trivalent cations. 2. Effects of cation structure. *Biopolymers* **30**, 631-643 (1990).

32. Fang, Y. & Hoh, J.H. Early intermediates in spermidine-induced DNA condensation on the surface of mica. *J Am Chem Soc* **120**, 8903-8909 (1998).

33. Widom, J. & Baldwin, R.L. Cation-induced toroidal condensation of DNA. Studies with Co3+(NH3)6. *J Mol Biol* **144**, 431-453 (1980).

34. He, S., Arscott, P.G. & Bloomfield, V.A. Condensation of DNA by multivalent cations: Experimental studies of condensation kinetics. *Biopolymers* **53**, 329-341 (2000).

35. Akinc, A., Lynn, D.M., Anderson, D.G. & Langer, R. Parallel synthesis and biophysical characterization of a degradable polymer library for gene delivery. *J Am Chem Soc* **125**, 5316-5323 (2003).

36. Jon, S., Anderson, D.G. & Langer, R. Degradable poly(amino alcohol esters) as potential DNA vectors with low cytotoxicity. *Biomacromolecules* **4**, 1759-1762 (2003).

37. Petersen, H., Kunath, K., Martin, A.L., Stolnik, S., Roberts, C.J., Davies, M.C. & Kissel, T. Star-shaped poly(ethylene glycol)-*block*-polyethylenimine copolymers enhance DNA condensation of low molecular weight polyethylenimines. *Biomacromolecules* **3**, 926-936 (2002).

38. Han, S.-O., Mahato, R.I., Sung, Y.K. & Kim, S.W. Development of biomaterials for gene therapy. *Mol Ther* **4**, 302-317 (2000).

39. Illum, L. Chitosan and its use as a pharmaceutical excipient. *Pharm Res* **15**, 1326-1331 (1998).

40. Lee, M., Nah, J.W., Kwon, Y., Koh, J.J., Ko, K.S. & Kim, S.W. Water-soluble and low molecular weight chitosan-based plasmid DNA delivery. *Pharm Res* **18**, 427-431 (2001).

41. Kubota, N. & Kikuchi, Y. Macromolecular complexes of chitosan. In *Polysaccharides: structural deversity and functional versatility*. (ed Dumitriu, S.) 595-628 (Marcel Dekker, Inc., New York, 1998).

42. Vårum, K.M., Anthonsen, M.W., Grasdalen, H. & Smidsrød, O. 13C-N.m.r. studies of the acetylation sequences in partially N-deacetylated chitins (chitosans). *Carbohydr Res* **217**, 19-27 (1991).

43. Anthonsen, M.W. & Smidsrød, O. Hydrogen ion titration of chitosans with varying degrees of N-acetylation by monitoring induced ^{1}H-NMR chemical shifts. *Carbohydr Polym* **26**, 303-305 (1995).

44. Vårum, K.M. Ottøy, M. H. & Smidsrød, O. Water-solubility of partially N-acetylated chitosans as a function of pH: Effect of effect of chemical composition and depolymerisation. *Carbohydr Polym* **25**, 65-70 (1994).

45. Strand, S.P., Tømmeraas, K., Vårum, K.M. & Østgaard, K. Electrophoretic light scattering studies of chitosans with different degrees of N-acetylation. *Biomacromolecules* **2**, 1310-1314 (2001).

46. Mumper, R.J., Wang, J., Claspell, J.M. & Rolland, A.P. Novel polymeric condensing carriers for gene delivery. *Proceed Intern Symp Control Rel Bioact Mater* **22**, 178-179 (1995).

47. Köping-Höggård, M., Tubulekas, I., Guan, H., Edwards, K., Nilsson, M., Vårum, K.M. & Artursson, P. Chitosan as a nonviral gene delivery system. Structure-property relationship and characteristics compared with polyethylenimine *in vitro* and after lung administration *in vivo* . *Gene Ther* **8**, 1108-1121 (2001).

48. Erbacher, P., Zou, S., Bettinger, T., Steffan, A.-M. & Remy, J.-S. Chitosan-based vector/DNA complexes for gene delivery: Biophysical characteristics and transfection ability. *Pharm Res* **15**, 1332-1339 (1998).

49. Carreno-Gomez, B. & Duncan, R. Evaluation of the biological properties of soluble chitosan and chitosan microspheres. *Int J Pharm* **148**, 231-240 (1997).

50. Romøren, K., Pedersen, S., Smistad, G., Evensen, Ø. & Thu, B.J. The influence of formulation variables on in vitro transfection efficiency and physiochemical properties of chitosan-based polyplexes. *Int J Pharm* **261**, 115-127 (2003).

51. Köping-Höggård, M., Mel'nikova, Y.S., Vårum, K.M., Lindman, B. & Artursson, P. Relationship between the physical shape and the efficiency of oligomeric chitosan as a gene delivery system *in vitro* and *in vivo*. *J Gene Med* **5**, 130-141 (2003).

52. Liu, W.G. & Yao, K.D. Chitosan and its derivatives -a promising non-viral vector for gene transfection. *J Control Release* **83**, 1-11 (2002).

53. MacLaughlin, F.C., Mumper, R.J., Wang, J., Tagliaferri, J.M., Gill, I., Hinchchliffe, M. & Rolland, A.P. Chitosan and depolymerized chitosan oligomers as condensing carriers for in vivo plasmid delivery. *J Control Release* **56**, 259-272 (1998).

54. Köping-Höggård, M., Vårum, K.M., Issa, M., Danielsen, S., Christensen, B.E., Stokke, B.T. & Artursson, P. Improved chitosan-mediated gene delivery based on easily dissociated chitosan polyplexes of highly defined chitosan oligomers. *Gene Ther* **11**, 1441-1452 (2004).

55. Ishii, T., Okahata, Y. & Sato, T. Mechanism of cell transfection with plasmid/chitosan complexes. *Biochim Biophys Acta* **1514**, 51-64 (2001).

56. Sato, T., Ishii, T. & Okahata, Y. In vitro gene delivery mediated by chitosan. Effect of pH, serum, and molecular mass of chitosan on the transfection efficiency. *Biomaterials* **22**, 2075-2080 (2001).

57. Gao, S., Chen, J., Xu, X., Ding, Z., Yang, Y.H., Hua, Z. & Zhang, J. Galactosylated low molecular weight chitosan as DNA carrier for hepatocyte-targeting. *Int J Pharm* **255**, 57-68 (2003).

58. Jansma, C.A., Thanou, M., Junginger, H.E. & Borchard, G. Preparation and characterization of 6-O-carboxymethyl-N-trimethyl chitosan derivative as a potential carrier for targeted polymeric gene and drug delivery. *STP Pharma Sci* **12**, 63-67 (2003).

59. Mao, H.Q., Roy, K., Walsh, S.M., August, J.T. & Leong, K.W. DNA-chitosan nanospheres for gene delivery. *Proceed Intern Symp Control Rel Bioact Mater* **23**, 401-402 (1996).

60. Murata, J.-I., Ohya, Y. & Ouchi, T. Design of quaternary chitosan conjugate having antennary galactose residues as a gene delivery tool. *Carbohydr Polym* **32**, 105-109 (1997).

61. Köping-Höggård, M. *Chitosan polyplexes as non-viral gene delivery systems: Structure-property relationships and in vivo efficiency*. (Uppsala, 2003).

62. Thanou, M., Florea, B.I., Geldof, M., Junginger, H.E. & Borchard, J.G. Quaternized chitosan oligomers as novel gene delivery vectors in epithelial cell lines. *Biomaterials* **23**, 153-159 (2002).

63. Bloomfield, V.A., Crothers, D.M. & Tinoco, I. *Nucleic Acids. Structures, properties and functions*. (University Science Books, Sausalito, 2000).

64. Frank-Kamenetskii, M.D. Biophysics of the DNA molecule. *Physics reports* **288**, 13-60 (1997).

65. Clayton, J. & Dennis, C. (eds) *50 years of DNA*. (Palgrave Macmillan, Basingstoke, 2003).

66. Watson, J.D. & Crick, F.H.C. Molecular structure of nucleic acids. *Nature* **171**, 737-738 (1953).

67. Tinland, B., Pluen, A., Sturm, J. & Weill, G. Persistence length of single-stranded DNA. *Macromolecules* **30**, 5763-5765 (1997).

68. Tamarin, R.H. *Principles of genetics*. (McGraw-Hill, New York, 2002).

69. Stryer, L. *Biochemistry*. (W. H. Freeman and Company, New York, 1995).

70. Dautzenberg, H., Jaeger, W., Kötz, J., Philipp, B., Seidel, C. & Stscherbina, D. *Polyelectrolytes formation, characterization and application*. (Hanser/Gardner Publications, Inc., Cincinnati, 1994).

71. Rau, D.C. & Parsegian, V.A. Direct measurement of the intermolecular forces between counterion-condensed DNA double helices. Evidence for long range attractive hydration forces. *Biophys J* **61**, 246-259 (1992).

72. Rouzina, I. & Bloomfield, V.A. Macroion attraction due to electrostatic correlation between screening counterions. 1. Mobile surface-adsorbed ions and diffuse ion cloud. *J Phys Chem* **100**, 9977-9989 (1996).

73. Grosberg, A.Y., Nguyen, T.T. & Shklovski, B.I. The physics of charge inversion in chemical and biological systems. *Rev Mod Phys* **74**, 329-345 (2002).

74. Tanaka, M. & Grosberg, A.Y. Giant charge inversion of a macroion due to multivalent counterions and monovalent coins: Molecular dynamics study. *J Chem Phys* **115**, 567-574 (2001).

75. Matulis, D., Rouzina, I. & Bloomfield, V.A. Thermodynamics of DNA binding and condensation: Isothermal titration calorimetry and electrostatic mechanism. *J Mol Biol* **296**, 1053-1063 (2000).

76. Bloomfield, V.A. DNA condensation by multivalent cations. *Biopolymers* **44**, 269-282 (1997).

77. Manning, G.S. Thermodynamic stability theory for DNA doughnut shapes induced by charge neutralisation. *Biopolymers* **19**, 37-59 (1980).

78. Rouzina, I. & Bloomfield, V.A. Competitive electrostatic binding of charged ligands to polyelectrolytes: practical approach using the non-linear Poisson-Boltzmann equation. *Biophys Chem* **64**, 139-155 (1997).

79. Bloomfield, V.A. Condensation of DNA by multivalent cations. *Biopolymers* **31**, 1471-1481 (1991).

80. Israelachvili, J. & Wennerström, H. Role of hydration and water structure in biological and colloidal interactions. *Nature* **379**, 219-225 (1996).

81. Mascotti, D.P. & Lohman, T.M. Thermodynamic extent of couterion release upon binding oligolysines to single-stranded nucleic acids. *Proc Natl Acad Sci U S A* **87**, 3142-3146 (1990).

82. Stigter, D. & Dill, K.A. Binding of ionic ligands to polyelectrolytes. *Biophys J* **71**, 2064-2074 (1996).

83. Eickbush, T.H. & Moudrianakis, E.N. The compaction of DNA helices into either continous supercoils or folded-fiber rods and toroids. *Cell* **13**, 295-306 (1978).

84. Ivanov, V.A., Stukan, M.R., Vasilevskaya, V.V., Paul, W. & Binder, K. Structures of stiff macromolecules of finite chain length near the coil-globule transition: A Monte Carlo simulation. *Macromol Theory Simul* **9**, 488-499 (2000).

85. Hud, N.V., Downing, K.H. & Balhorn, R. A constant radius of curvature model for the organization of DNA in toroidal condensates. *Proc Natl Acad Sci U S A* **92**, 3581-3585 (1995).

86. Marx, K.A. & Reynolds, T.C. Spermidine-condensed ϕX174 DNA cleavage by micrococcal nuclease: torus cleavage model and evidence for unidirectional circumferential DNA wrapping. *Proc Natl Acad Sci U S A* **79**, 6484-6488 (1982).

87. Yoshikawa, K. & Matsuzawa, Y. Nucleation and growth in single DNA molecules. *J Am Chem Soc* **118**, 929-930 (1996).

88. Sakaua, T. & Yoshikawa, K. Folding/unfolding kinetics of a semiflexible polymer chain. *J Chem Phys* **117**, 6323-6330 (2002).

89. Matsuzawa, Y., Yonezawa, Y. & Yoshikawa, K. Formation of nucleation center in single double-stranded DNA chain. *Biochem Biophys Res Commun* **225**, 796-800 (1996).

90. Shen, M.R., Downing, K.H., Balhorn, R. & Hud, N.V. Nucleation of DNA condensation by static loops: Formation of DNA toroids with reduced dimensions. *J Am Chem Soc* **122**, 4833-4834 (2000).

91. Reich, Z., Ghirlando, R. & Minsky, A. Nucleic acids packaging processes: Effects of adenine tracts and sequence-dependent curvature. *J Biomol Struct Dyn* **9**, 1097-1109 (1992).

92. Maniatis, T., Venable, J.H. & Lerman, J.a.L.S. The structure of ψ DNA. *J Mol Biol* **84**, 37-64 (1974).

93. Schellman, J.A. & Parthasarathy, N. X-ray diffraction studies on cation-collapsed DNA. *J Mol Biol* **175**, 313-329 (1984).

94. Hud, N.V. & Downing, K.H. Cryoelectron microscopy of λ–phage DNA condensates in vitreous ice: The fine structure of DNA toroids. *Proc Natl Acad Sci U S A* **98**, 14925-14930 (2001).

95. Park, S.Y., Harries, D. & Gelbart, W.M. Topological defects and the optimum size of DNA condensates. *Biophys J* **75**, 714-720 (1998).

96. Jones, N.A., Hill, I.R.C., Stolnik, S., Bignotti, F., Davis, S.S. & Garnett, M.C. Polymer chemical structure is a key determinant of physicochemical and colloidal properties of polymer-DNA complexes for gene delivery. *Biochim Biophys Acta* **1517**, 1-18 (2000).

97. Howard, K.A., Dash, P.R., Read, M.L., Ward, K., Tomkins, L.M., Nazarova, O., Ulbrich, K. & Seymour, L.W. Influence of hydrophilicity of cationic polymers on the biophysical properties of polyelectrolyte complexes formed by self-assembly with DNA. *Biochim Biophys Acta* **1475**, 245-255 (2000).

98. Schaffer, D.V., Fidelman, N.A., Dan, N. & Lauffenburger, D.A. Vector unpacking as a potential barrier for receptor-mediated polyplex gene delivery. *Biotechnol Bioeng* **67**, 598-606 (2000).

99. Rungsardthong, U., Ehtezazi, T., Bailey, L., Armes, S.P., Garnett, M.C. & Stolnik, S. Effect of polymer ionization on the interacation with DNA in nonviral gene delivery systems. *Biomacromolecules* **4**, 683-690 (2003).

100. Putnam, D., Gentry, C.A., Pack, D.W. & Langer, R. Polymer-based gene delivery with low cytotoxicity by unique balance of side-chain termini. *Proc Natl Acad Sci U S A* **98**, 1200-1205 (2001).

101. Hill, I.R.C., Garnett, M.C., Bignotti, F. & Davis, S.S. In vitro cytotoxicity of poly(amidoamine)s: relevance to DNA delivery. *Biochim Biophys Acta* **1427**, 161-174 (1999).

102. Strand, S., Danielsen, S., Christensen, B.E. & Vårum, K.M. *In prep* (2004).

103. Zelikin, A.N., Trukhanova, E.S., Putnam, D., Izumrudov, V.A. & Llitmanovich, A.A. Competitive reactions in solutions of poly-L-histidine, calf thymus DNA, and synthetic polyanions: determining the binding constants of polyelectrolytes. *J Am Chem Soc* **125**, 13693-13699 (2003).

104. Maurstad, G. & Stokke, B.T. Metastable and stable states of xanthan polyelectrolyte complexes studied by atomic force microscopy. *Biopolymers* **74**, 199-213 (2004).

105. Lee, K.Y., Kwon, I.C., Kim, Y.-H., Jo, W.H. & Jeong, S.Y. Preparation of chitosan self-aggregates as a gene delivery system. *J Control Release* **51**, 213-220 (1998).

106. Stukan, M.R., Ivanov, V.A., Grosberg, A.Y., Paul, W. & Binder, K. Chain length dependence of the state diagram of a single stiff-chain macromolecule: Theory and Monte Carlo simulation. *J Chem Phys* **118**, 3392-3400 (2003).

107. Noguchi, H. & Yoshikawa, K. Folding path in a semiflexible homopolymer chain: A Brownian dynamics simulation. *J Chem Phys* **113**, 854-862 (2000).

108. Dias, R.S., Pais, A.A.C.C., Miguel, M.G. & Lindman, B. Modeling of DNA compaction by polycations. *J Chem Phys* **119**, 8150-8157 (2003).

109. Noguchi, H. & Yoshikawa, K. Morphological variation in a collapsed single homopolymer chain. *J Chem Phys* **109**, 5070-5077 (1998).

110. Duguid, J.G., Li, C., Shi, M., Logan, M.J., Alila, H., Rolland, A., Tomlinson, E., Sparrow, J.T. & Smith, L.C. A physicochemical approach for predicting the effectiveness of peptide-based gene delivery systems for use in plasmid-based gene therapy. *Biophys J* **74**, 2802-2814 (1998).

111. Stevens, M.J. Simple simulations of DNA condensation. *Biophys J* **80**, 130-139 (2001).

112. Shimada, J. & Yamakawa, H. Ring-closure probabilities for twisted wormlike chains. Application to DNA. *Macromolecules* **17**, 689-698 (1984).

113. Ruponen, M., Rönkkö, S., Honkakoski, P., Pelkonen, J., Tammi, M. & Urtti, A. Extracellular glycosaminoglycans modify cellular trafficking of lipoplexes and polyplexes. *J Biol Chem* **276**, 33875-33880 (2001).

114. Zifferer, G. Shape distribution and correlation between size and shape of tetrahedral lattice chains in athermal and theta systems. *J Chem Phys* **109**, 3691-3698 (1998).

115. Zifferer, G. & Olaj, O.F. Shape assymetry of random walks and nonreversal random walks. *J Chem Phys* **100**, 636-639 (1994).

116. Spisz, T.S., Fang, Y., Reeves, R.H., Seymour, C.K., Bankman, I.N. & Hoh, J.H. Automated sizing of DNA fragments in atomic force microscope images. *Med Biol Eng Comput* **36**, 667-672 (1998).

117. Glazer, A.N. & Rye, H.S. Stable dye-DNA intercalation complexes as reagents for high sensitivity fluorescence detection. *Nature* **359**, 859-861 (1992).

118. Cai, X.-E. & Yang, J. Molecular forces for the binding and condensation of DNA molecules. *Biophys J* **82**, 357-365 (2002).

119. Sletmoen, M., Skjåk-Bræk, G. & Stokke, B.T. Single-molecular pair unbinding studies of mannuronan C-5 epimerase AlgE4 and its polymer substrate. *Biomacromolecules* **5**, 1288-1295 (2004).

120. Hames, B.D. & Rickwood, D. *Gel electrophoresis of protein: a practical approach*. (IRL Press Limited, London, 1981).

Appendix

A.1 Image analysis

Quantitative analysis of the polyplex structures observed by AFM imaging were performed by a user-interactive software developed in the IDL language (Research System, Inc., Boulder USA). The analysis involved collecting the distribution of geometries as well as their dimensions within series of AFM height topographs, as summarized in Figure A.1.

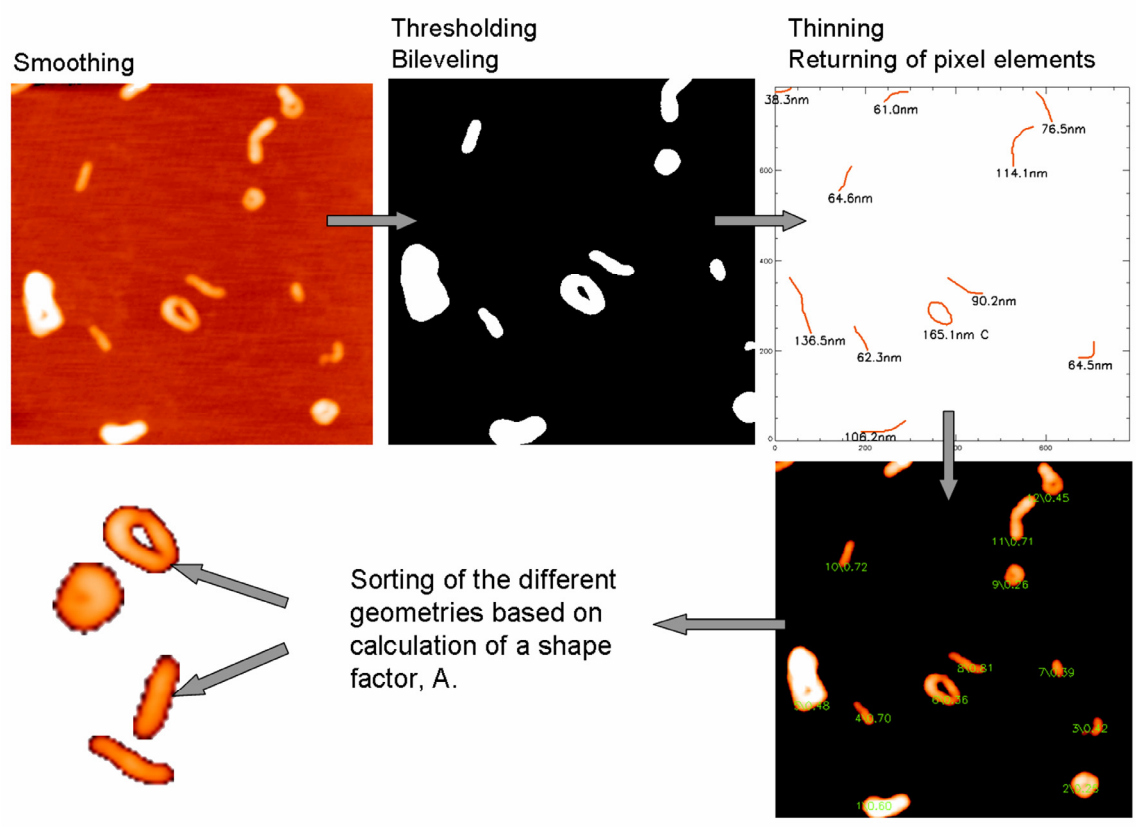

Figure A.1: Illustration of the steps involved in the image analysis of AFM topographs to extract information about distribution of geometries and their dimensions.

Individual structures were identified in the image by defining regions of interest (ROI), each containing one compacted structure. The ROIs were obtained by thresholding and bileveling of the line-smoothed height topographs and the AFM height data were returned in the ROI to provide the basis for the analysis. The structures were sorted into three different classes, linear, toroidal and globular, based on the calculation of a shape factor, the asphericity index *A*, for each structure [114, 115]:

$$A = \frac{\left(\lambda_1^2 - \lambda_2^2\right)^2 + \left(\lambda_2^2 - \lambda_3^2\right)^2 + \left(\lambda_1^2 - \lambda_3^2\right)^2}{2\left(\lambda_1^2 + \lambda_2^2 + \lambda_3^2\right)^2} \tag{A.1}$$

where the parameters λ_j, j = 1-3, are the eigenvalues of the tensor of the moment of inertia:

$$X_{\alpha,\beta} = \frac{1}{N}\sum_{i=1}^{N} S_i^{\alpha} S_i^{\beta}; \qquad \mathbf{S}_i = \mathbf{r}_i - \mathbf{R}_{CM}; \quad \alpha, \beta = x, y, z \tag{A.2}$$

where $\mathbf{r}_i$ and $\mathbf{R}_{CM}$ is the positional co-ordinate of the pixel element i in the structure, and the center of mass of the structure, respectively. The height data was included in the calculations of A by locating an element with z-extension equal to the height at the half height of the surface of the structure in each pixel and weighting the contribution to the tensor of the moment of inertia. The summation (eq. A.2) was therefore over all pixel elements, N, in the ROI. The asphericity index reflects the symmetry of the structure about the three axis of rotation and takes a value between 0 and 1 as illustrated in Figure A.2, with the theoretical values being A = 0 for a sphere, A = 0.25 for a circle without any width, and A = 1 for a rod without any width [109].

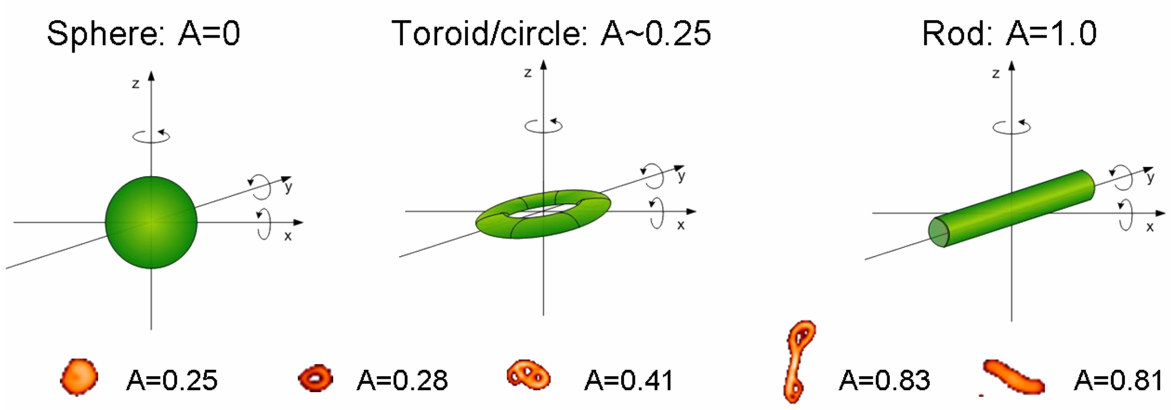

Figure A.2: Schematic illustration of the rotational symmetry of idealized structures with their corresponding asphericity indices. Examples of structures obtained from the AFM images are shown in the bottom row, illustrating how the asphericity index is used to differentiate between the various types of geometries.

Complexes were included in the toroidal ensemble provided $A \in$ (0.2- 0.35) and using the additional criteria of a distinct hole in the center. The ensemble of topologically linear polyplexes included species with $A \in$ (0.5- 1.0) to also allow for curved species.

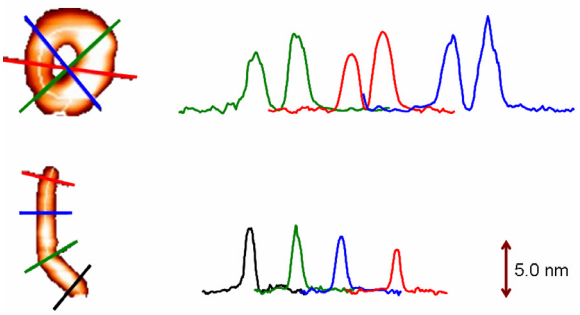

Figure A.3: The height along the structures was determined by measuring the peak value of the cross-sections taken successively along the structure.

The structures were further analyzed to extract contour length and height data within each ensemble. Branched species and species touching the edge of the topographs were excluded from the analysis. The linear structures were analyzed by a routine adapted from Hoh and coworkers [116] involving thinning of the structures with back-extrapolation of the pixels at the ends. The height along the contour length of the thinned images was used as the height of the structures, measured as the peak value of cross-sections taken along the structure (Figure A.3). For the toroidal structures, application of the thinning procedure often led to cutting of the circles. The contour lengths of the toroids were therefore obtained by determining the maximum height in the cross-section of the original image data returned to the ROI. These cross-sections were drawn radial from the center of the torus at incremental angles of 4º to cover the whole circumference, giving the height profile of the species. The contour lengths of the toroids were obtained from the maximum heights in the cross-sections collected for the individual toroids. This method allows the height of the structures to be measured continuously along the contour length and thus height differences within each complex to be determined. Globular structures were characterized with the volume contained within a perimeter of the half-height of the maximum. The number of species included in each ensemble for the quantitative determination of the dimensions was in the range 50 to 100.

A.2 DNA labeling for CLSM imaging

Distribution and uptake of DNA-chitosan complexes in multicellular spheroids were studied by labeling DNA with the fluorescent probe YOYO-1 (Molecular Probes, Eugene, OR, USA) and imaged by confocal laser scanning microscopy (CLSM). YOYO-1 exhibits an extremely high binding affinity to dsDNA and a very high fluorescence enhancement (a factor of 3200) upon binding while being essentially nonfluorescent in the absence of DNA [117]. Thus, YOYO-1 is exceptional sensitivity for DNA.

To label DNA (pBR322, ~4.4 kbp, Böringer Mannheim or D-1626, ~2 kbp, Sigma Aldrich), diluted YOYO-1 stock solution (1 mM in DMSO) was diluted in buffer and DNA was labeled by adding YOYO-1 to the DNA solution (10 µg/ml), yielding a final ratio of 1 dye molecule

per 50 base pairs [11]. DNA-chitosan complexes were prepared by adding chitosan solution to the DNA solution to obtain a charge ratio (+/-) of 0.5 to 6.

The fluorochrome-labeled DNA-chitosan complexes were incubated with human osteosarcoma multicellular spheroids for ~10 hours before imaging the spheroids with a CLSM (LSM510; Zeiss, Jena, Germany). Since YOYO-1 has its absorption maximum at 491 nm, the 488 line of the Ar-ion laser was employed for imaging and the fluorescence was recorded within the interval 500-550 nm which covers the emission maximum at 509 nm.

CLSM was also employed to study the distribution and diffusion of DNA-chitosan complexes in agarose gels. The gels were prepared by adding agarose powder to the desired amount of buffer, yielding a final agarose concentration of 0.2-2%, and heating to ~90°C until the agarose was completely dissolved. The agarose solution was then slowly cooled at room temperature to form a gel. Just before gelation (~40°C), the DNA-chitosan complexes were mixed with the agarose solution and left overnight to allow diffusion throughout the gel. Diffusion measurements were performed by recording the fluorescence recovery after photobeleaching (FRAP). This technique involves bleaching a small area by illuminating it with high intensity light, rendering the dye unable to fluoresce. Diffusion will cause photobleached molecules and the fluorescent molecules to mix. As the photobleached molecules move out of the bleached area, the fluorescent molecules will migrate into this area, causing the fluorescence from the bleached area to gradually increase in brightness. By measuring the rate at which this recovery takes place the diffusion constant can be estimated.

A.3 Immobilization of chitosan to mica and DNA to the AFM tip

The interaction between chitosan and DNA (D-1626, ~2 kbp, Sigma Aldrich) was determined using covalently immobilized chitosan on mica, and DNA on the AFM tip. The procedure for immobilizing DNA on the AFM tip and chitosan on the mica was adapted from Cai and Yang [118]. To clean the surface and facilitate silanization freshly cleaved mica discs and Si_3N_4 tips (MLCT-AUHW type Veeco, Santa Barbara, CA) were immersed in a 1:1 v/v concentrated HCl:MeOH mixture [119] for 120 and 30 minutes, respectively, followed by extensive rinsing in MeOH and Milli-Q H_2O. The mica discs were dried in a stream of N_2 gas and silanized by briefly immersing them into a 0.3% 3-(Trimethoxysilyl)propyl methacrylate (MEMO) (Acros Organics) solution, with MeOH as the base, for two hours. After extensive rinsing with MeOH and Milli-Q H_2O, followed by drying in a stream of N_2, the mica was submerged in a

chitosan solution (0.25 µg/ml in 10 mM TRIS, pH = 7.2) containing 0.2% of the catalytic agents ammonium persulfate (APS, w/w) and N,N,N',N'-tetramethylethylenediamine (TEMED, w/v). APS and TEMED facilitate the reduction of the alkene double bond of MEMO and covalently link the open bond to an OH or an ether group [118, 120]. The reaction was left to proceed for ~1 h [118]. To reduce the probability of getting long pulls that reflect the chitosan-mica rupture events caused by loosely bound chitosan to mica, the shorter chitosan C(0.01,32) was used for immobilization. Additionally, among the chitosans used in this study, C(0.01,32) is assumed to be most relevant for transfection [46, 50].

Silanization of the AFM tips were performed in the same way, except the incubation time in the MEMO liquid was reduced to 30 min and the concentration of the DNA in the last step was 3µg/ml. After cross-linking of the chitosan and DNA to the mica and tip, respectively, they were both carefully rinsed in Milli-Q H_2O and stored in the buffer to be used in the subsequent force spectroscopy experiments.

Paper I

Paper I is not included due to copyright.

Paper II

Glycosaminoglycan destabilization of DNA- chitosan polyplexes for gene delivery depends on chitosan chain length and GAG properties

Signe Danielsen[1], Sabina Strand[2], Catharina de Lange Davies[1], and Bjørn T. Stokke[1*]

[1]*Biophysics and Medical Technology, Dept. of Physics,*
[2]*NOBIPOL, Dept. of Biotechnology*
The Norwegian University of Science and Technology, NTNU, NO-7491 Trondheim, Norway

Abstract

Chitosan-based gene delivery systems are promising candidates for non-viral gene therapy. A wide range of chitosans have been studied to optimize the properties of the DNA-chitosan complexes to yield high transfection efficiencies. An important parameter to control is the polyplex stability to allow transport towards the cells, subsequent internalization and release of DNA intracellularly. The stability of the DNA-chitosan complexes was here studied after exposure to heparin and hyaluronic acid (HA) using atomic force microscopy (AFM) and ethidium bromide (EtBr) fluorescence assay. To study the effect of polycation chain length on the polyplex stability, chitosans with a degree of polymerization (DP) varying from ~10 to ~1000 were employed for DNA compaction. Whereas HA was unable to dissociate the complexes, the degree of dissociation caused by heparin depended on both the chitosan chain length and the amount of chitosan used for complexation. When increasing the chitosan concentration, larger heparin concentrations were required for polyplex dissociation. Furthermore, increasing the chitosan chain length yielded more stable complexes. Varying the chitosan chain length thus provides a tool for controlling the ability of the polyplex to deliver therapeutic gene vectors to cells.

Keywords: chitosan, DNA, polyplex, stability, AFM, fluorescence

Accepted for publication in BBA General subjects
* Corresponding author: Bjørn T. Stokke, Dept. of Physics, NTNU, NO-7491 Trondheim, NORWAY,
Fax: +47 73 59 77 10, e-mail: bjorn.stokke@phys.ntnu.no

Introduction

The development of efficient gene delivery systems is important for the advancement of gene therapy. Although viral vectors possess advantages such as high transfection efficiency and a wide range of cell targets, safety concerns and limited DNA carrying capacity have motivated the search for alternative delivery systems. A number of non-viral gene delivery systems based on the use of polycations have been studied (for recent reviews see [1, 2]). Among the polycations studied, chitosan has shown great potential as a gene delivery vehicle [3-6]. The non-toxic and biodegradable nature of chitosan are important features for this application [7-9]. A reduction in the molecular weight of chitosan is reported to yield a further reduction in toxicity [9] as well as increased transfection [6]. However, reduction of the molecular weight below that required for forming a complex with DNA yields an inefficient transfection. Effects of the polycation size have also been demonstrated for the use of polyethylenimine (PEI) and poly-L-lysine (PLL) in gene delivery [10, 11].

To achieve successful transfection the delivery system has to pass several barriers such as transport through the extracellular matrix and subsequent intracellular trafficking towards the nucleus. Interactions between glycosaminoglycans, GAGs, and the delivery system may impede the transport towards the target cell and limit the cellular uptake. Negatively charged GAGs may affect the delivery system e.g. by binding to the positively charged complexes and thereby altering the size and charge, or by causing dissociation of the polyplexes. Consistent with this, heparin and heparan sulphate are reported to bind to PEI and release DNA from the polyplexes [12, 13]. Thus, polyplex stability is important for its applicability as a gene delivery system where sufficient stability against environmental exposure extracellularly must be combined with the ability to dissociate inside the cell.

Cellular uptake of DNA-chitosan complexes is reported to take place through endocytosis [4, 14], followed by endosomal escape and nuclear accumulation [14]. Although the polyplexes are able to escape the endosomal degradation, efficient gene transfer is not obtained unless DNA is released from the complexes. High stability of polyplexes made from high molecular weight polycations is suggested to be a rate-limiting step in the overall transfection [3]. Shorter polycations are expected to release DNA more easily and appear to be candidates for improved gene delivery [11]. Several studies have shown that chitosan chain length, degree of acetylation (F_A) and A/P-ratio (defined as the ratio between the maximum number of protonable primary amines on chitosan and the number of negatively charged phosphate groups on DNA) are important factors for the transfection efficiency of chitosan-based delivery systems [5, 6, 15, 16].

Low F_A is reported to be preferable for chitosan-based delivery systems [5]. Chitosans with $F_A \leq 0.01$ were therefore used in this study to compact DNA, and the effect of chitosan chain length on the structure and stability of the DNA-chitosan complexes was studied. Since GAGs represent an important barrier for successful gene delivery, stability of the polyplexes after exposure to two of the most important GAGs, heparin and hyaluronic acid, was investigated. The morphology of the compacted polymers is believed to reflect the state with low free energy and is reported to depend on both the chain length and the chain stiffness [17-19]. Structural analysis of

the observed DNA-chitosan structures was therefore performed.

Materials and methods

Biopolymer samples

The DNAs used for complexation were the plasmids (pDNA) pCMV-luc (~4000 bp kindly provided by prof. Per Artursson, University of Uppsala) and pBR322 (4363 bp, Böhring Mannheim), and the linear calf thymus DNA (~10 kbp, D-1501 Sigma Aldrich). Preliminary studies revealed no differences between the structures formed from the two different plasmids and both are therefore referred to as pDNA. The chitosans used for DNA condensation, having a degree of acetylation (F_A) ≤ 0.01 and chain lengths varying from 10 to ~1000 monomers, were kindly provided by prof. K. M. Vårum (Dept. of Biotechnology, NTNU). Chitosan (F_A < 0.001) was depolymerized with nitrous acid degradation to obtain an oligomers fraction with a number average degree of polymerization (DPn) of 18 (DPn18) [20]. The DPn18 sample was subsequently fractionated by gel filtration as described previously [20] to yield 4 fractions differing in molecular weight. These chitosan fractions were denoted according to their number of monomers as DP10-14, DP15-21, DP22-35 and DP36-50. When referring to this group of oligomers in the following, the generic term low DP (LDP) chitosans are used. The high DP (HDP) chitosan used had a F_A = 0.01 and a DP of ~200 or ~1000. Heparin sodium salt (from porcine intestinal mucosa, ~17-19 kDa, H9399 Sigma Aldrich) and hyaluronic acid (HA, from rooster comb, H5388 Sigma Aldrich) were used to study the stability of DNA-chitosan complexes when exposed to biological polyanions.

Stock solutions (1 mg/mL) of the polymers were prepared in MQ H_2O and further diluted in either MQ H_2O or in 3-(N-Morpholino)propanesulfonic acid buffer (MOPS, 20 mM, Acros Organics) with pH adjusted to 6.5 and ionic strength, I, to 150 mM by adding NaCl. This pH was chosen to provide easy comparison complexation/ decomplexation in MQ H_2O, i.e. conditions equivalent to that used for preparation of complexes using the same chitosans for transfection studies [21].

Complex formation and stability studied by AFM imaging

Chitosan stock solutions (1mg/mL) were prepared in MQ H_2O. Both chitosan and pDNA were further diluted in MQ H_2O, and complexes were formed by adding chitosan to the DNA solution, yielding a final DNA concentration, c_{DNA}, in the formulation of 5-13μg/mL. The amount of chitosan added was adjusted to achieve an A/P-ratio between 1 and 60. The complexation was left to proceed for ~15 minutes. Heparin (5μg/mL) was added to the polyplex solution and incubated for 2 hours at room temperature or at 37°C to study possible destabilization of the polyplexes, and thus possible release of pDNA. Dried samples for AFM were prepared as previously described, and imaged by tapping mode AFM (TM-AFM) in air using a Digital Instrument Multimode IIIa [22, 23]. Quantitative analysis of the size and shape of the observed structures were performed using software developed in the IDL language (Research System Inc, Boulder, CO). About 100 structures were collected from several AFM topographs and sorted into rodlike and toroidal ensembles guided by the calculated asphericity index of each complex [22, 23].

Ethidium bromide fluorescence assay

Condensation of linear DNA by chitosan and stability of the polyplexes upon exposure to heparin and HA were studied by the ethidium bromide, EtBr, (Sigma Aldrich) fluorescence assay. The intercalation of EtBr into the DNA helix results in an increase of the fluorescence quantum yield of the dye [24]. Upon DNA condensation, EtBr is expelled from the DNA-EtBr complex, causing a decrease in the fluorescence signal [25]. As a consequence, compounds that destabilize the DNA condensates, release DNA from the polyplexes with a concomitant recovery of the fluorescence signal.

DNA-chitosan complexes were formed by adding chitosan to the DNA solution, yielding a final DNA concentration, c_{DNA}, in the formulation of 5-10µg/mL and an A/P-ratio between 1 and 50. Fifteen minutes after blending the solutions, EtBr was added in a molar ratio of one EtBr molecule for every 2nd base pair. Stability of the DNA-chitosan condensates when exposed to the biological polyanions was studied by adding increasing amounts of heparin and HA, respectively, to the polyplex formulation and incubated for ~2 hours. To get information about the affinity of chitosan binding to heparin and HA, compared to DNA, 10µg/mL of each of the polymers (DNA and heparin or DNA and HA) was mixed, together with EtBr, in buffer (MOPS, pH 6.5, I = 150 mM) and polyplexes were prepared by stepwise addition of chitosan.

Fluorescence of the EtBr-DNA complex was obtained by excitation at λ_{ex} = 511 nm. The effect of A/P and presence of heparin and HA on the fluorescence signal was studied in either 96 well plates, recording the emitted light at 603 nm using a Spectra MAX Gemini XS plate reader (Molecular Devices), or in 1.5 mL cuvettes, recording the emission spectrum from 500 nm to 700 nm using a Spex Spectramate Fluorolog (Spex Industries, Inc.). The fluorescence intensity was quantified by calculating the average intensity of the spectrum at 595-610 nm. Recording the whole emission spectrum has the advantage of reduced noise in the measured intensity compared to measuring the intensity at one wavelength only, and can additionally be used to provide information about possible shifts in the emission maximum.

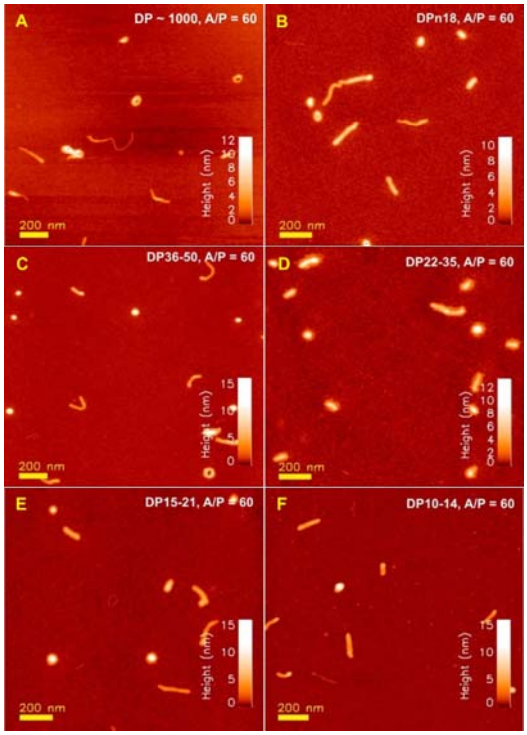

Figure 1: TM-AFM height topographs of pDNA (c_{DNA} = 13µg/mL) compacted with HDP (A) and LDP (B-F) chitosans, respectively, in MQ H_2O at an A/P-ratio of 60. The HDP chitosan used for compaction had a DP ~ 1000 (A). Five different samples of chitosan oligomers were employed: DPn18 (B), DP36-50 (C), DP22-35 (D), DP15-21 (E) and DP10-14 (F).

Results

Structural analysis of DNA-chitosan polyplexes

The size and shape of polyplexes formed when complexing pDNA with chitosans of varying DP was investigated by TM-AFM imaging. Polyplexes prepared in MQ H_2O at A/P-

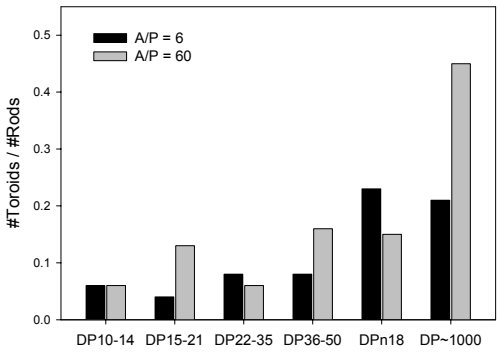

Figure 2: Ratio between the fraction of toroids and rods in the population when using chitosans of varying DP to compact pDNA. The pDNA-chitosan complexation was performed in water at A/P-ratios of 6 (black bars) and 60 (gray bars), respectively.

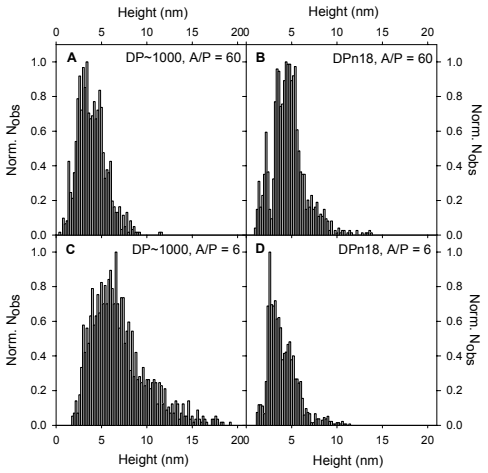

Figure 3: Normalized height distributions of the rodlike complexes obtained when compacting pDNA with the chitosans DP ~ 1000 (A, C) and DPn18 (B, D), respectively, in MQ H_2O at the two A/P-ratios 60 (A, B) and 6 (C, D).

ratios of 6 and 60 were chosen for this structural analysis to allow comparison to polyplexes employed in previous transfection studies [5, 6, 21]. The structures observed with AFM revealed that both HDP and LDP chitosans compact DNA into rodlike, toroidal and globular structures. Examples of structures observed when using HDP chitosans (DP~1000) and different chitosan oligomers to compact pDNA at an A/P-ratio of 60 are given in Figure 1. Whereas LDP chitosans tended to form fuzzy structures when complexed with pDNA at A/P=60 (Figure 1B-F), this was not the case when HDP chitosans were employed (Figure 1A). The term fuzzy structures here refer to complexes that appear to have a soft shell of oligomers surrounding its core.

The relative abundance of the polyplex geometries at the different conditions was compared by collecting polyplexes (~100) from several AFM topographs. The toroid-to-rod ratio obtained when using LDP chitosans was within the range 0.06-0.23 for all chitosan DPs, and was not altered by an increase in the A/P-ratio from 6 to 60 (Figure 2). Increasing the A/P-ratio from 6 to 60 for the HDP chitosan, on the other hand, resulted in an increase in the toroid-to-rod ratio from 0.21 to 0.45 (Figure 2). Detailed analysis of the size of the structures, determined as the height along the complex (Figure 3) and its contour length (Table 1), did not reveal any differences among complexes formed using either HDP or various LDP chitosans at A/P=60. The distributions of the heights of the polyplexes all showed a peak value close to 4 nm, independent on the chain length of the chitosan employed. However, whereas the height distributions obtained for HDP chitosan-DNA complexes became broader and slightly shifted towards larger heights when the A/P-ratio was reduced to 6, the structures obtained from LDP chitosans were not affected by this altered A/P-ratio (Figure 3).

Stability of polyplexes exposed to heparin and hyaluronic acid

The stability of the DNA-chitosan polyplexes when exposed to the biological polyanion heparin was studied by both AFM imaging and by determining changes in the EtBr-DNA fluorescence. Since the results obtained from two techniques were consistent, the effect of various parameters on the stability of DNA-chitosan complexes was studied mainly by the fluorescence

Table 1: Contour lengths of the toroidal and rodlike complexes formed when mixing pDNA with HDP chitosan (DP~1000) and LDP chitosans (oligomers) with DP ranging from 10 to 50.

Chitosan	Rods <L_c> ± sd (nm)		Toroids <L_c> ± sd (nm)	
	A/P 6	A/P 60	A/P 6	A/P 60
DP10-14	113 ± 37(N=113)	115 ± 37(N=51)	75 ± 25(N=7)	82 ± 11(N=3)
DP15-21	110 ± 41(N=92)	157 ± 60(N=111)	89 ± 8 (N=3)	98 ± 35(N=14)
DP22-35	110 ± 42(N=63)	114 ± 38(N=49)	93 ± 44(N=5)	124 ± 17(N=4)
DP36-50	118 ± 46(N=116)	140 ± 53(N=64)	154 ± 76(N=9)	110 ± 42(N=10)
DPn18	141 ± 67(N=91)	166 ± 82(N=68)	86 ± 24(N=21)	110 ± 60(N=9)
DP~1000	75 ± 29 (N=206)	117 ± 47(N=114)	80 ± 40(N=44)	130 ± 53(N=51)

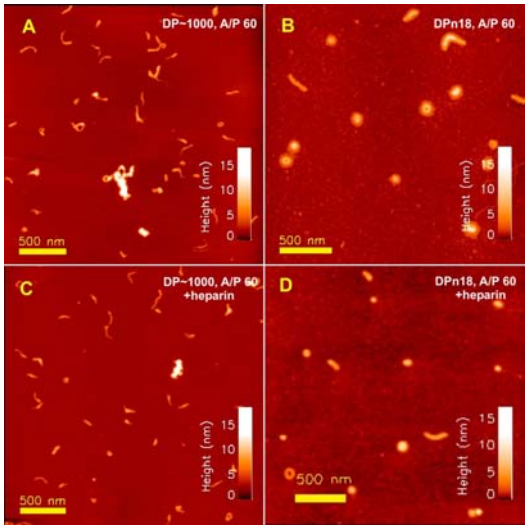

Figure 4: TM-AFM height topographs of pDNA-chitosan complexes before (A, B) and after two hours exposure to heparin ($c_{heparin}$ = ½ c_{DNA} = 5µg/mL; $q_{heparin}/q_{DNA}$ ~ 1) at room temperature (C, D). The two chitosans DP ~ 1000 (A, C) and DPn18 (B, D), respectively, were complexed with pDNA in MQ H_2O. An amount of chitosan corresponding to A/P=60 was employed.

assay and complementary information obtained for selected parameters with the AFM.

pDNA (10µg/mL) compacted by chitosan DP~1000 and DPn18, respectively, at an A/P-ratio of 60 (in MQ H_2O) were exposed to 5µg/mL heparin for two hours at room temperature. Since the equivalent molecular weight per unit charge of DNA is almost twice that of heparin, this mass concentration ratio corresponds to a heparin to DNA average charge ratio in the solution ($q_{heparin}/q_{DNA}$) of ~1. As seen from the AFM topographs, heparin did not induce dissociation of the pDNA-chitosan complexes at an A/P-ratio of 60, independent of the chitosan used (Figure 4). Neither did an increase in the temperature to 37°C during exposure cause destabilization of the polyplexes (data not shown). Whereas exposure to heparin affected the structure of the polyplexes made from LDP chitosan by making them less fuzzy, no structural changes were evident in the AFM topographs for polyplexes made from HDP chitosan (Figure 4). Decreasing the amount of chitosan used for complex formation to A/P=2 yielded a partly destabilization of the polyplexes following exposure to heparin for 2 hours. Dissociation of the polyplexes was seen as a presence of uncomplexed pDNA alongside a few remaining compacted structures (Figure 5). Furthermore, the tendency to release pDNA from the complexes appeared to be more pronounced when the temperature during incubation with heparin was increased from room temperature to 37°C (Figure 5).

Recording the fluorescence emission of EtBr labeled linear DNA upon addition of chitosan, showed that both DPn18 and DP~1000 chitosans induced a strong concentration dependent decrease in the fluorescence

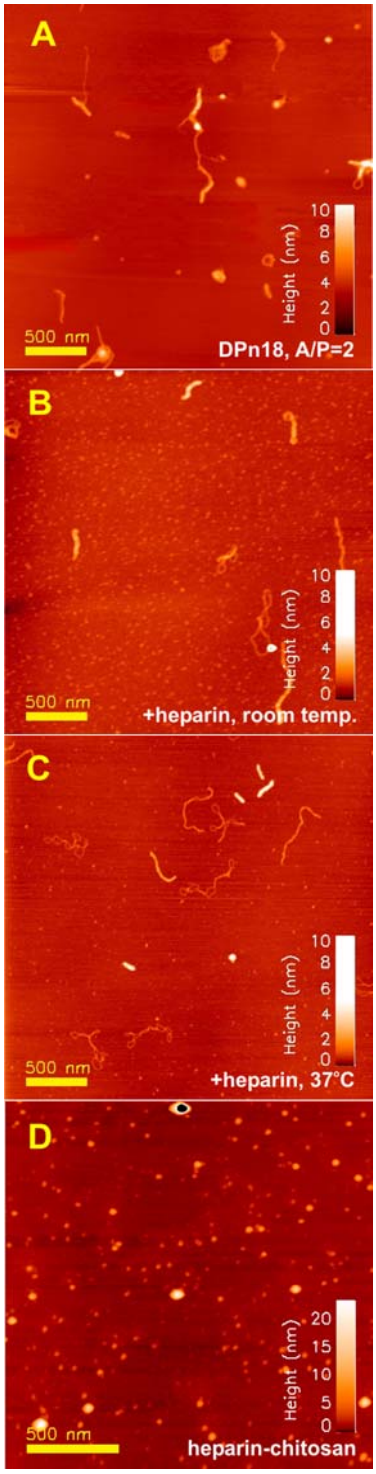

Figure 5: TM-AFM height topographs illustrating the release of pDNA from DNA-chitosan polyplexes upon exposure to heparin ($c_{heparin}$ = ½ c_{DNA} = 5µg/mL; $q_{heparin}/q_{DNA}$ ~ 1) for two hours. Complexation was performed in MQ H_2O employing the chitosan DPn18 at an A/P-ratio of 2. The images show the compacted pDNA before (A) and after exposure to heparin at room temperature (B) and at 37°C (C). Complexes formed from mixing heparin and chitosan are shown in (D).

intensity. Exposing the polyplexes to heparin gave a recovery in the fluorescence signal, depending on both the A/P-ratio and the heparin concentration. In general, the higher A/P-ratio, the more heparin was required to destabilize the DNA-chitosan complexes (Figure 6). Although the trends were similar when using HDP and LDP chitosans, the DNA-LDP chitosan complexes appeared to be more easily dissociated than the DNA-HDP chitosan complexes. Consistent with observations by AFM, the fluorescence measurements showed a transition from compacted DNA to a partly dissociated state around an A/P-ratio of 2 after exposure to heparin at a mass concentration equal to half that of the DNA, $c_{heparin}$ = ½·c_{DNA} ($q_{heparin}/q_{DNA}$~1) (Figure 6). Similar trends were observed when performing the measurements at a controlled pH (6.5) and I = 150 mM (Figure 7). The ability of the DNA-chitosan complexes to resist dissociation increased with increasing chitosan chain length (Figure 7). The fluorescence data showed that the degree of DNA compaction at low A/P-ratios was quite different when using HDP and LDP chitosans (Figure 6 and 7). At conditions where the LDP chitosan-DNA complexes were easily dissociated, the reduction in the fluorescence intensity had not reached its minimum (indicating that DNA was not fully compacted) before addition of heparin. To obtain information about the selectivity of chitosan binding to heparin compared to DNA, chitosan was titrated to a solution containing DNA and heparin ($c_{heparin}$ = c_{DNA}). The results showed that the presence of heparin in the solution completely inhibited the chitosan from binding to DNA (Figure 8).

Unlike heparin, hyaluronic acid (HA) was found not to induce dissociation of the DNA-chitosan

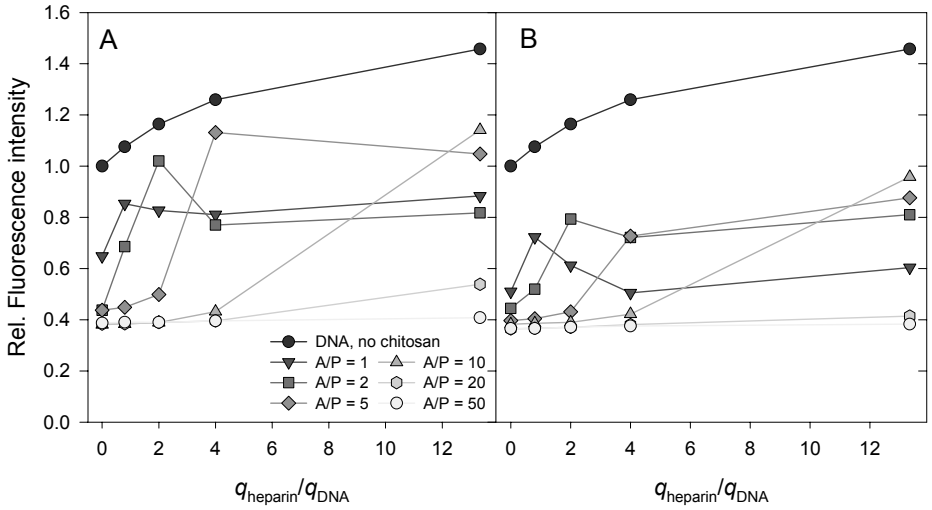

Figure 6: The destabilization of DNA-chitosan complexes at various A/P-ratios by exposure to increasing amounts of heparin, measured as a recovery in the EtBr-DNA fluorescence. Fluorescence intensities were recorded in well plates after two hours incubation of the polyplexes with heparin. The plotted values represent the measured intensities at the various conditions relative to the intensity recorded for DNA-EtBr before addition of chitosan and heparin. The amount of heparin used for destabilization was given in terms of $q_{heparin}$ relative to q_{DNA}. The chitosans DPn18 (A) and DP~1000 (B) were used to compact calf thymus DNA (7.5μg/mL) in MQ H_2O.

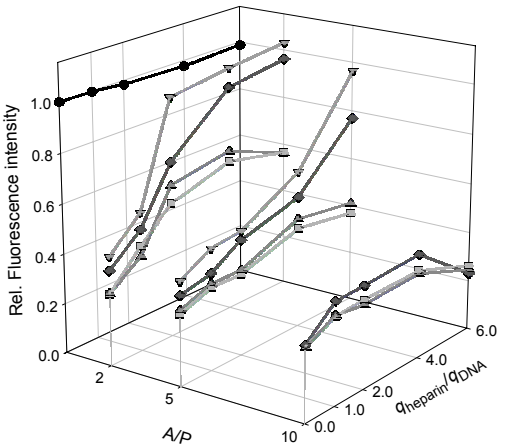

Figure 7: The destabilization of DNA-chitosan complexes as a function of the chitosan chain length and the A/P-ratio when exposed to increasing amounts of heparin. The reported intensities at various conditions are relative to the intensity determined for DNA-EtBr before addition of chitosan (•) and heparin. The chitosans DP ~ 1000 (Δ), DP ~ 200 (□), DPn18 (◇) and DP15-21 (▽), respectively, were used to compact calf thymus DNA (5μg/mL) in a buffer solution of pH 6.5 and *I*=150 mM.

complexes (data not shown). This was found by exposing DNA-chitosan complexes with different A/P-ratios to increasing amounts of HA at pH 6.5 and I = 150 mM. The HA concentrations used was similar to those employed for heparin, corresponding to HA to DNA charge ratios ranging from 0.4 to 2.5. Even polyplexes prepared at a low A/P-ratio were unaffected when exposed to large HA-concentrations. Furthermore, titration of chitosan to a solution of DNA and HA showed that unlike heparin, the binding of chitosan to DNA was unaffected by the presence of HA in the solution (data not shown).

Discussion

Heparin and HA are present in the extracellular matrix surrounding the cells as well as intracellularly and on the cell surface of various cell types [26-28]. Interaction between polyplexes and these GAGs may thus impede the transport through the extracellular matrix, across the plasma membrane, and through the cytoplasm. Positively charged polyplexes may act as a substrate for binding of anionic substances, impeding the gene delivery by altering the cellular uptake and/or the intracellular trafficking. Uptake of

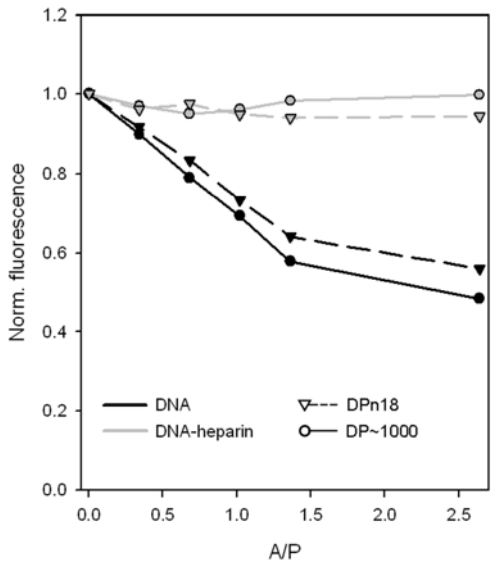

Figure 8: Titration curves obtained when titrating chitosan (DPn18 (circles) and DP ~ 1000 (triangles)) to a DNA-EtBr solution in the presence of heparin ($c_{heparin}$ = c_{DNA} = 5µg/mL; $q_{heparin}/q_{DNA}$ ~ 2) at pH 6.5 and I = 150 mM. The DNA used was the calf thymus DNA.

polyplexes with bound heparin and heparan sulfate are reported to strongly inhibit transfection of the polyplexes, whereas the binding of HA are not found to limit the transfection [29]. Complexes bound to different GAGs are therefore suggested to be directed to different paths inside the cell [29, 30]. Different concentrations of HA and heparin in different types of tissue (e.g. HA occurs to a large extent in connective tissue where there is no heparin [28]) thus represent different barriers to gene delivery of various types of tissue. If polyplexes are dissociated by the interaction with GAGs before they reach their target cell, transfection is expected to be reduced because of reduced cellular uptake. Furthermore, very stable polyplexes also seem to be unfavorable for gene delivery as they will not dissociate and release DNA intracellularly.

Formation and stability of DNA-chitosan complexes were here studied by AFM imaging and EtBr fluorescence displacement. Both techniques revealed that the ability of DNA-chitosan polyplexes to resist dissociation upon exposure to heparin increased with increasing A/P-ratio (Figure 4, 5, 6 and 7), and that LDP chitosans released DNA more easily than HDP chitosans (Figure 6 and 7). The ability of the polyplexes to release DNA was further seen to be reduced in buffer solution with I = 150 mM compared to polyplexes in MQ H_2O.

The increased polyplex stability observed when increasing the chitosan chain length at a given A/P ratio, indicates that higher DP chitosans yield stronger interactions with DNA. HDP chitosans (DP~1000) have previously been reported to have higher affinity for DNA binding than shorter chitosans (DP~25) [23]. This was based on the observation that larger amounts of LDP chitosans, compared to HDP chitosans, were necessary to fully compact DNA into well defined structures. Similar observations were done here when titrating chitosan to the DNA-EtBr solution, as a larger A/P-ratio was required for the LDP chitosans to reach minimum fluorescence intensity, indicating fully compacted DNA (Figure 6 and 7). Such molecular weight dependence has also been reported for DNA-PLL compaction [31]. Since the binding constant between a lattice like ligand and an oppositely charged polymer is reported to increase with the valency of the ligand [32, 33], the higher affinity of HDP chitosans for DNA is believed to be due to the increased valency following the increased chain length. The observed differences in polyplex stability are thus expected to be related to the polycation valency. The interplay between the A/P-ratio and various chitosan parameters such as chain length and F_A is reported to be important for the in vitro transfection efficiency [5, 6, 15]. Shorter chitosans were found to be

preferable at high A/P ratios, whereas longer chitosans were beneficial at low A/P ratios. It was further reported that LDP chitosan yielded a higher maximum transfection than HDP chitosan (when taken into consideration that maximum transfection is obtained at different A/P ratios for the different chitosans) [6, 21]. The importance of polycation charge has also been reported for other polycations with a reduction of the positive charges yielding increased transfection efficiencies [34, 35].

The increased stability obtained when increasing the amounts of chitosan used for complexation indicates that the intersegment attraction within the polyplex depends on the A/P ratio and/or that excess amounts of chitosan are required in the solution to prevent the polyplexes from dissociating. When large stoichiometric excess of chitosan is used for complex formation, some material can be expected to occur as uncomplexed chitosan. The addition of negatively charged heparin to the solution is thus expected to bind to uncomplexed chitosan and might explain the increased ability of the polyplexes to resist dissociation at higher A/P-ratios. This was confirmed by AFM-imaging showing that complexation of these two polymers gave small globular structures (data not shown). If excess amounts of chitosan are required for the polyplex to be stable, removal of free chitosan from the polyplex surroundings will initiate its dissociation. This was tested by exposing the polyplexes to HA, which also binds chitosan and form globular structures (data not shown). However, in contrast to heparin, exposure to high concentrations of HA ($q_{HA} \sim 2.5 \cdot c_{DNA}$) did not cause dissociation of any of the DNA-chitosan complexes (data not shown). Even when compensating for the higher equivalent mass pr. charge of HA compared to heparin (by increasing the HA concentration to yield comparable charge concentrations), HA was unable to dissociate the DNA-chitosan complexes.

The large differences in the ability of heparin and HA to dissociate the polyplexes is in accordance with previous studies [12] and has been suggested to be due to their different charge densities [29, 30]. Whereas the average distance between the charges, b, is 0.24 nm for heparin [36], it is 0.98 nm for HA [37]. Destabilization studies involving other polyanions with b parameters between that of heparin and HA (alginate and xanthan, both having b = 0.4-0.5) seem to provide supplementary information, indicating that the charge density might be important for the ability of a polyanion to destabilize compacted DNA [38]. Titration of chitosan to the EtBr-DNA solution in the presence of heparin ($q_{heparin} \sim 2q_{DNA}$) showed that the presence of heparin in the solution completely prevented chitosan from binding to DNA (Figure 8). Although $q_{heparin} > q_{DNA}$, the observation that no reduction in the DNA-EtBr fluorescence was determined until $q_{chitosan} > q_{DNA}$ indicates that heparin was preferred over DNA for chitosan binding. Similar experiments with HA did however not affect the interaction between DNA and chitosan (data not shown). Such titration curves have previously been used to determine the relative binding constant of a polycation to a polyanion as compared to DNA [39, 40]. Our results thus indicate that the ability of a polyanion to dissolve polyplexes is closely related to the polycation-polyanion interaction strengths. The stronger binding between heparin and chitosan, compared to DNA and chitosan, was also seen as an increased tendency of DNA release when increasing the temperature during heparin exposure. Since increasing the temperature facilitates the transition

from kinetically trapped states to a lower free energy state, this indicates that the heparin-chitosan complexes have lower free energy than the DNA-chitosan complexes.

The observation of a maximum in the fluorescence recovery upon adding increasing amounts heparin indicates that after being released from the polyplexes, DNA experiences structural changes that cause EtBr to be expelled from the helix again. These structural changes may be explained by interaction between DNA and positively charged chitosan-heparin complexes emerging in the solution upon addition of heparin and might result in the formation of aggregated structures.

The effect of chitosan chain length and concentration on the polyplex stability were found to induce similar trends when performing experiments in MQ H_2O and buffer (pH 6.5, I = 150 mM). Although different heparin to DNA charge ratios were employed, the trends observed in Figures 6 and 7 can be compared and indicate that the polyplexes appear to be more easily dissociated in MQ H_2O than in the buffer. At an A/P-ratio of 2, twice as much heparin was required to reach maximum fluorescence recovery in buffer compared to in MQ H_2O. Also, whereas polyplexes prepared at A/P=10 appeared to dissociate in MQ H_2O when adding large amounts of heparin (Figure 6), this was not the case in the buffer (Figure 7). pH in MQ H_2O was measured to be almost the same as in buffer (~6.5), it is therefore most likely that the weaker dissociation is due to the increased ionic strength in the buffer. Since the association between two oppositely charged polyelectrolytes is reported to decrease with increasing I [33, 41], altered I is expected to affect both the DNA-chitosan interactions and the heparin-chitosan interactions. Consistent with this the electrostatic interaction between heparin and positively charged peptides is reported to become weaker when increasing I [42]. Although increased I found to induce dissociation of DNA-chitosan polyplexes, they are found to rather stable for I < 200 mM (Strand, S. Danielsen, S. Christensen, B. E. Vårum, K. M., unpublished data). The reduced tendency for DNA-chitosan dissociation at the higher ionic strength thus implies that the dissociation is affected by chitosan sequestration by the added heparin, with a reduced relative binding constant following the increase in I preventing the dissociation.

The titration curves (Figure 6 and 7) indicate that at A/P-ratios reported to yield optimum transfection in vivo (A/P=60 for LDP chitosan [21]) no dissociation occurs. However, whereas the dissociation studies were performed at pH 6.5 (where transfection is reported to be very low [16]), the polyplexes are exposed to increased pH in tissue in vivo. Such increased pH is seen to increase the DNA release from polyplexes (Strand, S. Danielsen, S. Christensen, B. E. Vårum, K. M., unpublished data).

The structure and dimension of the DNA-chitosan polyplexes was observed to depend on both the chain length and concentration of chitosan used for polyplex formation. Hardly any toroids were observed when LDP chitosans were used to compact pDNA, while making up a considerable fraction of the morphologies when using HDP chitosan at large concentrations. Although all chitosans yielded stable complexes at high A/P-ratios, the general tendency was an increased stability with increasing chitosan chain length and concentration. Together with the observed tendency of increased toroid formation for HDP chitosans with increasing A/P-ratio, this indicates that the toroidal structures represent a more stable structure than the rods. The relation between structure and stability

is important in determining the preferred structures for gene delivery purposes. Since delivery systems based on LDP chitosans are reported to be more efficient in terms of transfection than those based on HDP chitosans, the toroid seem to be an unfavorable structure for these purposes.

Conclusion

The stability of DNA-chitosan complexes upon exposure to the important biological polyanions heparin and hyaluronic acid reveal that polyplex dissociation depends on chitosan chain length and A/P ratio, as well as the properties of the polyanions. Whereas heparin was able to dissociate the polyplexes, with increased heparin concentrations being required when increasing the chitosan chain length and A/P-ratio, hyaluronic acid was unable to dissociate the DNA-chitosan complexes. Polyplex stability is identified as an important parameter to control in designing efficient polycation based gene delivery systems. Varying the chitosan chain length thus appears to provide a tool for controlling the ability of DNA-chitosan complexes to deliver therapeutic genes to cells.

Acknowledgement

This work is supported by The Norwegian Research Council (grant numbers 129104/420 and 121894/420). We are grateful to dr. K. M. Vårum (Dept. of Biotechnology, Norwegian University of Science and Technology, NO-7491 Trondheim) for providing us with the chitosans. We also thank prof. T. B. Melø for many helpful discussions.

References

[1] T. Merdan., J. Kopecek. and T. Kissel, Prospects for cationic polymers in gene and oligonucleotide therapy against cancer, Adv. Drug Deliv. Rev. 54 (2002) 715-758.

[2] S.C. De Smedt., J. Demeester. and W.E. Hennink, Cationic polymer based gene delivery systems, Pharm. Res. 17 (2000) 113-126.

[3] F.C. MacLaughlin., R.J. Mumper., J. Wang., J.M. Tagliaferri., I. Gill., M. Hinchchliffe. and A.P. Rolland, Chitosan and depolymerized chitosan oligomers as condensing carriers for in vivo plasmid delivery, J. Control. Release 56 (1998) 259-272.

[4] P. Erbacher., S. Zou., T. Bettinger., A.-M. Steffan. and J.-S. Remy, Chitosan-based vector/DNA complexes for gene delivery: Biophysical characteristics and transfection ability, Pharm. Res. 15 (1998) 1332-1339.

[5] M. Köping-Höggård., I. Tubulekas., H. Guan., K. Edwards., M. Nilsson., K.M. Vårum. and P. Artursson, Chitosan as a nonviral gene delivery system. Structure-property relationship and characteristics compared with polyethylenimine *in vitro* and after lung administration *in vivo* , Gene Ther. 8 (2001) 1108-1121.

[6] M. Köping-Höggård., Y.S. Mel'nikova., K.M. Vårum., B. Lindman. and P. Artursson, Relationship between the physical shape and the efficiency of oligomeric chitosan as a gene delivery system *in vitro* and *in vivo*, J. Gene Med. 5 (2003) 130-141.

[7] L. Illum, Chitosan and its use as a pharmaceutical excipient, Pharm. Res. 15 (1998) 1326-1331.

[8] M. Lee., J.W. Nah., Y. Kwon., J.J. Koh., K.S. Ko. and S.W. Kim, Water-soluble and low molecular weight chitosan-based plasmid DNA delivery, Pharm. Res. 18 (2001) 427-431.

[9] S.C.W. Richardson., H.V.J. Kolbe. and R. Duncan, Potential of low molecular mass chitosan as a DNA delivery system: biocompatibility, body distribution and ability to complex and protect DNA, Int. J. Pharm. 178 (1999) 231-243.

[10] D. Fischer., T. Bieber., Y. Li., H.P. Elsässer. and T. Kissel, A novel non-viral vector for DNA delivery based on

low molecular weight, branched polyethylenimine: Effect of molecular weight on transfection efficiency and cytotoxicity, Pharm. Res. 16 (1999) 1273-1279.

[11] D.V. Schaffer., N.A. Fidelman., N. Dan. and D.A. Lauffenburger, Vector unpacking as a potential barrier for receptor-mediated polyplex gene delivery, Biotechnol. Bioeng. 67 (2000) 598-606.

[12] M. Ruponen., S. Ylä-Herttuala. and A. Urtti, Interactions of polymeric and liposomal gene delivery systems with extracellular glycosaminoglycans: physicochemical and transfection studies, Biochim. Biophys. Acta 1415 (1999) 331-341.

[13] I. Moret., J.E. Peris., V.M. Guillem., M. Benet., F. Revert., F. Dasi., A. Crespo. and S.F. Alino, Stability of PEI-DNA and DOTAP-DNA complexes: effect of alkaline pH, heparin and serum, J. Control. Release 76 (2001) 169-181.

[14] T. Ishii., Y. Okahata. and T. Sato, Mechanism of cell transfection with plasmid/chitosan complexes, Biochim. Biophys. Acta 1514 (2001) 51-64.

[15] K. Romøren., S. Pedersen., G. Smistad., Ø. Evensen. and B.J. Thu, The influence of formulation variables on in vitro transfection efficiency and physiochemical properties of chitosan-based polyplexes, Int. J. Pharm. 261 (2003) 115-127.

[16] T. Sato., T. Ishii. and Y. Okahata, In vitro gene delivery mediated by chitosan. Effect of pH, serum, and molecular mass of chitosan on the transfection efficiency, Biomaterials 22 (2001) 2075-2080.

[17] H. Noguchi. and K. Yoshikawa, Morphological variation in a collapsed single homopolymer chain, J. Chem. Phys. 109 (1998) 5070-5077.

[18] V.A. Ivanov., M.R. Stukan., V.V. Vasilevskaya., W. Paul. and K. Binder, Structures of stiff macromolecules of finite chain length near the coil-globule transition: A Monte Carlo simulation, Macromol. Theory Simul. 9 (2000) 488-499.

[19] V.A. Ivanov., W. Paul. and K. Binder, Finite chain length effects on the coil-globule transition of stiff-chain macromolecules: A Monte Carlo simulation, J. Chem. Phys. 109 (1998) 5659-5669.

[20] K. Tømmeraas., K.M. Vårum., B.E. Christensen. and O. Smidsrød, Preparation and characterisation of oligosaccharides produced by nitrous acid depolymerisation of chitosan, Carbohydr. Res. 333 (2001) 137-144.

[21] M. Köping-Höggård., K.M. Vårum., M. Issa., S. Danielsen., B.E. Christensen., B.T. Stokke. and P. Artursson, Improved chitosan-mediated gene delivery based on easily dissociated chitosan polyplexes of highly defined chitosan oligomers, Gene Ther. 11 (2004) 1441-1452.

[22] G. Maurstad., S. Danielsen. and B.T. Stokke, Analysis of compacted semiflexible polyanions visualized by atomic force microscopy: Influence of chain stiffness on the morphologies of polyelectrolyte complexes, J. Phys. Chem. B 107 (2003) 8172-8180.

[23] S. Danielsen., K.M. Vårum. and B.T. Stokke, Structural analysis of chitosan mediated DNA condensation by AFM: Influence of chitosan molecular parameters, Biomacromolecules 5 (2004) 928-936.

[24] J.-B. LePecq. and C. Paoletti, A fluorescent complex between ethidium bromide and nucleic acids, J. Mol. Biol. 27 (1967) 87-106.

[25] A.J. Geall. and I.S. Blagbrough, Rapid and sensitive ethidium bromide fluorescence quenching assay of polyamine conjugate-DNA interactions for the analysis of lipoplex formation in gene therapy, J. Pharm. Biomed. Anal. 22 (2000) 849-859.

[26] S.O. Kolset., K. Prydz. and G. Pejler, Intracellular proteoglycans, Biochem. J. 379 (2004) 217-227.

[27] T.N. Wight., D.K. Heinegård. and V.C. Hascall, Proteoglycans structure and function, in: Hay, E. (Ed.), Cell biology of extracellular matrix, Plenum press, New York, 1991, pp. 45-78.

[28] D.K. Apps., B.B. Cohen. and C.M. Steel, Biochemistry, Baillière Tindall, London, 1992, pp. 343-354.

[29] M. Ruponen., P. Honkakoski., S. Rönkkö., J. Pelkonen., M. Tammi. and A. Urtti, Extracellular and intracellular barriers in non-viral gene delivery, J. Control. Release 93 (2003) 213-317.
[30] M. Ruponen., S. Rönkkö., P. Honkakoski., J. Pelkonen., M. Tammi. and A. Urtti, Extracellular glycosaminoglycans modify cellular trafficking of lipoplexes and polyplexes, J. Biol. Chem. 276 (2001) 33875-33880.
[31] P.R. Dash., V. Toncheva., E. Schacht. and L.W. Seymour, Synthetic polymers for vectorial delivery of DNA: characterisation of polymer-DNA complexes by photon correlation spectroscopy and stability to nuclease degradation and disruption by polyanion in vitro, J. Control. Release 48 (1997) 269-276.
[32] D.P. Mascotti. and T.M. Lohman, Thermodynamic extent of couterion release upon binding oligolysines to single-stranded nucleic acids, Proc. Natl. Acad. Sci. U. S. A. 87 (1990) 3142-3146.
[33] D. Stigter. and K.A. Dill, Binding of ionic ligands to polyelectrolytes, Biophys. J. 71 (1996) 2064-2074.
[34] P. Erbacher., A.C. Roche., M. Monsigny. and P. Midoux, The reduction of the positive charges of polylysine by partial gluconoylation increases hte transfection efficiency of polylysine/DNA complexes, Biochim. Biophys. Acta 1324 (1997) 27-36.
[35] D. Putnam., C.A. Gentry., D.W. Pack. and R. Langer, Polymer-based gene delivery with low cytotoxicity by unique balance of side-chain termini, Proc. Natl. Acad. Sci. U. S. A. 98 (2001) 1200-1205.
[36] J. Mattai. and J.C.T. Kwak, Mg and Ca binding to heparin in the presence of added univalent salt, Biochim. Biophys. Acta 677 (1981) 303-312.
[37] E. Atkins, Polysaccharides: Biomolecular shape and structure, in: Happey, F. (Ed.), Applied fibre science, **3**, Academic press, London, 1979, pp. 311-369.
[38] S. Danielsen., G. Maurstad. and B.T. Stokke, DNA-polycation complexation and polyplex stability in the presence of competing polyanions, Biopolymers (2004, in press).
[39] A.N. Zelikin., E.S. Trukhanova., D. Putnam., V.A. Izumrudov. and A.A. Llitmanovich, Competitive reactions in solutions of poly-L-histidine, calf thymus DNA, and synthetic polyanions: determining the binding constants of polyelectrolytes, J. Am. Chem. Soc. 125 (2003) 13693-13699.
[40] B.F. Cain., B.C. Baguley. and W.A. Denny, Potential antitumor agents. 28. deoxyribonucleic acid polyintercalating agents, J. Med. Chem. 21 (1978) 658-668.
[41] D. Matulis., I. Rouzina. and V.A. Bloomfield, Thermodynamics of DNA binding and condensation: Isothermal titration calorimetry and electrostatic mechanism, J. Mol. Biol. 296 (2000) 1053-1063.
[42] D.P. Mascotti. and T.M. Lohman, Thermodynamics of charged oligopeptide-heparin interactions, Biochemistry (N. Y.) 34 (1995) 2908-2915.

Paper III

Paper III is not included due to copyright.

Paper IV

DNA-polycation complexation and polyplex stability in the presence of competing polyanions

Signe Danielsen,* Gjertrud Maurstad* and Bjørn T. Stokke§

Biophysics and Medical Technology, Dept. of Physics,
The Norwegian University of Science and Technology, NTNU, NO-7491 Trondheim, Norway

Abstract

Polyelectrolyte complex (polyplex) formation was studied by employing tapping mode atomic force microscopy (AFM) and an ethidium bromide fluorescence assay. The polycations chitosan and poly-L-lysine were used to compact DNA and the stability of the polyplexes was evaluated upon exposure to competing polyanions (alginate and xanthan). Furthermore, the relative preference of these polycations for DNA and the competing polyanion was investigated. The results showed that neither poly-L-lysine nor chitosan displayed any selectivity in binding to DNA relative to the competing polyanions, demonstrating the importance of electrostatics in the binding of a polycation to a polyanion. However, the ability of the polyanions to destabilize the DNA-polycation complexes depended on both the polyanion and the polycation employed, indicating that also polymer specific properties are important for the complexation behavior and polyplex stability. Destabilization experiments further showed that annealing yielded complexes that were less prone to disruption upon subsequent exposure to alginate. Annealing experiments of plasmid DNA-chitosan complexes showed an increased fraction of rods following temperature treatment, indicating that the rods most likely are the more stable morphology for this system.

Keywords: DNA, xanthan, alginate, chitosan, poly-L-lysine, AFM, fluorescence

This is a preprint of an article published in Biopolymers, vol 77(2), 2004, 86-97.

http://www3.interscience.wiley.com/journal/28380/home

Accepted for publication, Biopolymers

* The authors contributed equally to the work
§ Corresponding author: Bjørn T. Stokke, Dept. of Physics, NTNU, NO-7491 Trondheim, NORWAY,
Fax: +47 73 59 77 10, e-mail: bjorn.stokke@phys.ntnu.no

Introduction

Oppositely charged polyelectrolytes interact through an electrostatic exchange mechanism and form polyelectrolyte complexes (polyplexes) when mixed in solution.[1] The release of counterions from the polyelectrolytes upon interaction promotes the polyplex formation by increasing the entropy of the system. Polyplexes represent different levels of organization. Experimental studies have verified the presence of ordered structures within different polyplex systems.[2] The transition of an extended polymer into ordered structures can also be mediated by a poor solvent in which the polymer chains tend to collapse into a compact state to minimize the polymer-solvent contacts. This has been explored in simulation studies to predict the type of structures formed upon collapse of a polymer. For semiflexible chains such as DNA, there will be substantial energetic penalties associated with sharp bends, thus favoring extended chains and preventing the formation of compact globular states. For a given range of chain stiffness and polymer segment attractions, the toroidal structure is predicted to be the stable one as this shape is believed to be a balance between the energy penalty associated with bending a relatively stiff chain, and the intersegment attraction between segments of the polymer chain.[3-5] The formation of the collapsed state can be viewed as driven by intersegment attraction, irrespective of the nature of the forces.[6] In the case of polyplex formation, the intersegment attraction is assumed to arise from local charge reversal.[7] Different polycations interacting with the polyanion may therefore represent various interaction strengths.

Ethidium bromide, EtBr, interacts with DNA mainly by intercalation between the base pairs in the double helix, resulting in a significant increase in the EtBr fluorescence intensity.[8] The ability of various species to interact with DNA and displace EtBr, yielding a subsequent decrease in the EtBr fluorescence, provides a convenient indirect way of measuring the affinity of polycations for DNA and to monitor the DNA compaction.[9] One of the motivations for studying polyplex formation is their potential application for gene delivery.[10-12] Both poly-L-lysine (PLL) and chitosan has been evaluated for this purpose. In this study these two polycations were employed and their ability to compact DNA was contrasted by means of AFM and EtBr fluorescence assay. The interaction between the polycations and DNA was further studied in mixtures of DNA and a competing polyanion, xanthan or alginate. The EtBr-assay was also applied to study the stability of compacted DNA when exposing the polyplexes to the competing polyanions. Xanthan and alginate are semiflexible polyanions possessing chain stiffness and equivalent mass per unit charge above and below, respectively, that of DNA. Employing such general polyions is thus believed to aid in understanding the general aspects of polyplex formation,[2] which is also of importance for the improvement of polycation-based gene delivery systems.

Materials and methods

Biopolymer samples

The linear calf thymus DNA (D-1501, M_w 10-15 $\times 10^6$g/mol, Sigma Aldrich) was employed in most of the DNA condensation studies. Xanthan (M_w 5×10^6g/mol) was purified from a fermentation broth (Statoil, Bioferm, Norway).[2] The employed alginate is from *Laminara hyperborea* stipe (FMC Biopolymers, Drammen, Norway), with a molecular weight ~ 450×10^3g/mol and a fraction of guluronic acid residues of 0.68. To compact the polyanions either a chitosan with a degree of acetylation (F_A) equal to 0.1 and a molecular weight of ~33 $\times 10^3$g/mol or a poly-L-lysine (PLL), M_w 22.1×10^3g/mol (P2658, Sigma Aldrich) was used. Additional experiments were

Table 1. Characterization of the polyelectrolyte samples used in this study, in terms of molecular weight (M_w), pK_a value, persistence length (L_p) and equivalent molecular weight per unit charge (m/q).

	M_w(10^3 g/mol)	pK_a	L_p (nm)	m/q (g/mol e^{-1})
Alginate[a,b]	450	3.38 (Man*p*A)[28] 3.65 (Gul*p*A)[28]	5-17[29,30]	170
DNA		1[31]	50[32-35]	330
Plasmid	2880			
Linear	10000-15000[c]			
Xanthan	5000	2.6-3.5[36,37]	120[38]	940
Chitosan[a]		6.5[39]	6-12[40]	
F_A=0.1	33			165
F_A = 0.15	196			167
Poly-L-lysine	22	10.68	1.8[41]	128

[a] The fraction of Man*p*A (alginate) and Glc*p*NAc (chitosan) varies among different samples of these polysaccharides.[42-44]
[b] For the alginate sample used, the fraction of α-Gul*p*A (F_G) is 0.68.
[c] Sigma product information

performed with the plasmid DNA pBR322 (4363 bp, M_w 2.88×10^6g/mol, Börhing Mannheim) and a chitosan F_A 0.15 (M_w 196×10^3g/mol). Chitosan stock solutions (1mg/mL) were prepared in acetic acid (1%), the other polymers were dissolved in MQ-water (1mg/mL), and further diluted in ammonium acetate (NH_4Ac) or acetate buffer at pH 5.5 and an ionic strength, c_s, of 5 or 150 mM before use. Table 1 summarizes the characteristics of the polyanion and polycation samples used in this study.

Polyelectrolyte complex formation

The complexation was studied in NH_4Ac or acetate buffer at two different ionic strengths (5mM and 150mM) and a pH equal to 5.5, chosen based on the pK_a-values of the polymers (Table 1). Complexes were formed by adding the chitosan- or PLL solution to the polyanion (PA) solution, yielding a final PA concentration, (c_{PA}) in the formulation of 5-10 μg/mL and a ratio between the maximum number of protonable primary amines on the polycation and the number of negatively charged groups on the PA from 1 to 10. In the case of DNA-polycation complexes this ratio is determined as the A/P-ratio, in which A and P refers to the charged groups of the polycation and DNA, respectively. The complexation was left to proceed for ~15 minutes. Annealing of xanthan-chitosan polyplexes is reported to drive the complexes to a more stable state.[13] DNA-polycation complexes were therefore subject to annealing experiments. The temperature was chosen below the melting temperature (T_m) of the DNA double helix:

$$T_m = 81.5°C + 16.6 \cdot \log c_s + 0.41 \cdot \chi_{CG}$$

with χ_{CG} being the fraction of CG pairs in the DNA,[14] and equal to 0.49 for calf thymus DNA and 0.52 for pBR322. For the

annealing experiments, the complexation reaction proceeded at room temperature (~20°C) for 15 minutes, followed by annealing of the polyplex solution in a thermostated water bath set at 50°C for 5.5 hours.

AFM imaging and analysis

Dried samples for AFM were prepared and imaged by tapping mode AFM in air using a Digital Instrument Multimode IIIa as described previously.[2,15] To evaluate the effect of annealing of pBR322-chitosan complexes, the AFM images of these structures were subject to quantitative analysis. The fractions of toroids and rods in the images were determined by sorting the complexes into characteristic ensembles based on the calculation of a shape factor (the asphericity index) for each individual species.[2] The structures (100-200 in each ensemble) were further analyzed to yield information about heights and contour lengths of the polyplexes as described previously.[2]

Ethidium bromide exclusion assay

The complexation of DNA with chitosan and PLL, respectively, and the effect of exposing the polyplexes to other polyanions were studied by recording the fluorescence obtained with the fluorescent probe ethidium bromide, EtBr (Sigma Aldrich). Intercalation of EtBr into DNA increases the fluorescence quantum yield of the dye.[8] Upon DNA compaction EtBr is expelled from the DNA-EtBr complex, causing a decrease in the fluorescence signal.[9] Consequently, destabilization of the DNA condensates is expected to cause a recovery of the fluorescence signal. EtBr (stock solution of 1 mg/mL) was added to the formulation to yield one dye molecule for every 2nd base pair. The fluorescence was measured in 1.5 mL cuvettes using a Spex Spectramate Fluorolog (Spex Industries, Inc., Metuchen, NJ USA). The excitation wavelength, λ_{ex}, was 511 nm

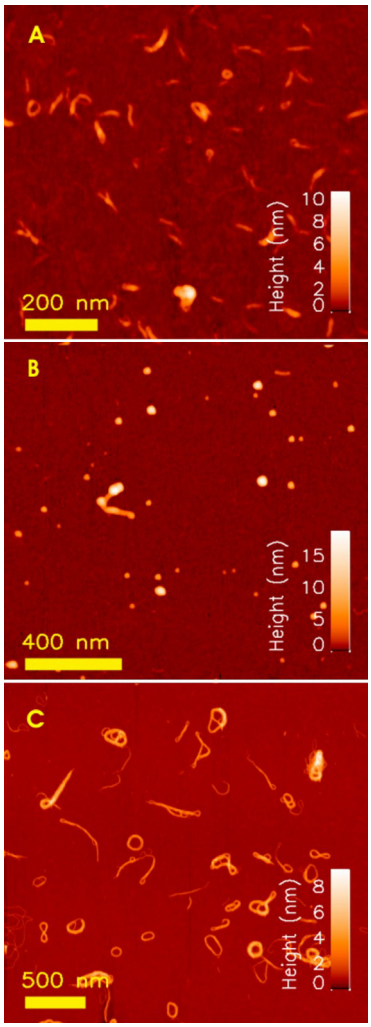

Figure 1. AFM topographs of polyelectrolyte complexes of chitosan (F_A 0.1) and alginate (A), DNA calf thymus (B) and xanthan (C). In all cases c_s = 5mM, and c_{PA} = 2-10 µg/mL.

and the emission spectrum from 500 nm to 700 nm was recorded. A measure of the fluorescence intensity was obtained from the spectrum by calculating the average intensity within the wavelengths 595-610 nm. In reporting the titration curves, the fluorescence intensity (I) was normalized relative to the fluorescence signal of DNA-EtBr (I_0) without subtracting the background fluorescence, and results from 2-3 independent experiments were averaged ($\langle I/I_0 \rangle$).

To investigate the compaction of DNA by chitosan and PLL, respectively, the fluorescence signal was recorded during stepwise addition of the polycations (PC) at time intervals of 15 minutes. Polyanions competing with DNA for the

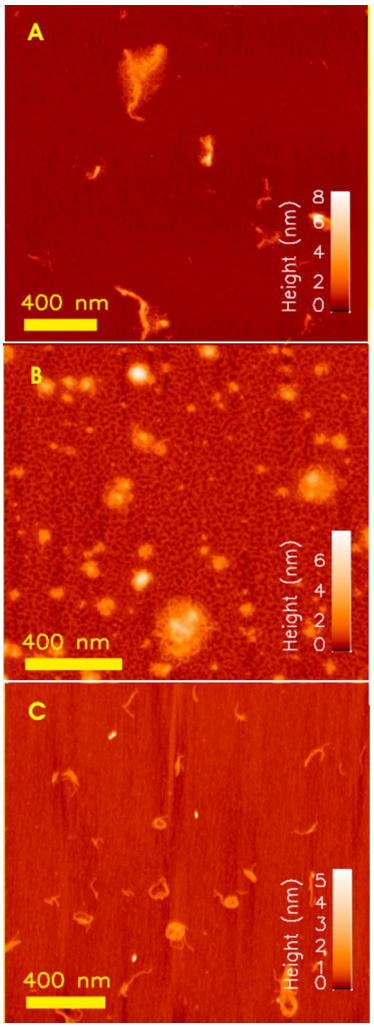

Figure 2. AFM topographs of polyelectrolyte complexes of PLL (M_w ~22×10^{3}g/mol) and alginate (A), DNA calf thymus (B) and xanthan (C). In all cases c_s = 5mM and c_{PA} = 2-10 µg/mL.

polycation will cause a less efficient reduction in the fluorescence signal upon polycation addition. To obtain information about the ability of the polycations to bind to alginate or xanthan instead of DNA, increasing amounts of the polycation was added to a mixture of DNA and one of these competing polyanions (PA) while recording the fluorescence. An efficient binding of the PC to the PA will be seen as a smaller reduction in the DNA-EtBr signal than in the absence of PA. The stability of the DNA-PC polyplexes (A/P = 2) when exposed to the competing PA (q_{PA}/q_{DNA} ~2.5) was studied by adding the EtBr and PA to the polyplex solution and measuring the fluorescence signal (λ_{em} =

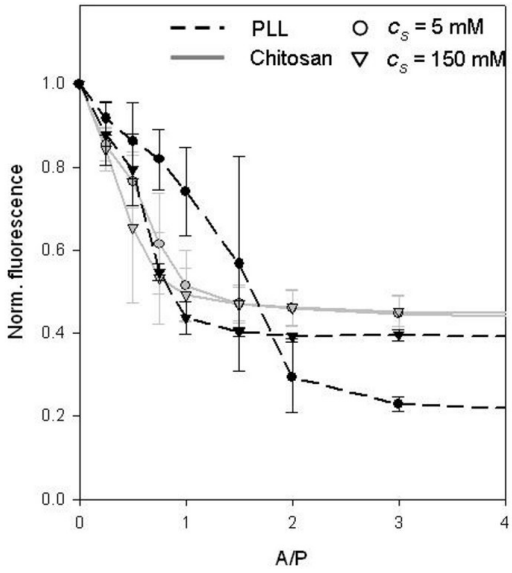

Figure 3. Titration curves illustrating the release of EtBr from calf thymus DNA (c_{DNA} = 10µg/ml) upon compaction with chitosan (grey) or PLL (black) at the two ionic strengths 5mM (circles) and 150mM (triangles).

599 nm and 603 nm) as a function of time for ~2 hours.

Results

Tapping mode AFM topographs of the polyanions alginate, DNA and xanthan complexed with chitosan (Figure 1A, B and C, respectively), showed that the different polyanions yield different polyplex structures.[2] Whereas chitosan compacted DNA (calf thymus) into globular shapes, toroidal as well as other species identified as metastable structures were observed for the xanthan-chitosan system.[13] The most flexible polyanion alginate was compacted into less well defined structures, however some toroidal-like and rodlike structures could be observed. Compaction of the polyanions with PLL at low ionic strength (5mM) yielded more hairy complexes, with polymer threads extending from the structures (Figure 2A, B and C, respectively). However, whereas both DNA-PLL and alginate-PLL complexes appeared to have a rather compact core with polymers extending from it, the

Table 2. The A/P-ratio at which the relative fluorescence intensity $\langle I/I_0 \rangle$ reaches its plateau value (transition A/P) for the titration of a polycation (chitosan or PLL) to a solution of DNA (c_{DNA}=10μg/mL) and a competing polyanion (alginate or xanthan) at c_s=5 mM.

PA	$\frac{q_{DNA}+q_{PA}}{q_{DNA}}$	Transition A/P	
		PLL	Chitosan
-	1	2-3	1-1.5
Xanthan	1.5	4-5	2-3
"	2	4.5-5.5	2.5-3.5
"	3	>10	5-6
Alginate	1.5	2-3	1.5-2
"	2	3-4	2.5-3.5
"	3	9-10	5-6

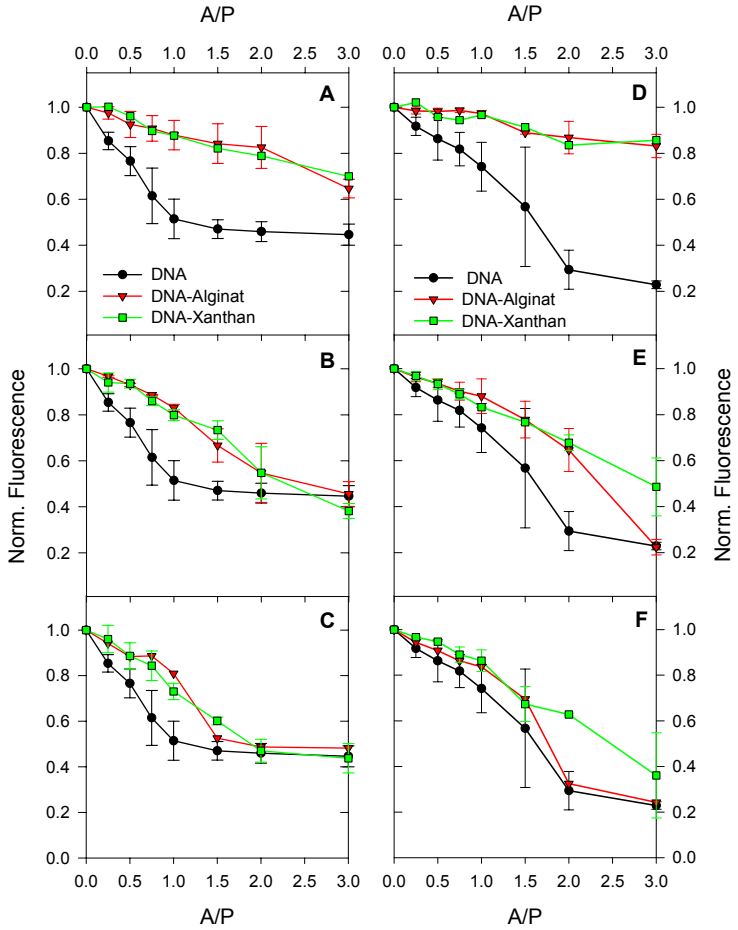

Figure 4. Titration of chitosan (left panel, A-C) or PLL (right panel, D-F) to EtBr-DNA in the presence of either alginate (red triangles) or xanthan (green squares). The experiments were performed with c_s = 5mM and c_{DNA} = 10μg/mL and the amount of either of the polyanions used was calculated to yield q_{DNA}/q_{PA} equal to 0.5 (A, D), 1 (B, E) and 2 (C, F), respectively.

complexes of xanthan appeared to be looser, lacking this core. For all polyanions, the overall structure of the complexes was independent of the selected polycation, i.e. globular for DNA.

Fluorimetric titration curves obtained by recording the fluorescence emission of DNA-EtBr upon addition of the polycations chitosan and PLL, respectively, yielded a decrease in the relative fluorescence intensity, $\langle I/I_0 \rangle$, reflecting a displacement of EtBr concomitant with the compaction of DNA. At high ionic strength, c_s, (150mM) the

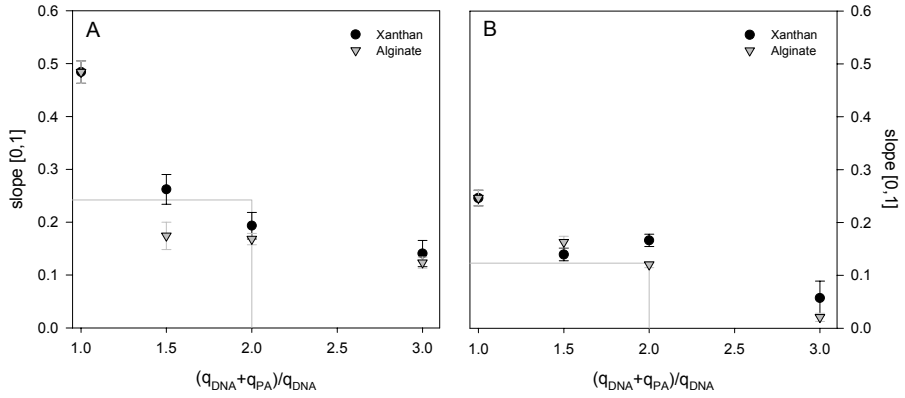

Figure 5. The slope of the titration curves in Figure 4 was extracted up to an A/P ratio of 1 for chitosan (A) and PLL (B) as the polycation. At $q_{DNA}=q_{PA}$ ($(q_{DNA}+q_{PA})/q_{DNA}=2$) the slope is compared to the half value of the slope for only DNA in the titrate solution, $(q_{DNA}+q_{PA})/q_{DNA}=1$ (grey lines). A value of the slope in the mixed solution higher than the half-value, represents more PC binding to DNA than to the competing PA.

titration curves for both polycations decreased with the same slope and reached a plateau value when an amount of the polycation corresponding to an A/P-ratio of 1 was added (Figure 3). This indicates that the polycations are equally effective in compacting DNA. Similar titration curves were observed for chitosan titration at low c_s (5mM) (Figure 3). Titration with PLL, however, was clearly affected by a reduction in the ionic strength. For A/P-ratios < 2, the reduction in $\langle I/I_0 \rangle$ due to addition of PLL was less efficient at low c_s than at high c_s. Thus, a larger amount of PLL is needed to fully compact DNA at low c_s than at high c_s, with $\langle I/I_0 \rangle$ reaching the plateau value at an A/P-ratio close to 3 (Figure 3).

Titration of chitosan and PLL, respectively, to the DNA-EtBr solution additionally containing one of the polyanions alginate or xanthan, gave a reduction in $\langle I/I_0 \rangle$ depending on the concentration of the competing polyanion (Figure 4). For both polycations, the presence of an additional polyanion caused a reduction in the slope of the titration curve. This reflects a competition between DNA and the added polyanion with respect to polycation binding. Binding of polycations to the added polyanion will cause a less efficient compaction of DNA, as observed in the fluorescence assay. Titration curves have previously been used to determine the affinity between a polyanion and a polycation.[16,17] To differentiate between the different polyanions' ability to compete for the polycation, the slope of the titration curves in the region A/P = [0,1] was extracted and plotted as a function of the total polyanion charge relative to DNA in the solution, $(q_{DNA}+q_{PA})/q_{DNA}$ (Figure 5). If, at stoichiometric charge ratio between DNA and PA ($q_{DNA}=q_{PA}$), the polycation binds to DNA and PA to the same extent, the slope is expected to be reduced to half of the value observed without added PA. Using chitosan as the polycation, this analysis revealed no difference between the two polyanions, with chitosan binding to a somewhat larger extent to the PA than to the DNA (Figure 5A). Upon titration to a solution of DNA and alginate, PLL bound to the two polyanions to the same extent. However, when replacing alginate with xanthan, DNA appeared to be the polyanion preferred for PLL binding (Figure 5B).

In addition to changing the slope of the titration curves, the presence of a competing PA shifted the A/P-ratio for reaching the plateau level of $\langle I/I_0 \rangle$ to higher values. At sufficiently large A/P-ratios, the fluorescence for the DNA-PA system was decreased to the same plateau level as for DNA alone. However, the A/P ratio at which the plateau level was

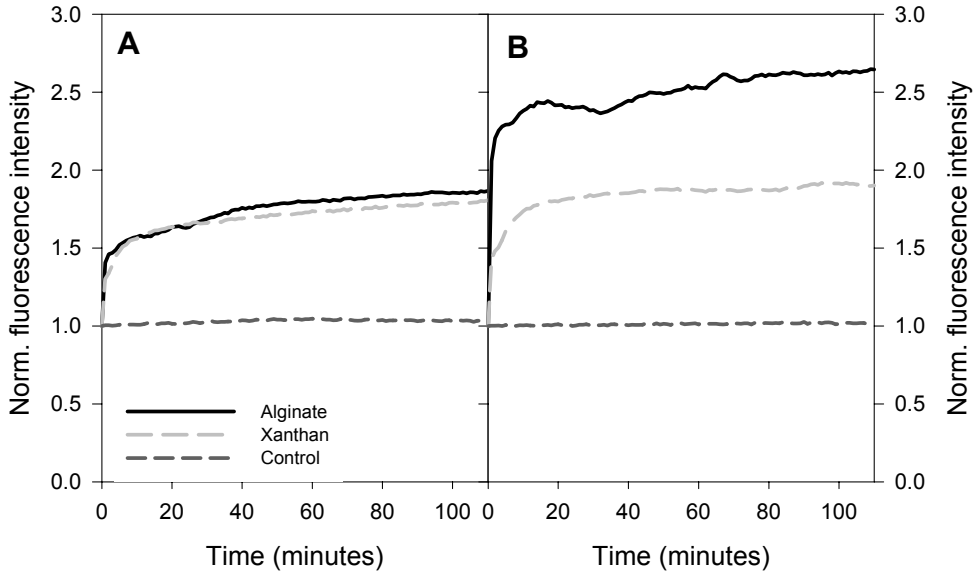

Figure 6. Fluorescence recovery illustrating the dissociation of DNA-chitosan (A) or DNA-PLL (B) complexes when exposed to alginate or xanthan. Complexation and destabilization were carried out in acetate buffer at pH 5.5 and c_s = 5mM with c_{DNA} = 5µg/mL, A/P =2 and $q_{PA} \sim 2.5\ q_{DNA}$. The control represents polyplexes that are not exposed to either of the polyanions.

reached increased with increasing PA concentration, c_{PA} (Figure 4 and Table 2).

The stability of DNA-PC complexes (A/P = 2) upon exposure to excess amounts of alginate or xanthan (q_{PA}/q_{DNA} ~2.5)was determined by measuring the recovery of the fluorescence as a function of time. The excess of PA would make dissociation possible by ensuring that the PA not only binds to excess amounts of PC. In the absence of added polyanion, the DNA-PC complexes were stable. This was based on the observation that no recovery of fluorescence was obtained over a time span of 2 hours (Figure 6). The constant level of the fluorescence intensity further indicates that EtBr was not photo-bleached within the duration of the experiments. Addition of either xanthan or alginate to either of the DNA-PC complexes resulted in a recovery of the fluorescence signal reflecting the dissociation of the polyplexes induced by the added polyanion (Figure 6). Both polyanions dissociated the DNA-chitosan polyplexes to the same extent, yielding a 30-40% recovery of the fluorescence as compared to uncomplexed DNA (Figure 6A). In contrast to the DNA-chitosan complexes, the DNA-PLL complexes were destabilized to different extents by the two polyanions (Figure 6B). While the retrieval of fluorescence upon exposure to xanthan reached the same level as for the DNA-chitosan complexes (30-40%), exposure to alginate yielded a recovery of 60-70% of the fluorescence. In all cases, 90% of the recovered fluorescence was obtained within the first 30 minutes.

It has previously been shown that temperature treatment of xanthan-chitosan condensates will drive these towards more stable structures, identified as the toroid.[13] To investigate whether metastability is an inherent feature also of the DNA-chitosan complexes, the complexes were exposed to alginate both before and after temperature treatment. These experimental series were carried out employing a plasmid DNA (pBR322) and a chitosan with F_A 0.15. From the AFM topographs (Figure 7) the observed toroids appeared to be denser following the annealing (5.5 hours at 50°C) with a reduced inner radius compared to before heat treatment. In most of the toroids, the hole in the middle was hardly visible at all. Analysis of the AFM topographs showed that the fraction of

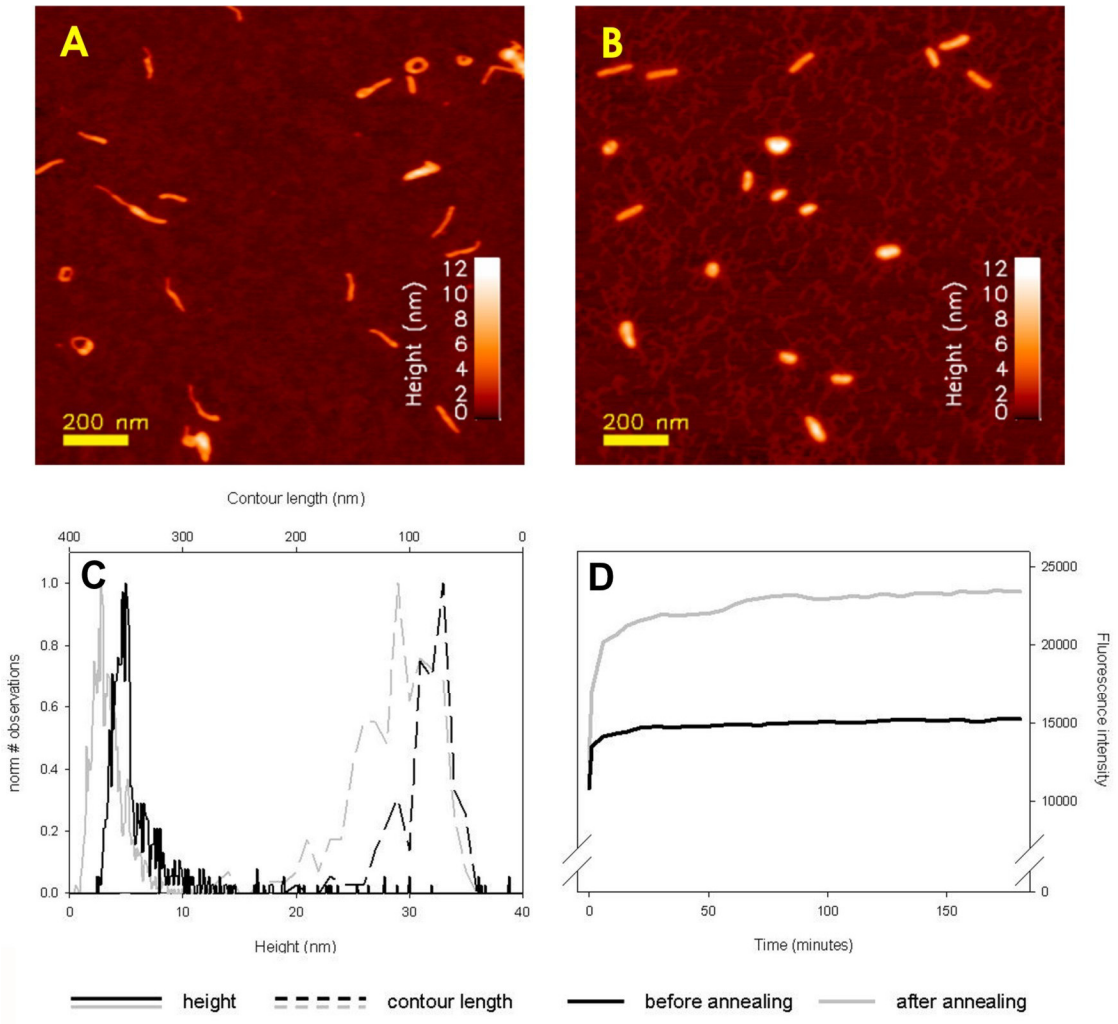

Figure 7. The upper panel shows AFM height topographs before (A) and after (B) annealing plasmid DNA–chitosan complexes (c_{DNA} = 5µg/mL, A/P =2) at 50°C for 5.5 hours. The height- (C, straight line) and contour length (C, dashed line) distributions following analysis of the linear complexes illustrates the shift towards shorter and thicker rods following annealing. The fluorescence recovery curve as a function of time when exposed to alginate ($q_{alginate}$ = 2.5 q_{DNA}) is compared before (grey) and after (black) annealing (D). In this series a chitosan F_A 0.15 was employed and c_s = 5mM.

toroids relative to rods decreased from 0.62 to 0.32 following annealing. In both situations more than 90% of the observed structures could be classified into well-defined structural categories. Annealing further affected both the height and contour length of the polyplexes. Whereas temperature treatment caused the distributions of polyplex contour lengths to be shifted towards shorter lengths, the height distributions were seen to be shifted towards larger heights (Figure 7 and Table 3). After annealing, several peaks were found in the height distribution of the toroids contrary to a single peak before the temperature treatment. Furthermore, based on their asphericity index a number of structures observed after heat treatment appeared to fall into the category of globular structures.[15]

The stability of plasmid DNA-chitosan complexes following exposure to alginate was compared before and after annealing. Before heat treatment of the complexes, alginate was found to destabilize the complexes, retrieving fluorescence to a level more than half of that obtained for uncomplexed pDNA (55-60% recovery). Monitoring the fluorescence as a function of time (Figure

Table 3. Effect of temperature treatment on the average height (h) and contour length (L_c) of the polyplexes observed when mixing plasmid DNA (pBR322) with chitosan F_A 0.15. c_{DNA} = 5µg/mL and A/P = 2.

	Toroids		Rods	
	<h> ± sd (nm)	<L_c> ± sd (nm)	<h> ± sd (nm)	<L_c> ± sd (nm)
Before annealing	3.5 ± 1.3	122 ± 40	3.4 ± 1.5	110 ± 40
After annealing	8.5 ± 4.8	77 ± 25	6.1 ± 4.4	81 ± 26

6 and 7) showed that the destabilization of the complexes mainly occurred within the first 30 minutes after addition of alginate. Exposing the complexes to alginate after annealing caused a less efficient fluorescence recovery (~35%). However, the time scale of destabilization was the same as before annealing the complexes.
Similarly, exposing temperature treated polyplexes of calf thymus DNA and chitosan (F_A 0.1) to alginate retrieved 36% of the fluorescence as compared to before annealing. In comparison, annealing of calf thymus DNA-PLL complexes resulted in 7% retrieval of the fluorescence (relative to before annealing) upon exposure to alginate.

Discussion

Polycation-induced compaction of semiflexible polyanions is driven mainly by electrostatic interactions.[4] Thus, the amount of charges available for polymer interactions is expected to be of importance. Although having approximately the same charge spacing parameter (*b* parameter), alginate and xanthan have different equivalent mass per unit charge (Table 1). The above results were therefore presented based on the charge stoichiometry between DNA and the competing polyanion, rather than mass concentrations. When presented in this way, data obtained when employing the two different polyanions nearly coincides, suggesting that electrostatics is a main factor influencing the interactions between the various PA-PC pairs. Studying the slope of the titration curves the relative association of PA-PC compared to DNA-PC seemed to be independent on the polyanion for binding of chitosan, while only minor differences were observed for PLL. If the polycation showed a strong preferential binding to the competing polyanion compared to DNA, this would appear as an initial plateau in the $<I/I_0>$ curve, representing complete binding to the PA before binding to DNA. As this was not observed in the systems studied, the important factor in a competitive binding appeared to be the number of charges available for binding, indicative of an electrostatically determined interaction. Any specific interactions in the investigated systems were not revealed in the PA-PC binding.

The reduction in DNA-EtBr fluorescence intensity upon complexation of DNA with the polycations chitosan and PLL showed that both polycations interact with DNA. This was also confirmed by AFM imaging, where individual complexes were observed. Comparison of the fluorimetric titration data obtained for the two polycations showed that DNA had higher affinity for chitosan than for PLL at low ionic strength (Figure 3). A larger A/P-ratio was thus needed to effectively compact DNA when PLL was used instead of chitosan at this condition. The decline in the fluorescence signal upon addition of PC to DNA at high ionic strength indicated that at this ionic strength both polycations had high affinity for DNA. However, although the titration curve for PLL at low c_s was less steep than the one obtained for PLL at high c_s and for chitosan at both ionic strengths, PLL at low c_s caused the overall strongest displacement of the EtBr from DNA (Figure 3). Conformational changes in DNA, such as bending

associated with polycation induced DNA condensation, displaces EtBr from DNA, decreasing the fluorescence yield.[9] Thus, a higher $<I/I_0>$ plateau value might represent the presence of pockets within the polyplex available for the fluorescent dye, caused by either a lower affinity between the polycation and DNA or a smaller bending of the DNA upon compaction. Differences in the fluorimetric titration curves might thus result from different compaction behavior. The plateau values achieved was lower for PLL than for chitosan at both ionic strengths, but being most pronounced at 5mM. Differences in the final plateau level have also been reported for other systems and seen to be related to the charge density of the polycation, decreasing with increasing charge density.[9,18-20] The average distances between the charges in a line-charge model for chitosan and PLL is 0.58 nm and 0.38 nm respectively, consistent with such an interpretation. Increased screening at high c_s might lead to a less pronounced effect of the polycation charge density, and hence the reduced difference between the two polycations at 150mM.

The titration studies indicated that PLL was less efficient in compacting DNA at low c_s compared to high c_s, implying that PLL has a higher association for DNA at high c_s than at low c_s. This is in contrast to the fact that the association constant between two oppositely charged polyelectrolytes is known to decrease with increasing c_s.[21,22] AFM images of PLL-DNA showed that at high ionic strength two populations of structures existed (data not shown), where larger structures were present in addition to some very small complexes. This was in contrast to observations at low ionic strength where the size distribution of the complexes was less heterogeneous (Figure 2B). The stronger decline in fluorescence upon increasing the PLL concentration at 150 mM might be caused by a more rapid aggregation of DNA and PLL into large aggregates compared to that at 5mM. Both techniques thus showed that the influence of ionic strength on the DNA compaction is polycation-dependent.

The slopes of the titration curves, reflecting the relative association of PA-PC to DNA-PC, appeared to be independent on the polyanion for binding of chitosan. Only minor differences were observed when PLL was employed, but with a slightly higher preference for alginate as compared to xanthan (Figure 5). Although there was only a slight selectivity in the binding of the polycations to the two different competing polyanions, the polyanions displayed differences in their ability to destabilize the compacted DNA. For DNA-chitosan complexes the polyanions were equally effective. However, while xanthan did not discriminate between DNA-chitosan and DNA-PLL complexes, alginate was more efficient in releasing DNA from DNA-PLL complexes. For the systems investigated in this study, the potential of the polyanions to destabilize the compacted DNA can not easily be predicted from the titration curves. The titration curves indicate that the available charge is the important factor in determining the competitive binding, thus pointing toward a general electrostatic mechanism. However, the destabilization experiments imply that there are also other more polymer-specific interactions involved. The employed polyanions have almost the same b parameter, being 0.45nm for alginate and 0.47nm for xanthan, indicative of Manning condensation. Together with other studies where destabilization by polyanions with a high (hyaluronic acid) and low (heparin) b parameter has been explored,[23] it appears that this b parameter might be important for the ability of the polyanion to destabilize compacted DNA, a topic that needs to be further explored.

When two different DNA's (linear vs plasmid) were compacted with slightly different chitosans, AFM images revealed that whereas the plasmid was compacted into toroidal and rodlike structures, small

globular structures were observed for the compacted linear calf thymus DNA. The difference in compaction behavior was also confirmed when using chitosan F_A 0.1 to compact the plasmid. Simulation studies indicate that the existence of different compacted morphologies depend on the intersegment attraction and chain stiffness of the compacted polymer.[3,24] The effect of chain stiffness on the polyplex morphology has previously been shown experimentally by compacting different polyanions with chitosan.[2] For polymers with high chain stiffness, the high energy associated with bending will favor toroidal condensates, a structure often reported for compacted DNA. Additionally, the most stable morphology is also reported to depend on the chain length. For long chains the spherical globule is reported to be preferable over the toroid.[25] The observed change in the apparent equilibrium of species of the DNA-chitosan complexes from toroids and rods to globular species with increasing chain length of DNA were thus consistent with the theoretical predictions. Although drying the specimens for AFM imaging may affect the precise nature of the observed states, as well as arrest the dynamics of the system, this correspondence suggests that the main trends are reflected by the selected approach.

Fluorescence studies of destabilizing DNA-chitosan complexes together with AFM imaging of the complexes indicated that the stability of the complexes was related to their morphology. Since the structures formed upon compaction of DNA also depended on the DNA used it is likely that also the stability is linked to the DNA chain length. This was confirmed by exposing DNA-chitosan complexes prepared from different DNAs to alginate, which yielded a higher fluorescence recovery from the plasmid DNA than the linear DNA. The polyplex morphology and stability towards a competing polyanion were further investigated by annealing of the plasmid DNA-chitosan complexes. The compaction of semiflexible polymers is believed to take place through a cascade of intermediate states.[26] Due to high energy barriers, some complexes might get trapped in intermediate states during compaction. Increasing the temperature of the system is therefore thought to drive the system closer to equilibrium.[13] Many simulation studies refer to the toroid as the energetically most stable state for semiflexible polymers,[27] while others find the rod to be the most stable morphology for intermediate chain stiffness.[24] However, as analysis of AFM topographs revealed that the fraction of rods increased following annealing, the rod appeared to be the most stable structure for this DNA-chitosan system. In terms of a phase diagram for the coil-globule transition,[3] this would place the DNA-chitosan system in the transition region. The complexes were also more stable against disruption by a competing polyanion after temperature treatment than before, as fluorescence was retrieved to a much lesser extent upon addition of alginate. The increased stability of the polyplexes following annealing is evidence in favor for a system driven closer to equilibrium. Even though indirectly, it also indicates that the rod is the most stable structure for this system.

Conclusion

Titration of a polycation to a mixed solution of DNA-EtBr and a second polyanion demonstrates the importance of electrostatics in determining the binding of a polycation to a polyanion. Comparison based on molar charge ratios revealed that competing polyanions, differing in molecular structure, stiffness, and mass per unit charge, are equally effective in reducing the efficiency of DNA compaction. Furthermore, AFM-imaging and changes in EtBr-fluorescence upon binding of a polycation to DNA was found to yield complementary information about polyplex formation and stability. The ability of polycations to compact DNA

depends on both the polycation used and the ionic strength at which compaction takes place. Although the relative binding of either chitosan or PLL to alginate or xanthan did not discriminate between the two polyanions, stability of the DNA-PLL complexes was higher when exposed to xanthan than to alginate. Combining the two techniques, information about the relation between stability and morphology was obtained. For the plasmid DNA-chitosan system, rods were found to be the most difficult morphology to dissociate.

Acknowledgment

This work is supported by The Norwegian Research Council (grant numbers 129104/420, 121894/420 and 134674/140). We are grateful to prof. Thor Bernt Melø (Dept. of Physics, Norwegian University of Science and Technology, NO-7491 Trondheim) for helpful discussions. We are indebted to Dr. Kjell Morten Vårum, Dept. of Biotechnology, NTNU, Norway for providing the chitosan samples. The assistance of Kristin Sæterbø and Baukje Kuitert in carrying out some of the experiments is gratefully acknowledged.

References

1. Thünemann, A.F.; Müller, M.; Dautzenberg, H.; Joanny, J.-F.; Löwen, H. Adv Polym Sci 2004, 166, 113-171.
2. Maurstad, G.; Danielsen, S.; Stokke, B.T. J Phys Chem B 2003, 107, 8172-8180.
3. Ivanov, V.A.; Stukan, M.R.; Vasilevskaya, V.V.; Paul, W.; Binder, K. Macromol Theory Simul 2000, 9, 488-499.
4. Stevens, M.J. Biophys J 2001, 80, 130-139.
5. Noguchi, H.; Yoshikawa, K. J Chem Phys 2000, 113, 854-862.
6. Stukan, M.R.; Ivanov, V.A.; Grosberg, A.Y.; Paul, W.; Binder, K. J Chem Phys 2003, 118, 3392-3400.
7. Grosberg, A.Y.; Nguyen, T.T.; Shklovski, B.I. Rev Mod Phys 2002, 74, 329-345.
8. LePecq, J.-B.; Paoletti, C. J Mol Biol 1967, 27, 87-106.
9. Geall, A.J.; Blagbrough, I.S. J Pharm Biomed Anal 2000, 22, 849-859.
10. De Smedt, S.C.; Demeester, J.; Hennink, W.E. Pharm Res 2000, 17, 113-126.
11. Vijayanathan, V.; Thomas, T.; Thomas, T.J. Biochemistry 2002, 41, 14085-14094.
12. Merdan, T.; Kopecek, J.; Kissel, T. Adv Drug Deliv Rev 2002, 54, 715-758.
13. Maurstad, G.; Stokke, B.T. Biopolymers 2004, 74, 199-213.
14. Cantor, C.R. & Schimmel, P.R. *Biophysical Chemistry. III The behavior of biological macromolecules*. (W. H. Freeman & Co, San Francisco, 1980).
15. Danielsen, S.; Vårum, K.M.; Stokke, B.T. Biomacromolecules 2004, 5, 928-936.
16. Zelikin, A.N.; Trukhanova, E.S.; Putnam, D.; Izumrudov, V.A.; Llitmanovich, A.A. J Am Chem Soc 2003, 125, 13693-13699.
17. Cain, B.F.; Baguley, B.C.; Denny, W.A. J Med Chem 1978, 21, 658-668.
18. Wiethoff, C.M.; Gill, M.L.; Koe, G.S.; Koe, J.G.; Middaugh, C.R. J Pharm Sci 2003, 92, 1272-1285.
19. Strand, S.; Danielsen, S.; Christensen, B.E.; Vårum, K.M. In prep 2004.
20. Wolfert, M.A.; Dash, P.R.; Nazarova, O.; Oupicky, D.; Seymour, L.W.; Smart, S.; Strohalm, J.; Ulbrich, K. Bioconjug Chem 1999, 10, 993-1004.
21. Stigter, D.; Dill, K.A. Biophys J 1996, 71, 2064-2074.
22. Matulis, D.; Rouzina, I.; Bloomfield, V.A. J Mol Biol 2000, 296, 1053-1063.
23. Danielsen, S.; Strand, S.; de Lange Davies, C.; Stokke, B.T. submitted 2004.
24. Noguchi, H.; Yoshikawa, K. J Chem Phys 1998, 109, 5070-5077.
25. Ivanov, V.A.; Paul, W.; Binder, K. J Chem Phys 1998, 109, 5659-5669.
26. Schnurr, B.; MacKintosh, F.C.; Williams, D.R.M. Europhys Lett 2000, 51, 279-285.
27. Schnurr, B.; Gittes, F.; MacKintosh, F.C. Phys Rev E 2002, 65, 061904-1-061904-13.
28. Haug, A. Report no 30, Norwegian Institute of Seaweed Research 1964,
29. Strand, K.A.; Bøe, A.; Dalberg, P.S.; Sikkeland, T.; Smidsrød, O. Macromolecules 1982, 15, 570-579.
30. Smidsrød, O.; Haug, A. Acta Chem Scand 1968, 22, 797-810.
31. Bloomfield, V.A., Crothers, D.M. & Tinoco, I. *Nucleic Acids. Structures, properties and functions*. pp 13-43 (University Science Books, Sausalito, 2000).
32. Borochov, N.; Eisenberg, H. Biopolymers 1984, 23, 1757-1769.
33. Hagerman, P.J. Biopolymers 1983, 22, 811-814.
34. Smith, S.B.; Cui, Y.; Bustamante, C. Science 1996, 271, 795-799.
35. Wenner, J.R.; Williams, M.C.; Rouzina, I.; Bloomfield, V.A. Biophys J 2002, 82, 3160-3169.

36. Zhang, L.; Takematsu, T.; Norisuye, T. Macromolecules 1987, 20, 2882-2887.
37. Young, S.-L.; Martino, M.; Kienzle-Sterzer, C.; Torres, J.A. J Sci Food Agric 1994, 64, 121-127.
38. Sato, T.; Norisuye, T.; Fujita, H. Polymer J 1984, 16, 341-350.
39. Moe, S.T.; Elgsaeter, A.; Skjåk-Bræk, G.; Smidsrød, O. Carbohydr Polym 1993, 20, 263-268.
40. Cölfen, H.; Berth, G.; Dautzenberg, H. Carbohydr Polym 2001, 45, 373-383.
41. Brant, D.A.; Flory, P.J. J Am Chem Soc 1965, 87, 2788-2791.
42. Grasdalen, H.; Larsen, B.; Smidsrød, O. Carbohydr Res 1981, 89, 179-191.
43. Vårum, K.M.; Anthonsen, M.W.; Grasdalen, H.; Smidsrød, O. Carbohydr Res 1991, 211, 17-23.
44. Vårum, K.M.; Anthonsen, M.W.; Grasdalen, H.; Smidsrød, O. Carbohydr Res 1991, 217, 19-27.

Paper V

Chitosan-mica interactions by force spectroscopy: a model system for DNA-chitosan condensation

Signe Danielsen[1,2], Emin Oroudjev[2], Thomas Gutsmann[2,3], Bjørn T. Stokke[1*] and Helen G. Hansma[2]

[1]*Biophysics and Medical Technology, Dept. of Physics, The Norwegian University of Science and Technology, NTNU, NO-7491 Trondheim, Norway*
[2]*Dept. of Physics, University of California Santa Barbara, UCSB, California 93106, USA*
[3]*Research Center Borstel, Leibniz-Center for Medicine and Biosciences, Dept. of Immunochemistry and Biochemical Microbiology, D-23845 Borstel, Germany*

Abstract

DNA-chitosan complexation has been studied for the potential of chitosan as a gene delivery vehicle. The ability of chitosan to compact DNA into well-defined structures has been found previously to depend on several factors, involving both molecular parameters (chain length and charge density, measured in terms of the degree of acetylation, F_A) and solution parameters (ionic strength, I, and pH). Also transfection studies have shown that such parameters are important for the ability of the DNA-chitosan complex to transfect cells. In this study the interaction between chitosan and negatively charged mica surface and/or the silicon nitride tip of the cantilever was investigated by using AFM based force spectroscopy. Chitosan was physiosorbed onto mica and the force-distance profile was recorded when pulling on chitosan. The effect of both solution parameters (pH and I) and molecular parameters (F_A) was evaluated and the interaction strength between chitosan and the surface was found to depend on these parameters, being strongest for low pH, low I and low F_A, as expected from electrostatic considerations. The shape of the force-spectra was also found to depend on pH and I in the solution, reflecting the adsorption characteristics of chitosan onto the surface at these conditions.

Keywords: Chitosan, DNA, force spectroscopy, polyplexes

* Corresponding author: Bjørn T. Stokke, Dept. of Physics, NTNU, NO-7491 Trondheim, NORWAY,
Fax: +47 73 59 77 10, e-mail: bjorn.stokke@phys.ntnu.no

Introduction

Polycation-induced compaction of dsDNA vectors for gene delivery is one of the popular routes for gene therapy. The function of the polycation is to reduce the physical size of the vector and thereby potentially facilitate passage through the extracellular matrix. Two additional advantages are that the compact form of DNA is less accessible for nuclease attacks and thereby protected from digestion [1-3], and that the charge reversal of DNA upon compaction increases the residence time at the cell membrane and thereby facilitates cell internalization [4-6]. DNA compaction by polycations has previously been studied by several groups using atomic force microscopy (AFM) [7-12]. Based on AFM topographs, we have previously reported that the polycation chitosan effectively compacts DNA into toroidal, rodlike and globular structures with the relative abundance of the different morphologies depending on the molecular properties of the different chitosans [13]. For high-charge-density chitosans, which have a low degree of acetylation, toroids dominated, whereas an abundance of rods were seen for lower charge density chitosans. Chitosans are partly or completely de-N-acetylated derivatives of the naturally occurring polysaccharide chitin and was chosen for its potential as a gene delivery system [14-18]. The aim of the present study is to investigate the interactions of chitosans with solid surfaces (mica and the silicon nitride of the tip of the cantilever) on a single molecular level.

Single-molecule interactions between polymers and surfaces have been reported using various polymers in contact with homogenous and heterogeneous surfaces. A molecular interpretation of the pull-off of polymers from surfaces needs to address several issues. These issues are related to the number of molecules being stretched, and eventually desorbed, and to adsorption features such as types of chain conformations of the adsorbed polymer, as well as molecular details of the polymers. The conformation of a polymer adsorbed onto a surface is commonly described in terms of trains, loops and tails (Figure 1). Adsorption of a polyelectrolyte onto mica has similarities to the formation of polyelectrolyte complexes. Both processes are electrostatically driven by entropy gain upon release of counterions from the surface and the polymer [19, 20]. It is therefore likely that factors important for the morphology of polyelectrolyte complexes also will affect the adsorption of a polyelectrolyte onto a charged surface. Thus, details of the adsorbed chain conformation can be expected to be influenced by both surface and polymer chain properties, as well as solution parameters affecting the structure of the chain at the surface. Force-distance spectra obtained when desorbing a polymer from a surface are

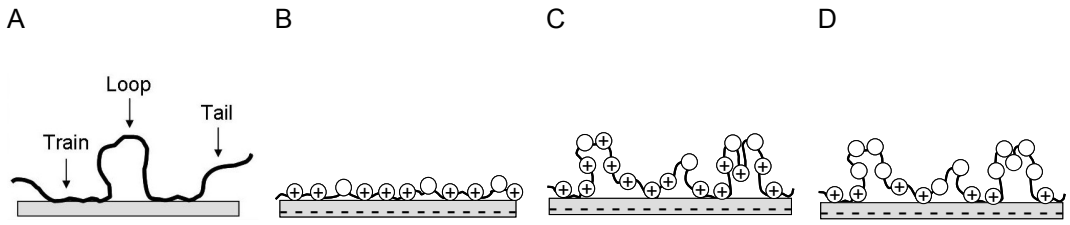

Figure 1: Diagrams of different ways that a polymer can adsorb onto a surface illustrating typical adsorption characteristics of a polymer chain onto a surface which is described in terms of trains, loops and tails (A). High charge density and low *I* cause a train-like conformation on the surface (B) whereas both high *I* (C) and low charge density (D) result in the formation of polymer loops.

believed to reflect adsorption characteristics of the polymer [21].

The interaction between chitosan and negatively charged solid surfaces was studied at a molecular level by using the Molecular Force Probe. This instrument, working in one dimension, is analogous to the AFM, but specifically designed to perform high precision force spectroscopy. Pulling experiments of chitosan adsorbed to mica focused on the chitosan molecular parameters (degree of acetylation) and the solvent conditions (pH and ionic strength, I). The electrostatic properties of DNA in high ionic strength solutions (I > 90 mM) can be represented by a planar surface with a certain charge density [22]. In such a context, mica can be viewed to model the features of the electrostatic interaction between DNA and chitosan.

Materials and methods

Biopolymer samples

Chitosans with four different degrees of acetylation (F_A) (Table 1) were used for the interaction studies. The chitosans, prepared by deacetylation of chitin from shrimp shells [23, 24], were kindly provided by Dr. K. M. Vårum (Dept. of Biotechnology, NTNU). In the following the notation C(F_A, M_n) was used when referring to the different chitosans. The buffers used for dilution of polymers, for complex formation, and to maintain the four different pH values throughout the experiments were citrate (50 mM, pH = 5.4), 2-Morpholino-ethanesulfonic acid (MES, 20 mM, pH = 6.3), 3-(N-Morpholino)propanesulfonic acid (MOPS, 20 mM, pH 7.4) and N-[Tris(hydroxymethyl)methyl]-3-amino-propanesulfonic acid (TAPS, 20 mM, pH = 8.4) (all from Sigma Aldrich). NaCl was added to these aqueous buffer solutions to achieve the desired ionic strength (50 mM, 150 mM or 500 mM, respectively) and pH was adjusted by adding NaOH.

Table 1: Properties of the chitosans used for the interaction studies. The number averaged molecular weight, M_n, was calculated from the intrinsic viscosity, [η], using the MHKS equation [46]. The average length of the chitosan polymers, L_c, was calculated assuming a monomer length of 0.52 nm [47].

F_A	[η] (ml/g)	~DP[a]	M_n (kDa)	L_c (nm)	Term for identification
0.01	220	200	32	105	C(0.01,32)
0.01	610	1005	162	525	C(0.01,162)
0.15	740	1170	196	610	C(0.15,196)
0.35	760	1035	182	540	C(0.35,182)
0.49	450	560	102	290	C(0.49,102)

[a] Degree of polymerization

Chitosan desorption from solid surfaces by force spectrocopy

To determine the force-vs.-distance spectra when pulling on chitosan, the chitosan was physiosorbed onto mica. 120 µl of the chitosan solution (1µg/ml) was transferred to freshly cleaved mica discs (glued onto a glass slide) and incubated in a closed chamber for ~1 hour. After incubation, excess chitosan was removed from the solution by washing the sample a few times in fresh buffer. The mica was then covered by fresh buffer and the sample was used for investigating molecular stretching and interactions with the surface.

The molecular elongation and interaction experiments were performed in aqueous solution employing a Molecular Force Probe (MFP-SA, Asylum Research, Santa Barbara, CA) and "D" silicon nitride cantilevers (MLCT-AUHW type Veeco, Santa Barbara, CA) with a nominal spring constant and resonance frequency of 0.03 nN/nm and 15 kHz, respectively. The spring constant was estimated for each cantilever from the measured amplitude of its thermal fluctuations (sampling for 10 s), using a build-in thermal calibration module in the

Asylum Research supplied software [25]. The retract and approach velocity was in all experiments equal to 300 nm/s (~0.15 Hz, ~10 nN/s) with a 1 s delay at the surface. To make sure that the observed pulling curves were caused by the presence of chitosan on the surface, and not contaminations in the buffer, the buffer solutions were filtered (pore size of 0.2 μm) and controls were performed with bare tip and mica only in the presence of buffer.

The distribution of physiosorbed chitosan (C(0.01,162)) on the mica surface at the various pH values was verified by tapping mode AFM (TM-AFM) imaging in air using a Multimode IIIa AFM (Veeco, Santa Barbara, CA) as previously described [13]. Chitosan was adsorbed to the mica as explained above, except NH_4Ac was used to adjust the ionic strength [13].

Data analysis

Before extracting and analyzing data from the force plots, the cantilever deflection-vs.-piezo extension curves were transformed into force-vs.-distance curves by using software from Asylum Research based on IGOR Pro (WaveMetrics, Lake Oswego, OR). The more detailed analysis, involving the extraction of rupture forces and rupture lengths, was also performed using IGOR Pro. Possible drift in the baseline was adjusted for by normalization. For the analysis of unbinding events, only the last rupture event was included in the analysis even though some of the force-distance spectra were observed to contain additional unbinding events. This was done to reduce the probability of measuring a convolution of multiple unbinding events. To achieve information about interaction strengths, the rupture force of the last unbinding event (either in the form of a peak or a plateau) was extracted from force-vs-elongation spectra and presented as force distribution histograms. The numbers of spectra analyzed for each data set is presented in Table 2. In the same way the observed polymer segment lengths at the final unbinding event, here referred to as the rupture length, was extracted to obtain length histograms.

Table 2: Number of recorded force-elongation spectra for the chitosan-surface interaction at varying pH and *I* from which last peak rupture force information was extracted. The last two columns list the number and percent of the recorded spectra that ended in a plateau.

pH	I (mM)	# recorded spectra	# spectra ending in plateau	% of spectra ending in plateau
5.4	150	189	13	7
6.3	150	221	45	20
7.4	50	66	13	20
7.4	150	197	5	3
7.4	500	87	2	2

To extract peak values and widths from the observed force distributions, these were fitted to a log-normal distribution:

$$P(f) = a \exp\left(-\tfrac{1}{2}\left(\ln\left(f/f_0\right)/\sigma\right)^2\right) \qquad (1)$$

where f_0 represents the peak force in the distribution, a a normalization parameter, and σ the shape parameter of the distribution. These parameters were used in the following as a basis for the influence of solvent parameters without an explicit connection to the molecular interpretation of the desorption. The parameters f_0 and σ was used to calculate the width of the distribution, represented as the full-width-half-maximum, FWHM. All fits gave a coefficient of determination, R_{sqr}, larger than 0.9.

Statistical significance of data was calculated by the Wilcoxon-Mann-Whitney test in Kaleidagraph (Ver. 3.6, synergy Software, Reading, PA, USA).

Results

Imaging chitosan C(0.01,162) physiosorbed onto mica at pH values from 5.4 to 8.4 showed that at pH 5.4, 6.3 and 7.4, chitosan formed a fairly

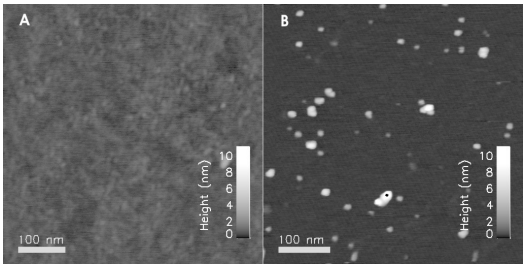

Figure 2: TM-AFM topographs of chitosan C(0.01,162) physiosorbed onto mica at pH 5.4 (A) and 8.4 (B). Adsorbing chitosan to mica at the pH values 5.4, 6.3 and 7.4 yielded identical images, as in (A), which shows a fairly uniform chitosan layer that is less smooth (roughness ≥ 0.08 nm) than the bare mica background (roughness = (0.05 ± 0.01) nm) in (B).

uniform layer on the mica surface (Figure 2A) with a roughness ≥ 0.08 nm. In contrast, at pH 8.4, the chitosan molecules appeared to be clumped into globular clusters on the surface (Figure 2B) with bare mica in between (roughness of the bare mica areas was equal to 0.05±0.01 nm). These globular clusters had heights of ~6 nm and were completely absent for adsorption at the lower pH values. Consistent with these observations from AFM-imaging, chitosan force-vs.-elongation spectra were observed only at certain distinct regions of the mica at pH 8.4. Additionally, at the locations where such spectra were seen, the pulls indicated that the surface was soft and contained several closely spaced unbinding events (data not shown). At locations where no chitosan spectra were seen, the surface was hard, as indicated by sharper change in the force curve when the tip touched the surface [26]. This behavior at pH 8.4 is probably due to precipitation since chitosans with low F_A are known to be insoluble at this high pH [27]. The force spectra obtained for chitosan at this pH are therefore more likely to reflect a convolution of phenomena such as disentanglement and multiple chains being desorbed. Analysis of force spectra obtained at pH 8.4 is therefore not presented in further detail.

Examples of force-distance curves obtained when pulling on chitosan

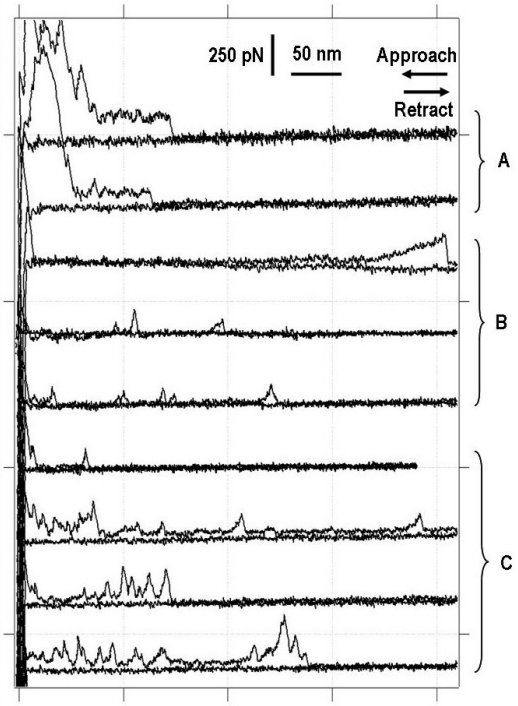

Figure 3: Examples of force-vs.-elongation displacement curves obtained when pulling on chitosan C(0.01,162) at I = 150 mM and pH 6.3 (A) and 7.4 (B), as well as the chitosan C(0.15,196) at pH 7.4 and I = 150 mM (C). The graphs illustrate the presence of plateaus and peaks in the force spectra. Upper curve in each pair is the retract (stretching) curve; lower curve is the approach (relaxation) curve. See arrows. "Retract" and "Approach" refer to the movement of the cantilever as it retracts from the sample surface and approaches it.

physiosorbed on mica are shown in Figure 3, were the chitosans C(0.01,162) and C(0.15,196), respectively, were adsorbed onto mica at pH 6.3 and 7.4 and I = 150 mM. Changes in pH and ionic strength affected the shape of the force-elongation spectra. Whereas a considerable fraction (~20%) of the force curves at pH 6.3 and I=150 mM ended in a plateau of constant force, very few such plateaus were observed when the pH was changed to 5.4 and 7.4 (I=150 mM, Table 2).

Furthermore, varying the ionic strength while keeping pH equal to 7.4 showed that ending plateaus were dominating at low ionic strength, I = 50 mM, while being completely absent at high ionic strength, I = 500 mM (Table 2). Increasing the ionic strength from 50

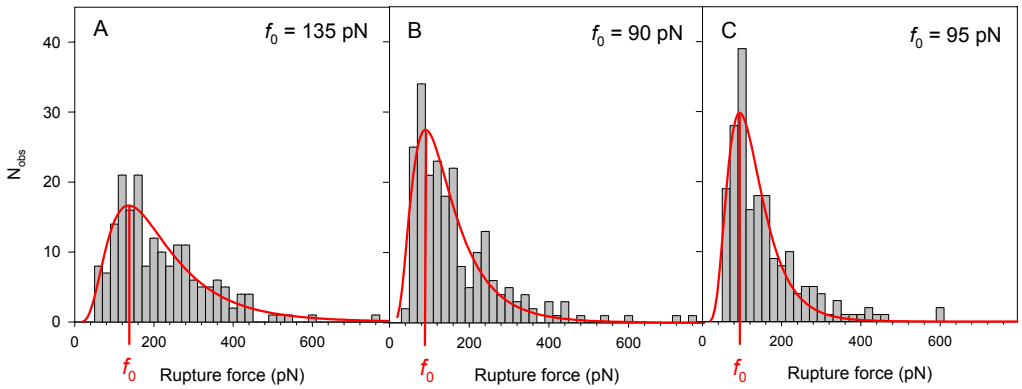

Figure 4: Force histograms were plotted on the basis of the recorded unbinding forces of the last peak when pulling on chitosan physiosorbed on mica. Example of such a force histogram is shown for C(0.01,162) at I = 150 mM and pH 5.4 (A), 6.3 (B) and 7.4 (C). The overlaid curve shows the fit of the histograms to a log normal distribution.

mM to 150 mM and 500 mM further seemed to cause an increased tendency of saw tooth-like pattern in the force spectra. Varying the chitosan charge by changing F_A, keeping the ionic strength at 150 mM and pH at 7.4, did not cause any noticeable effect on the shape of the force-elongation curves (data not shown).

Histograms of the observed unbinding forces for the last chitosan rupture yielded information about the most probable unbinding force (Figure 4) depending on the chitosan properties and solvent conditions. The properties of the last unbinding event were found to be altered by changes in pH (Figure 4, 5 and 6). In these experiments, the ionic strength was constant at 150 mM and the highly charged chitosan C(0.01,162) was used. Chitosan pulls at pH 5.4 had a significantly higher force (135 pN) and yielded broader distributions for both rupture forces and rupture lengths than chitosan pulls at either pH 6.3 and 7.4 (Figure 4, 5 and 6). Although the peak value, f_0, from the force distributions was similar at pH 6.3 and 7.4 (90 pN, Figure 4 and 5), the force distribution was broader at pH 6.3 than at pH 7.4 (Figure 5). This resulted in a significantly higher median force value at pH 6.3 compared to pH 7.4.

Lowering the ionic strength from 150 mM to 50 mM caused a significant increase in the rupture force (Figure 4 and 5). However, increasing the ionic strength from 150 mM to 500 mM did not affect the value of the rupture force (Figure 5). At both 50 mM and 500 mM the rupture length distributions were narrower than at 150 mM and the peak was shifted towards shorter lengths. In all of these experiments pH was 7.4 and

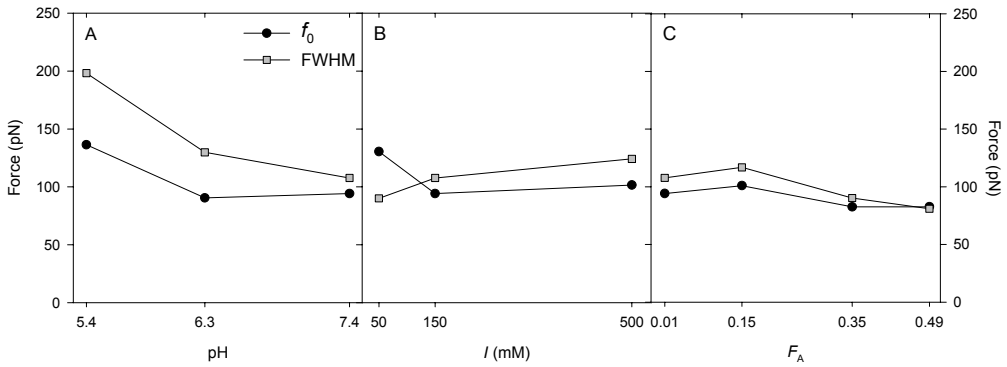

Figure 5: Fitting the histograms to a log normal distribution yielded a measure of the peak force, f_0, and the width, FWHM, of the distribution. The chitosan C(0.01,162) was studied at varying pH while keeping I = 150 mM (A) and varying ionic strength at pH 7.4 (B), and the effect of varying chitosan F_A was studied at pH 7.4 and I = 150 mM (C).

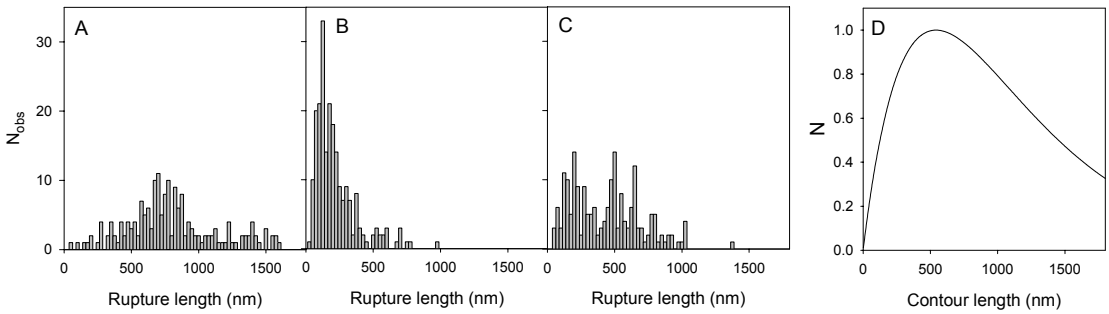

Figure 6: Histograms showing the distribution of rupture lengths when pulling on chitosan C(0.01,162) at pH 5.4 (A), 6.3 (B) and 7.4 (C). The length distribution as calculated from the theoretical weight distribution of the chitosan sample is shown in (D).

pulls were performed on the chitosan C(0.01,162).

Changes in the chitosan F_A showed only small variabilities in the value of the unbinding force (90-100 pN) at pH 7.4 and I=150 mM, but there was a slight trend toward lower rupture force as F_A increased. All chitosans yielded rather broad rupture length distributions, being slightly broader for the chitosans C(0.01,162) and C(0.49,102), when differences in their degree of polymerization were taken into account (data not shown).

The final rupture lengths for the chitosan C(0.01,162) were observed to make up rather broad distributions (Figure 6), being quite different for the 3 different pH values. The longest ruptures and the broadest distribution were seen at low pH of 5.4, while the shortest ruptures and the narrowest distribution are seen at the intermediate pH of 6.3 (Figure 6).

Discussion

Force spectroscopy of chitosan on mica revealed molecular scale interactions of chitosans with the surfaces of mica and the AFM tip, both possessing capacity for a significant electrostatic interaction by their net negative charge (Figure 7). The surface of the AFM tip is predominantly a silicon oxide surface. Both mica and silanol on the AFM tip acquire their negative charges from proton loss by acidic hydroxyl groups. The apparent pK_a of mica is reported to be ~3.5 [28] while pK_a of silanol groups on the surface of the AFM tip is 6-7 [29]. Chitosan obtains its positive charge from the glucosamine residues generated by the de-acetylation of N-acetyl glucosamine. Since pK_a of the chitosan amine groups is ~6.5 [30, 31], a decrease in pH causes increased protonation of chitosan.

We measured the forces and distances for the last rupture event for chitosans with 4 degrees of de-acetylation and for one of these chitosans at 3 ionic strengths and 3 pH's. The 3 pH's affect the charge densities of mica, chitosan, and the AFM tip differently as schematically illustrated in Figure 7. Adsorption of polyelectrolytes onto charged surfaces is an

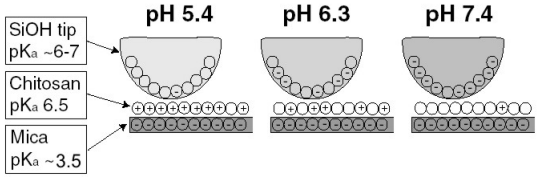

Figure 7: pH vs charge on tip, chitosan, and mica. Tip: Outer surface of Si-N tip is silanol (SiOH) with pK_a ~ 6-7 [29]. Tip shading is proportional to the fraction of SiO^- at each pH (~10% SiO^- at pH 5.4, 50% SiO^- at pH 6.3, and 90% SiO^- at pH 7.4. Chitosan: With pK_a = 6.5 [30, 31], chitosan amino groups are ~90% NH_3^+ at pH 5.4, 50% NH_3^+ at pH 6.3 and 10% NH_3^+ at pH 7.4. Mica hydroxyls are ~100% negatively charged (O^-) at all 3 pH's.

electrostatically driven process where the charge density and Debye screening length are observed to be important parameters [19, 32]. Since changes in pH will affect the electrostatic interaction between chitosan and a negatively charged surface, the adsorption of chitosan to these surfaces can be expected to be influenced by pH in the solution. The chitosan-surface rupture forces for the final peak were found to be largest at pH 5.4 (Figure 4A and 5A). The trends of decreasing rupture forces observed for the C(0.01, 162) with increasing pH, can be due to the decreasing chitosan-mica interaction associated with the reduced effective charge density of chitosan. Chitosan-surface rupture forces were significantly higher at pH 5.4 than at pH's 6.3 or 7.4. A similar effect of pH on the interaction strength between chitosan and mica has also been reported from surface force measurements [33]. As the pH increases, the cationic chitosan becomes less charged, the anionic tip becomes more charged, and the mica remains anionic (Figure 7).

Experiments carried out at different ionic strengths yielded data that can be explained by considering the effect of the electrostatic double-layer on the chitosan-surface interactions. The rupture force was significantly reduced when increasing *I* from 50 mM to 500 mM (Figure 5B). This decrease in *I* corresponds to an increase in the Debye screening length from 0.4 nm to 1.4 nm. Also the chitosan charge affected the rupture force. The less charged chitosans C(0.35,182) and C(0.49,102) yielded lower rupture forces than the more charged chitosans C(0.01,162) and C(0.15,196) (Figure 5B). This is consistent with our hypothesis that electrostatic interactions dominate in the binding of chitosan to the surface.

The rupture forces observed for the chitosan-mica interaction are in the range of forces reported for the interaction between DNA and different surfaces (among them mica) in the presence of Mg^{2+}-ions [34]. Also interactions between polyvinylamine and mica are reported to be in the same range (50-150 pN, depending on *I*) [32].

The distances to the final rupture peak showed a much more complex pattern (Figure 6). Rupture lengths varied over an eight-fold range, unlike rupture forces, which showed only a two-fold variation. The width of the rupture length distributions have been used to describe the polydispersity in the molecular weight of the polymer sample studied [35]. Comparing the rupture length histograms achieved from the recorded rupture length when pulling on chitosan with the theoretical weight distribution [36] revealed that all rupture lengths are short enough to result from pulls on single molecules (Figure 6). Since polymers from the same batch of preparation (C(0.01,162)) were used at the different pH values, the differences in the rupture length distributions are not due to differences in the polydispersity in the chitosan molecular weight. In addition to reflecting polydispersities of the sample, the rupture length distributions also reflect the distribution of the anchoring site to the AFM tip on the polymer chain. Both the specific location and the number of anchoring sites on the polymer chain will depend on the conformation of the polymer on the surface as it is easier to pick up polymer loops and loose ends than trains from the surface. Pulling on the chitosan C(0.49,102) at pH 5.4 did not yield the long rupture lengths that were observed for C(0.01,162) (data not shown). This supports the suggestion that a highly charged polymer will adopt a train-like conformation on the surface whereas a reduction in the polymer charge density increases the probability for formation of polymer loops due to lack of interacting sites on the polymer. The combined effect of pH and residue sequence of

chitosan may support longer relative rupture lengths for the C(0.01, 162) than C(0.49, 102) at pH 5.4 due to differences in number of contiguous residues interacting with the mica and thereby yielding difference the overall lifetime of the zipper-like interaction. The interaction between chitosan C(0.01,162) and mica at pH 5.4 will be supported by a much longer average length of GlcN residues at this small degree of acetylation, compared to the C(0.49,102) sample. In the dynamic equilibrium, the overall lifetime of the C(0.01,162) can therefore be longer and support longer rupture lengths than the C(0.49,102) at pH 5.4.

Conformation of an adsorbed polyelectrolyte on a charged surface, commonly described in terms of loops and trains (Figure 1), is important in describing its behavior at various conditions. It has been observed that at low I and conditions were the polymer charge is high, the polymer adopts a flat, train-like, conformation on the surface (Figure 1A), whereas at conditions with high I (Figure 1B) or low charge density (Figure 1C), the polymer will form loops on the surface [37]. The force-distance spectra recorded when using AFM tips to detach polymers from surfaces has been suggested to reflect adsorption characteristics of the polymer to the surface [38] as well as the strength of the unbinding event. Whereas trains yield plateaus in the force-elongation spectra, loops in between the trains give rise to saw-tooth like desorption spectra and the detachment of a long loop or tail structure causes a force spectrum containing a single peak [38]. Thus, the observation of plateaus in the force profile when detaching C(0.01,162) from mica at pH 6.3 (I = 150 mM) indicates that the polymer adopts a rather flat conformation at this condition whereas the presence of peaks (one or a few) in the force-elongation curve when pH was increased to 7.4 indicates that a considerable amount of loops are present in the adsorbed layer. Because of the large degree of protonation at pH 5.4 and the observed strong interaction with mica, C(0.01,162) is expected to adopt a train-like conformation on the mica surface at this condition. However, the shape of the force-elongation curve, containing one or a few peaks and only a few plateaus, indicates the presence of one or a few large loops in addition to some short trains. The presence of peaks instead of plateaus, which are expected for a train-like structure, might be due to a reduction in the dissociation rate of amino groups from the surface because of the stronger binding at this high charge density. This is based on reports predicting that details of force-elongation spectra for the continuous desorption of a weakly adsorbed polymer from a solid substrate will depend on the force loading rate relative to the on-off rate of the adsorption process [39, 40]. Since increasing F_A of the chitosan while keeping pH = 7.4 yielded force-elongation profiles with similar characteristic features, we believe that this additional decrease in charge density did not induce a further development of loop structures on the surface. Furthermore, comparing the force-elongation profiles collected at varying I leads to the suggestion that chitosan adsorbs predominantly with a train configuration at low ionic strength with an increased tendency for loop formation at higher I as previously reported for other polyelectrolytes [41-43].

The variation in the force-elongation spectra obtained here at the different pH values indicates that the loading rate is not the only parameter important for the features of a typical desorption pattern. As a continuous desorption of polymers from the surface requires a train-like structure on the surface, the average distance between the charged segments

is important in determining the presence of plateaus vs. peaks in the force curves.

Both the polycation charge and ionic strength of the solution have been reported to be important for the polyelectrolyte complexes formed when interacting with DNA. Increased size of the DNA-chitosan polyplexes has been reported upon increase in the pH from 5.5 to 7 [18]. This might be related to the increased pH reducing the net charge of chitosan in solution, and thus mediate weaker intersegment attraction between the DNA segments. The larger charge density of chitosan at pH 5.5 can thus be viewed to mediate stronger DNA intersegment attraction and thereby tolerate the opposing energy associated with smaller radius of curvature in the toroidal and rodlike polyplexes. Alternatively, polyplexes prepared from weakly charged chitosan may be able to come close together and form aggregated structures as a result of uncharged polymer loops extending from the polyplexes. Similar effect on the polyplex size is also reported when reducing the chitosan charge density by increasing F_A [18].

It was previously found that whereas an increase in the ionic strength at which complex formation takes place has no effect on the dimension of the structures formed, it affects the type of structures formed (data not shown). An increase in I from 5 to 500 mM caused an almost complete depletion of the toroidal structures for the DNA-chitosan system, independent of the chitosan F_A. Screening of the electrostatic potential due to increased ionic strengths may cause the complexes to be brought close together to form aggregated structures. Such increased tendency for aggregation is previously observed for DNA-PLL complexes upon increasing I [1], but could not be observed from the AFM studies here. Aggregated structures might still be present in the solution in addition to the smaller and well-defined structures. This needs to be further evaluated.

Stability of the polyplexes is important for their function as a gene delivery system. The total interaction energy between a polymer and its adsorption substrate or between two molecular pairs can in principle be obtained by integration under the force spectrum. The shape of the curves and the size of the loops must therefore be considered when estimating the interaction energy and the size of the polymer segment available for interaction with DNA. In fact, the total interaction energy would involve the area under all peaks, provided that they result from a single polymer chain. However, since immersing the tip into the polymer layer probably involves the attachment of more than one chain to the tip, the various peaks probably reflect a convolution of unbinding events from multiple chains. Quantification of the total interaction energy is therefore difficult. Although no correlation was seen between rupture length and rupture force for the individual pulls, the increased forces observed for pH 5.4 reflect stronger interactions, compared to the higher pH, as expected from the effect of pH on the chitosan charge density [44]. This might further be of importance for the stability of the resulting DNA-chitosan complexes.

DNA, with a pK_a of ~1 [45], is similar to mica in its acidity as none of these are affected by the pH values employed in this study. Therefore these results provide insights into optimizing the conditions for chitosan-induced condensation of DNA, which is a potential delivery system for gene therapy. For investigating interactions at the single-molecule level, the chitosan-surface system has great advantages over a chitosan-DNA system. In the simple system of chitosan and the 2 surfaces, there are few possible interactions; and few controls are needed. The only

'unwanted' interaction in a clean system of this type is the interaction between tip and substrate. In contrast, a system for investigating single-molecule chitosan-DNA interactions requires that chitosan be covalently immobilized on one surface via a bi-functional crosslinker, while DNA is covalently immobilized on the other surface. In this system, with surface - linker - biomolecule at both the tip and the substrate, there are many possible artifacts due to interactions of either surface or either linker with the other surface or the other linker or the other biomolecule. AFM imaging is also of little benefit for monitoring these interactions, since the tip cannot be imaged, and the surface characterization will be more ambiguous. Therefore the indirect but simple approach used here is valuable for guiding further research on the preparation and analysis of chitosan-DNA condensates.

Acknowledgement

This work is supported by The Norwegian Research Council (grant numbers 129104/420 and 121894/420) and the National Science Foundation (MCB0236093 to HGH). We are grateful to dr. K. M. Vårum (Dept. of Biotechnology, Norwegian University of Science and Technology, NO-7491 Trondheim) for providing us with the chitosans.

References

1. Kwoh, D.Y., Coffin, C.C., Lollo, C.P., Jovenal, J., Banaszczyk, M.G., Mullen, P., Phillips, A., Amini, A., Fabrycki, J., Bartholomew, R.M., Brostoff, S.W. & Carlo, D.J. Stabilization of poly-L-lysine/DNA polyplexes for in vivo gene delivery to the liver. *Biochim Biophys Acta* **1444**, 171-190 (1999).
2. Dash, P.R., Toncheva, V., Schacht, E. & Seymour, L.W. Synthetic polymers for vectorial delivery of DNA: characterisation of polymer-DNA complexes by photon correlation spectroscopy and stability to nuclease degradation and disruption by polyanion in vitro. *J Control Release* **48**, 269-276 (1997).
3. Richardson, S.C.W., Kolbe, H.V.J. & Duncan, R. Potential of low molecular mass chitosan as a DNA delivery system: biocompatibility, body distribution and ability to complex and protect DNA. *Int J Pharm* **178**, 231-243 (1999).
4. Hill, I.R.C., Garnett, M.C., Bignotti, F. & Davis, S.S. In vitro cytotoxicity of poly(amidoamine)s: relevance to DNA delivery. *Biochim Biophys Acta* **1427**, 161-174 (1999).
5. Akinc, A., Lynn, D.M., Anderson, D.G. & Langer, R. Parallel synthesis and biophysical characterization of a degradable polymer library for gene delivery. *J Am Chem Soc* **125**, 5316-5323 (2003).
6. Jones, N.A., Hill, I.R.C., Stolnik, S., Bignotti, F., Davis, S.S. & Garnett, M.C. Polymer chemical structure is a key determinant of physicochemical and colloidal properties of polymer-DNA complexes for gene delivery. *Biochim Biophys Acta* **1517**, 1-18 (2000).
7. Dunlap, D.D., Maggi, A., Soria, M.R. & Monaco, L. Nanoscopic structure of DNA condensed for gene delivery. *Nucleic Acids Res* **25**, 3095-3101 (1997).
8. Hansma, H.G., Golan, R., Hsieh, W., Lollo, C.P., Mullen-Ley, P. & Kwoh, D. DNA condensation for gene therapy as monitored by atomic force microscopy. *Nucleic Acids Res* **26**, 2481-2487 (1998).
9. Golan, R., Pietrasanta, L.I., Hsieh, W. & Hansma, H.G. DNA toroids: Stages in condensation. *Biochemistry* **38**, 14069-14076 (1999).
10. Fang, Y. & Hoh, J.H. Early intermediates in spermidine-induced DNA condensation on the surface of

mica. *J Am Chem Soc* **120**, 8903-8909 (1998).
11. Martin, A.L., Davies, M.C., Rackstraw, B.J., Roberts, C.J., Stolnik, S., Tendler, S.J.B. & Williams, P.M. Observations of DNA-polymer condensate formation in real time at a molecular level. *FEBS Lett* **480**, 106-112 (2000).
12. Rackstraw, B.J., Martin, A.L., Stolnik, S., Roberts, C.J., Garnett, M.C., Davies, M.C. & Tendler, S.J.B. Microscopic investigations into PEG-cationic polymer induced DNA condensation. *Langmuir* **17**, 3185-3193 (2001).
13. Danielsen, S., Vårum, K.M. & Stokke, B.T. Structural analysis of chitosan mediated DNA condensation by AFM: Influence of chitosan molecular parameters. *Biomacromolecules* **5**, 928-936 (2004).
14. Köping-Höggård, M., Tubulekas, I., Guan, H., Edwards, K., Nilsson, M., Vårum, K.M. & Artursson, P. Chitosan as a nonviral gene delivery system. Structure-property relationship and characteristics compared with polyethylenimine *in vitro* and after lung administration *in vivo*. *Gene Ther* **8**, 1108-1121 (2001).
15. Köping-Höggård, M., Mel'nikova, Y.S., Vårum, K.M., Lindman, B. & Artursson, P. Relationship between the physical shape and the efficiency of oligomeric chitosan as a gene delivery system *in vitro* and *in vivo*. *J Gene Med* **5**, 130-141 (2003).
16. MacLaughlin, F.C., Mumper, R.J., Wang, J., Tagliaferri, J.M., Gill, I., Hinchchliffe, M. & Rolland, A.P. Chitosan and depolymerized chitosan oligomers as condensing carriers for in vivo plasmid delivery. *J Control Release* **56**, 259-272 (1998).
17. Erbacher, P., Zou, S., Bettinger, T., Steffan, A.-M. & Remy, J.-S. Chitosan-based vector/DNA complexes for gene delivery: Biophysical characteristics and transfection ability. *Pharm Res* **15**, 1332-1339 (1998).
18. Romøren, K., Pedersen, S., Smistad, G., Evensen, Ø. & Thu, B.J. The influence of formulation variables on in vitro transfection efficiency and physiochemical properties of chitosan-based polyplexes. *Int J Pharm* **261**, 115-127 (2003).
19. Rojas, O.R., Ernstsson, M., Neuman, R.D. & Claesson, P.M. Effect of polyelectrolyte charge density on the adsorption and desorption behaviour on mica. *Langmuir* **18**, 1604-1612 (2002).
20. Stevens, M.J. Simple simulations of DNA condensation. *Biophys J* **80**, 130-139 (2001).
21. Zhang, W. & Zhang, X. Single molecule mechanochemistry of macromolecules. *Progress in Polymer Science* **28**, 1271-1295 (2003).
22. Rouzina, I. & Bloomfield, V.A. Competitive electrostatic binding of charged ligands to polyelectrolytes: practical approach using the non-linear Poisson-Boltzmann equation. *Biophys Chem* **64**, 139-155 (1997).
23. Ottøy, M.H., Vårum, K.M. & Smidsrød, O. Compositional heterogeneity of heterogeneously deacetylated chitosans. *Carbohydr Polym* **29**, 17-24 (1996).
24. Draget, K.I., Vårum, K.M., Moen, E., Gynnild, H. & Smidsrød, O. Chitosan cross-linked with Mo(VI) polyoxyanoins: a new gelling system. *Biomaterials* **13**, 635-638 (1992).
25. Hutter, J.L. & Bechhoefer, J. Calibration of atomic-force microscopy tips. *Rev Sci Instrum* **64**, 1868-1873 (1993).
26. Laney, D.E., Garcia, R.A., Parsons, S.M. & Hansma, H.G. Changes in the elastic properties of cholinergic synaptic vesicles as measured by atomic force microscopy. *Biophys J* **72**, 806-813 (1997).
27. Vårum, K.M., Ottøy, M.H. & Smidsrød, O. Water-solubility of partially N-acetylated chitosans as a function of pH: effect of chemical composition and depolymerisation. *Carbohydr Polymers* **25**, 65-70 (1994).
28. Pashley, R.M. DLVO and hydration forces between mica surfaces in Li^+, Na^+, K^+ and Cs^+ electrolyte solutions: A correlation of double-layer and hydration forces cation exchange properties. *J Colloid Interface Sci* **83**, 531-546 (1981).
29. Hoh, J.H., Cleveland, J.P., Prater, G.B., Revel, J.P. & Hansma, P.K. Quantized

adhesion detected with the atomic force microscope. *J Am Chem Soc* **114**, 4917-4918 (1992).
30. Anthonsen, M.W. & Smidsrød, O. Hydrogen ion titration of chitosans with varying degrees of N-acetylation by monitoring induced ^{1}H-NMR chemical shifts. *Carbohydr Polym* **26**, 303-305 (1995).
31. Strand, S.P., Tømmeraas, K., Vårum, K.M. & Østgaard, K. Electrophoretic light scattering studies of chitosans with different degrees of N-acetylation. *Biomacromolecules* **2**, 1310-1314 (2001).
32. Seitz, M., Friedsam, C., Jöstl, W., Hugel, T. & Gaub, H. Probing solid surfaces with single polymers. *ChemPhysChem* **4**, 986-990 (2003).
33. Claesson, P.M. & Ninham, B.W. pH-dependent interactions between adsorbed chitosan layers. *Langmuir* **8**, 1406-1412 (1992).
34. Cai, X.-E. & Yang, J. Molecular forces for the binding and condensation of DNA molecules. *Biophys J* **82**, 357-365 (2002).
35. Al-Maawali, S., Bemis, J.B., Akhremitchev, B.B., Leecharoen, R., Janesko, B.G. & Walker, G. Study of the polydispersity of grafted poly(dimethylsiloxane) surface using single-molecule atomic force microscopy. *J Phys Chem B* **105**, 3965-3971 (2001).
36. Flory, P.J. *Principles of polymer chemistry*. (Cornell University Press, New York, 1953).
37. Fleer, G.J., Cohen Stuart, M.A., Scheutjens, J.M.H.M., Cosgrove, T. & Vincent, B. *Polymers at interfaces*. (Chapmann & Hall, London, 1993).
38. Zhang, W. & Zhang, X. Single molecule mechanochemistry of macromolecules. *Progress Polymer Science* **28**, 1271-1295 (2003).
39. Evans, E. & Ritchie, K. Dynamic strength of molecular adhesion bonds. *Biophys J* **72**, 1541-1555 (1997).
40. Haupt, B.J., Ennis, J. & Sevick, E.M. The detachment of a polymer chain from a weakly adsorbing surface using an AFM tip. *Langmuir* **15**, 3886-3892 (1999).
41. Marra, J. & Hair, M.L. Forces between two poly(2-vinylpyridine)-covered surface as a function of ionic strength and polymer charge. *J Phys Chem* **92**, 6044-6051 (1988).
42. Dahlgren, M.A.G., Waltermo, Å., Blomberg, E., Claesson, P.M., Sjöström, L., Åkesson, T. & Jönsson, B. Salt effects on the interaction between adsorbed cationic polyelectrolyte layers - theory and experiment. *J Phys Chem* **97**, 11769-11775 (1993).
43. Dahlgren, M.A.G., Hollenberg, H.C.M. & Claesson, P.M. The order of adding polyelectrolyte and salt affects surface forces and layer structures. *Langmuir* **11**, 4480-4485 (1995).
44. Stigter, D. & Dill, K.A. Binding of ionic ligands to polyelectrolytes. *Biophys J* **71**, 2064-2074 (1996).
45. Bloomfield, V.A., Crothers, D.M. & Tinoco, I. *Nucleic Acids. Structures, properties and functions*. pp 13-43 (University Science Books, Sausalito, 2000).
46. Anthonsen, M.W., Vårum, K.M. & Smidsrød, O. Solution properties of chitosans: Conformation and chain stiffness of chitosans with different degrees of N-acetylation. *Carbohydr Polymers* **22**, 193-201 (1993).
47. Minke, R. & Blackwell, J. The structure of α-chitin. *J Mol Biol* **120**, 167-181 (1978).